Voltammetric study of the formation of heteropolyanions in solutions

片野, 肇

(Degree)
博士（理学）

(Date of Degree)
1994-03-31

(Date of Publication)
2008-10-28

(Resource Type)
doctoral thesis

(Report Number)
甲1274

(JaLCDOI)
https://doi.org/10.11501/3078402

(URL)
https://hdl.handle.net/20.500.14094/D1001274

博 士 論 文

VOLTAMMETRIC STUDY OF THE FORMATION OF HETEROPOLYANIONS IN SOLUTIONS

（溶液中でのヘテロポリ酸アニオン生成のボルタンメトリー的研究）

平成 6 年 1 月

神戸大学大学院自然科学研究科

片野　肇

CONTENTS

Introduction ····· 1

Chapter Ⅰ. Hydrophobicity Scale of Heteropoly- and Isopolyanions · 3

1.1. Introduction ····· 3

1.2. Experimental ····· 4

1.3. Results ····· 10

1.4. Discussion ····· 16

Chapter Ⅱ. Solvation Energy of Heteropoly- and Isopolyanions ··· 20

2.1. Introduction ····· 20

2.2. Experimental ····· 21

2.3. Results ····· 22

2.4. Discussion ····· 27

Chapter Ⅲ. Formation Equilibrium of Heteropolymolybdates in Aqueous Solutions ····· 32

3.1. Introduction ····· 32

3.2. Experimental ····· 34

3.3. Results ····· 45

3.3.1. Molybdosilicates ····· 45

3.3.2. Molybdogermanates ····· 56

3.3.3. Molybdophosphates ····· 63

3.3.4. Molybdoarsenates ····· 77

3.4. Discussion ····· 85

Chapter Ⅳ. Formation Kinetics of Heteropolymolybdates in Aqueous Solutions ····· 88

4.1. Introduction ····· 88

4.2. Experimental ····· 90

4.3. Theoretical ····· 92

4.4. Results ····· 99

4.5. Discussion ····· 111

Chapter Ⅴ. Analytical Application — A Voltammetric Phosphate Sensor — ····· 112

5.1. Introduction ····· 112

5.2. Experimental ····· 113

5.3. Results and Discussion ····· 116

Conclusion ····· 124

Acknowledgement ····· 127

References ····· 128

List for Frequently Used Symbols

Symbol	Meaning	Usual Dimensions
A	surface area of an interface	cm^2
a_j^α	activity of ion j in phase α	usual, M
D_j^α	diffusion coefficient of ion j in phase α	$cm^2\ sec^{-1}$
E	potential	V
E_j°	standard potential of ion j	V
E_{mid}	midpoint potential; $(E_{pa} + E_{pc})/2$	V
E_{pa}	anodic (positive current) peak potential	V
E_{pc}	cathodic (negative current) peak potential	V
ΔE_{ref}	reference electrode potential	V
F	Faraday constant	C
$\Delta G_{tr,j}^{\circ,\beta\rightarrow\alpha}$	standard Gibbs free energy of the transfer of ion j from β to α	J
I, i	current	μA, A
I_{pa}	anodic (positive current) peak current	μA
I_{pc}	cathodic (negative current) peak current	μA
k	rate constant	sec^{-1}
R	gas constant	$J\ mol^{-1}\ K^{-1}$
s	Laplace plane variable, usually complementary to t	
T	temperature	usual, K
t	time	sec
γ_j^α	activity coefficient of ion j in phase α	M
$\Delta_\alpha^\beta\phi_j$	interfacial potential difference (across the interface between phases α and β)	V
$\Delta_\alpha^\beta\phi_j^\circ$	standard ion-transfer potential difference of ion j (across the interface between phases α and β)	V

Introduction

Heteropolyanions [1,2] have been utilized in various fields. The formation and subsequent precipitation or reduction of heteropolyanions are the basis of gravimetric or colorimetric analyses of such oxoanions as silicate, germanate, orthophosphate, arsenate, etc. They have been also used as heterogeneous and homogeneous catalysts for a broad variety of reactions [3]. Recently, there have been reports on their applications to biochemistry [4] and as ion-exchange materials [5].

In addition, a wide variety of heteropolyanions have been synthesized. However, no systematic procedure for their syntheses has been established. This seems to be ascribed to the lack of a consideration of their solvation behaviors. Although most polyanions have been prepared from aqueous solutions, a number of new heteropolyanions have been recently isolated from aqueous organic solvents [6-11]. It should be also noted that certain polyanions unstable in water are stabilized by the addition of water-miscible organic solvents [12-19]. Thus it may be speculated that hydrophobic characters of polyanions play an important role in their formation. Nevertheless, there has been no available measure for evaluating the hydrophobicity (or hydrophilicity).

A recently developed voltammetric technique using a polarizable oil/water interface, so-called ion-transfer voltammetry [20-22], provides quantitative information on the phase transfer characteristics of an individual ion. It offers a promising possibility for understanding the interfacial processes including extraction [23-27] and liquid-membrane transport [28]. In particular, the standard ion transfer potential, which is related to the Gibbs standard transfer energy of the ion from oil to water, can provide useful criteria for evaluating the affinity of the ion to organic solvents. It should be also noted that the voltammetric current proportional to the bulk concentration of a transferring species enables us to study solution equilibria of polyanions. Thus, in order to understand the formation of polyanions systematically, ion-transfer voltammetry has been

employed.

In this thesis, the author's contribution to the study of the formation of heteropolyanions in solutions has been summarized in five chapters. In Chapter I, the solution chemistry of heteropoly- and isopolyanions is considered. The transfer of polyanions at the nitrobenzene/water interface has been studied by ion-transfer voltammetry. Through analyses of the voltammetric waves, a simple linear dependence of the standard ion-transfer potentials on the surface charge densities of polyanions has been obtained. On the basis of this finding, the author has proposed a hydrophobicity scale of polyanions. In Chapter II, ion-transfer voltammetric measurements have been extended to the 1,2-dichloroethane/water interface. The author has discussed the solvation energy of polyanions. In Chapter III, the formation equilibrium of heteropolymolybdates in aqueous solutions is mentioned. Ion-transfer voltammetry with the nitrobenzene/water interface has been applied to the characterization of aqueous molybdate solutions containing such a heteroanion as silicate, germanate, phosphate, or arsenate. Some solute species have been identified and their formation equilibria have been discussed on the basis of the hydrophobicity scale proposed in Chapter I. Chapter IV deals with the formation kinetics of heteropolymolybdates. To date, the formation mechanisms of heteropolymolybdates have not been elucidated well. The author has developed a novel technique based on the amperometric detection of polyanions using an oil/water interface for the research of the formation mechanisms of Keggin-type heteropolymolybdates. In Chapter V, an analytical application is described. On the basis of the study described in Chapters III and IV, the author has developed a new method for the determination of oxoanions, which relies on electrochemical formation of a molybdophosphate at the interface and on the subsequent detection of the voltammetric current due to its transfer. A novel voltammetric sensor for phosphate ion has been constructed and its performance has been examined.

CHAPTER I

Hydrophobicity Scale of Heteropoly- and Isopolyanions[a)]

1.1. Introduction

Heteropolyanions [1,2] are widely used as acid and redox catalysts for various synthetic reactions in both heterogeneous and homogeneous systems[3]; they have also played important roles in the analysis of such oxoanions as orthophosphate and silicate ions. While trying to understand these catalytic and analytical processes, detailed solution studies of heteropolyanions were carried out using electrochemical and spectroscopic techniques. One of the important facts obtained is that although certain heteropolyanions, like $[PMo_{12}O_{40}]^{3-}$, are unstable in water, they are stabilized by addition of water-miscible organic solvents, such as 1,4-dioxane and acetone. [12-19] It should also be noted that in recent synthetic studies [6-11] a wide variety of new heteropolyanions, e.g., $[S_2Mo_{18}O_{62}]^{4-}$, $[S_2VMo_{17}O_{62}]^{5-}$, $[VMo_{12}O_{40}]^{3-}$, and $[P_2Mo_{18}O_{61}]^{4-}$(containing $P_2O_7^{4-}$), have been successfully prepared from mixed aqueous solutions. Thus, although many heteropolyanions possess hydrophobic characteristics, there has been no available measure for evaluating the affinity of heteropolyanions to organic solvents.

The transfer of heteropoly- and isopolyanions at the interface between two immiscible electrolyte solutions (ITIES), viz., the nitrobenzene(NB)/water(W) interface [30-35] has been studied by a novel voltammetric technique (so-called ion-transfer voltammetry) [20-22]. Moderately hydrophobic polyanions, such as $[SiW_{12}O_{40}]^{4-}$, $[P_2Mo_{18}O_{62}]^{6-}$, and $[Mo_6O_{19}]^{2-}$, produced voltammetric waves due to their transfer across the ITIES. Through analyses of the voltammetric waves, the values of the standard ion-transfer potential ($\Delta_o^w \phi^\circ$), which is related to the standard Gibbs free energy of transfer by Eq. 1-3 (see below), were determined for the polyanions of various size and ionic charge. As for the determined $\Delta_o^w \phi^\circ$-values, a simple linear dependence on the surface charge densities of polyanions has been observed. On the basis

of this finding, the author will hereinafter propose a hydrophobicity scale of heteropoly- and isopolyanions.

1.2. Experimental

Chemicals

TBA$^+$ salt of $[VMo_5O_{19}]^{3-}$

A *n*-tetrabutylammonium (TBA^+) salt of $[VMo_5O_{19}]^{3-}$ was prepared according to the reported method. [36] A polyhedral representation of the anion is shown in Fig. 1-1(a).

TBA$^+$ salt of α-$[Mo_8O_{26}]^{4-}$

A 10 g quantity of $(NH_4)_6Mo_7O_{24}\cdot 4H_2O$ was dissolved in 100 ml of water. After filtration of the turbidity, the pH of the solution was adjusted to 5.5-6.5 with 1 M NaOH. The addition of TBABr produced white precipitates. They were collected by filtration, washed with ethanol and then dried at 50℃. The identification of the salt was based on an elemental analysis and IR spectroscopy. [37]

Anal. Calcd for $(TBA)_4[Mo_8O_{26}]$: Mo, 35.64; C, 35.70; H, 6.74; N, 2.60%. Found: Mo, 35.9; C, 35.42; H 6.74; N, 2.59%. IR(cm^{-1}) 950(w), 923(vs), 912(vs), 905(vs), 854(s), 806(vs), 665(vs), 560(w), 502(w).

In TG-DTA no evolution of water was observed up to 220℃. A polyhedral representation is shown in Fig. 1-1(b).

n-Tetrapentylammonium tetraphenylborate (TPnATPB)

TPnATPB was prepared by mixing equimolar ethanolic solutions of *n*-

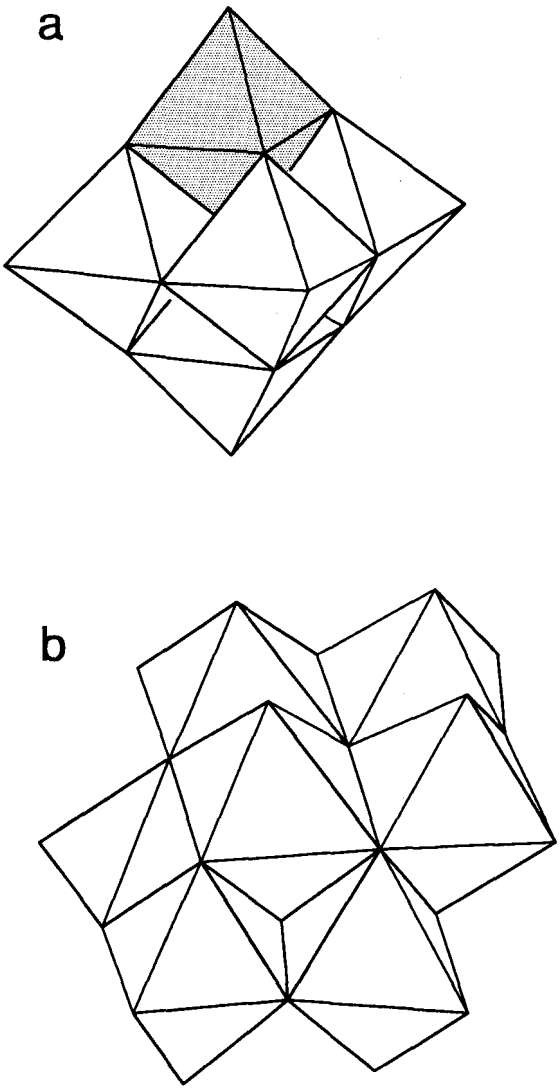

Fig. 1-1. Structures of (a) $[VMo_5O_{19}]^{3-}$ and (b) α-$[Mo_8O_{26}]^{4-}$.

tetrapentylammonium bromide (Wako Pure Chemical Industries, Ltd.) and sodium tetraphenylborate (Dojindo Laboratories); the precipitate was washed five times with distilled water and twice with ethanol and further purified by recrystallization from acetone.

n-Tetrapentylammonium chloride (TPnACl)

TPnACl (Wako's practical grade) was dissolved in distilled water, treated several times with active carbon to remove yellowish impurities and used for preparing phase I in cell A; the concentration of TPnCl was determined by potentiometric titration with a standard silver nitrate solution.

The crystals of *n*-Tetrabutylammonium tetraphenylborate (TBATPB) were obtained according to the reported method [38].

n-Tetrabutylammonium chloride (TBACl)

Analytical grade TBACl was frequently contaminated by a trace iodide ion, which was removed by metathesis with silver chloride in the aqueous solution; the concentration of TBACl was determined by potentiometrically in the same manner as TPnACl.

Analytical grade nitrobenzene(Wako) was purified by shaking with active alumina overnight. The nitrobenzene solutions of the heteropolyanions were prepared immediately before use to avoid gradual reduction of the heteropolyanions.

Other chemicals were of analytical grade and were used as received.

Electrochemical measurements

Ion transfer voltammetric measurements were made by using a microcomputer-assisted system [39].

In studing of the transfer of $[VMo_5O_{19}]^{3-}$ and α-$[Mo_8O_{26}]^{4-}$ at the NB/W interface, the following electrochemical cell (cell A) was used:

	I	II	III	IV	V	
	0.02M TPnACl	0.1 M	0.1 M TPnATPB	0.05 M $MgCl_2$	0.05M $MgCl_2$	
Ag/AgCl (RE2)	0.1 M MgSO4	TPnATPB	x mM TBA^+ salt of heteropolyanion	0.5M $MgSO_4$ buffer	0.5 M $MgSO_4$	AgCl/Ag (RE1)
	(W)	(NB)	(NB)	(W)	(W)	

The polyanion was added to phase III as the TBA^+ salt*) , and its transfer across the interface (area, 0.127 cm^2) between phases III and IV was examined. (*: In this study, polyanions to be tested were usually dissolved in the organic-solvent phase, not in the water phase where most polyanions are very labile.) The pH of phase IV was adjusted with 0.1 M ammonia buffer (pH > 7), CH_3COOH + $(CH_3COO)_2Mg$ buffer ($[CH_3COO^-]$ = 0.1 M; pH 3 - 5), and HCl (pH < 3). A three-electrode cell assembly shown in Fig. 1-2 was used for cell A. The 0.1 M TPnATPB NB solution without a TBA^+ salt of heteropolyanion was loaded into Luggin capillary to prevent the equilibrium potential difference between phases I and II from being disturbed by TBA^+ ion. Phases IV and V were separated by a glass sinter. The potential difference across the test interface, $\Delta_O^W\phi$ ($\equiv\phi^W-\phi^O$; ϕ^W and ϕ^O being the potentials of W and O phases), was controlled by using two reference electrodes, *i.e.* the Ag/AgCl|I|II electrode (RE2) and Ag/AgCl|V electrode (RE1). The potential difference E between the metal phases of the two reference electrodes, being controlled by means of a laboratory-made potentiostat with a positive feedback iR compensation, is related to $\Delta_O^W\phi$ as

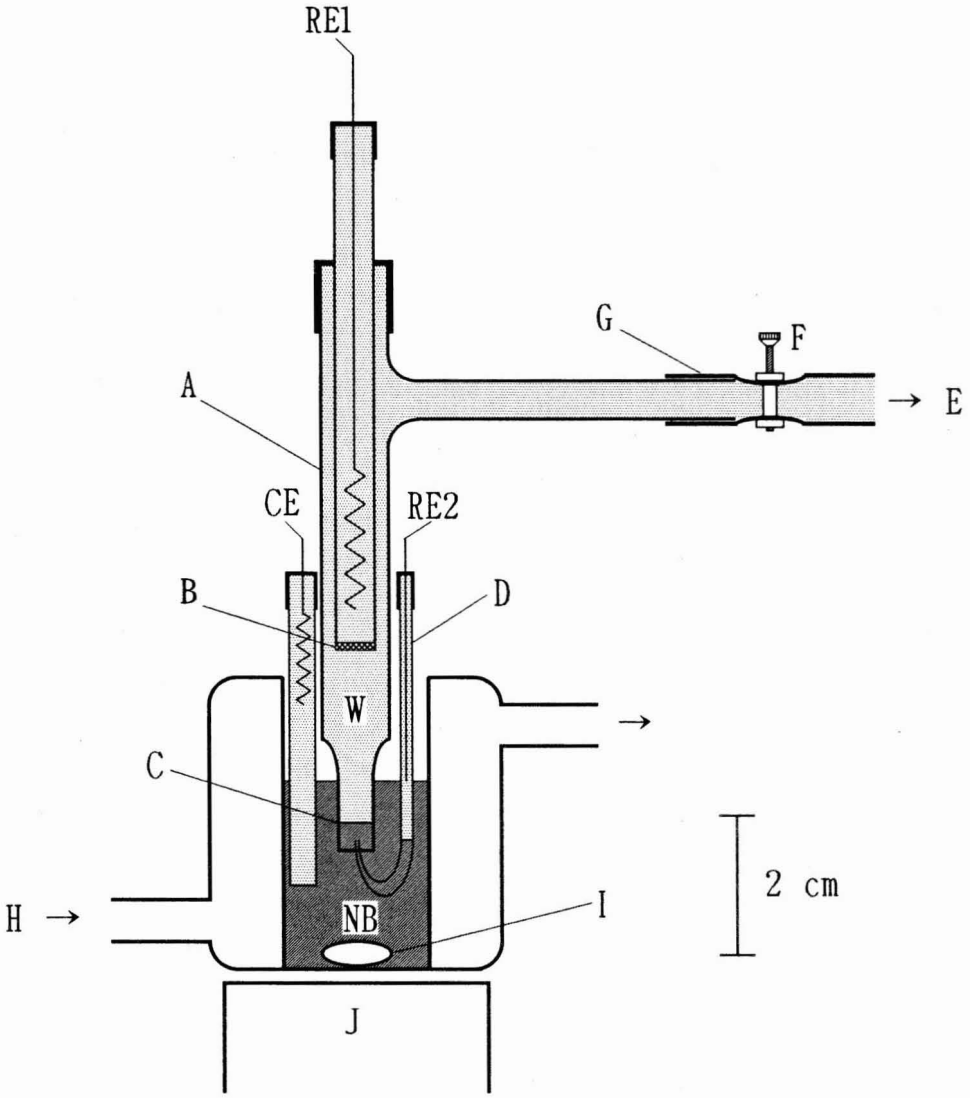

Fig. 1-2. Electrolytic cell :

(W) water phase, (NB) nitrobenzene phase, (RE1 and RE2) reference electrodes, (CE) counter electrode, (A) glass tube, (B) sintered glass, (C) test interface, (D) Luggin capillary, (E) to solution reservoir, (F) screw cock for the interface adjustment, (G) silicone tube, (H) thermostated water (25±0.1 ℃), (I) stirring bar, and (J) magnetic stirrer.

$$E = \Delta^{W}_{O}\phi + \Delta E_{ref}$$

where ΔE_{ref} is a constant which depends only on the reference electrode system. The ΔE_{ref} for cell A has been evaluated to be 0.323 V. [40] The current flowing through the test interface was detected by using the Ag/AgCl|V electrode (RE1) and additional Ag/AgCl|0.02 M TPnACl + 0.1 M $MgSO_4$ (W) electrode (CE in Fig. 1-2) immersed in NB (phase III).

For the study of the phase transfer using different supporting-electrolyte systems, the following cell (cell B) was used instead of cell A.

CELL B:

	I	II	III	
Ag/AgCl	0.1 M TBACl (W)	0.1 M TBATPB x mM heteropolyanion (NB)	0.5 M $MgCl_2$ buffer (W)	AgCl/Ag

CELL C:

	I	II	III	
Ag/AgCl	0.1 M TBACl (W)	0.1 M TBATPB x mM heteropolyanion (NB)	0.1 M LiCl buffer (W)	AgCl/Ag

The interface between phases II and III was to be tested. A two-electrode cell assembly [30] was employed for cells B and C.

1.3 Results

The voltammetric determinations of $\Delta_o^w \phi^\circ$ for the polyanions at the NB/W interface were reported in detail, [30-33] except for $[VMoO_{18}]^{3-}$ and α-$[Mo_8O_{26}]^{4-}$. Fig. 1-3 shows cyclic voltammograms for the transfer of $[VMo_5O_{19}]^{3-}$ at the NB/W(pH 4.8) interface, which were recorded using five different scan rates. In each voltammetric wave, the anodic (positive current) peak corresponds to the transfer of the polyanion from NB to W, whereas the cathodic (negative current) peak corresponds to its transfer back to NB. As can be seen in the figure, the cathodic peak became less prominent upon lowering the scan rate. This may be ascribed to the partial decomposition of the polyanion in the W phase (cf. [32]).

Nevertheless, the midpoint potential E_{mid} ($\equiv(E_{pa}+E_{pc})/2$; E_{pa} and E_{pc} being the anodic and cathodic peak potentials) was practically independent of the scan rate. As shown in Fig. 1-4, the values of E_{mid} were almost invariant at higher pH-values (>4), though they shifted to positive potentials at lower pH-values due to protonation of the polyanion in the organic-solvent phase [41]. The invariant value of E_{mid} at higher pH-values (viz., 0.201 V) was then considered as the reversible half-wave potential ($E_{1/2}^{rev}$) for the individual ion transfer accompanying no protonation.

The $E_{1/2}^{rev}$ is related to $\Delta_o^w \phi^\circ$ as [25]

$$E_{1/2}^{rev} = \Delta_o^w \phi^\circ + \Delta E_{ref} \qquad (1\text{-}1)$$

and

$$\Delta_o^w \phi_{1/2}^{rev} = \Delta_o^w \phi^\circ + \frac{RT}{zF} \ln \frac{\gamma^{o}\sqrt{D^{w}}}{\gamma^{w}\sqrt{D^{o}}}, \qquad (1\text{-}2)$$

where z is the ionic valence (here z = -3); γ^α and D^α (α = O or W) are the activity coefficient and the diffusion coefficient of transferred ion in the organic-solvent phase (O) or water phase (W); F, R, and T have their usual meanings. The second term of the right-hand side of Eq. 1.2 is quite small; the contribution was evaluated to be only -0.003

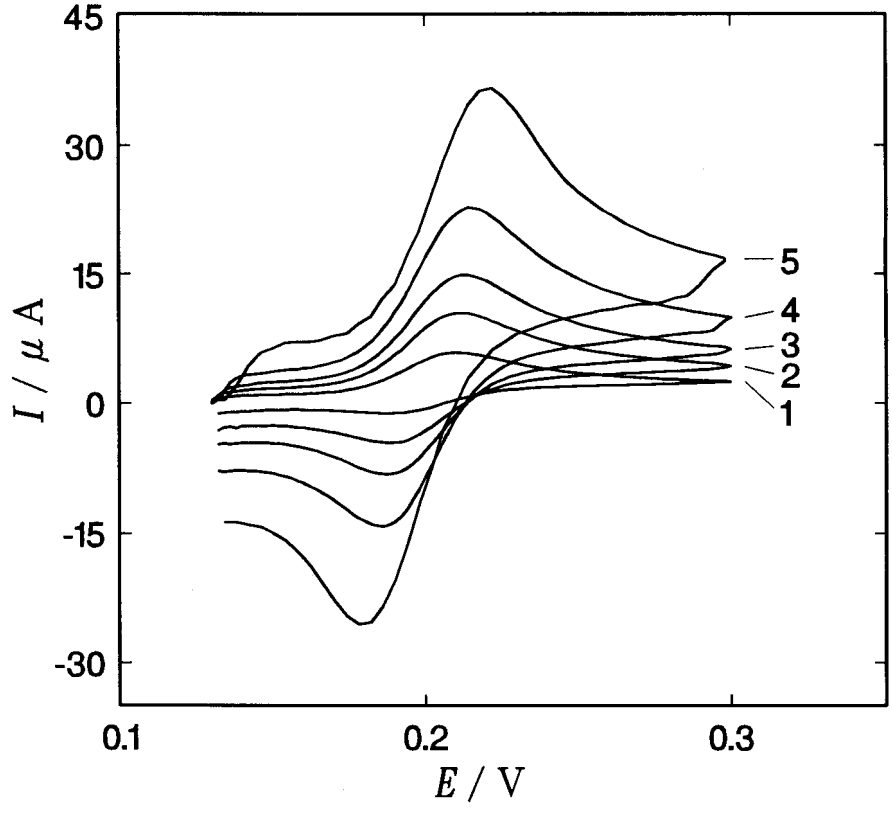

Fig. 1-3. Cyclic voltammgrams of the transfer of $[VMo_5O_{19}]^{3-}$ at the NB/W (pH 4.8) interface. The polyanion was added to the NB phase as the TBA^+ salt so that the concentration became 0.20 mM. The scan rates were (1) 0.02 ; (2) 0.05 ; (3) 0.1 ; (4) 0.2 ; (5) 0.5 V s^{-1}.

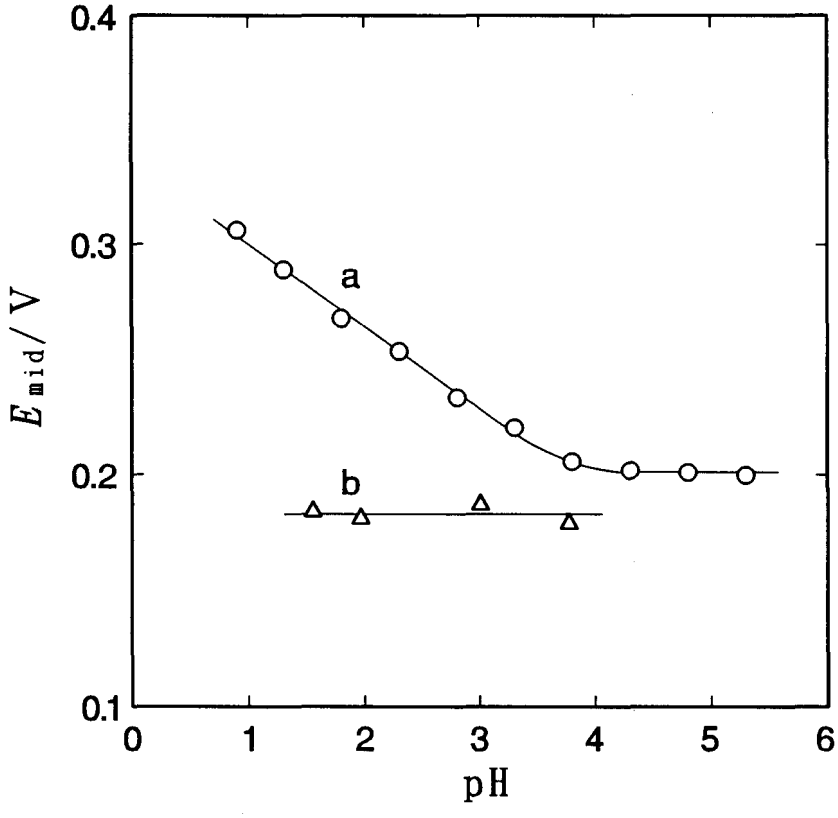

Fig. 1-4. pH dependences of the midpoint potentials of the cyclic voltammograms for the transfer of (a) $[VMo_5O_{19}]^{3-}$ and (b) α-$[Mo_8O_{26}]^{4-}$ at the NB/W interface.

V (for z = -3) by assuming $\gamma^{o}/\gamma^{w} = 1$ and $D^{o}/D^{w} = 2.07$ [42] (Walden rule). Finally, $\Delta_{o}^{w}\phi^{o}$ was determined to be -0.119 V for $[VMo_5O_{19}]^{3-}$. Further, using a well-known relation [20,22],

$$\Delta G_{tr}^{o,\,o\rightarrow w} = -zF\Delta_{o}^{w}\phi^{o} \qquad (1\text{-}3)$$

$\Delta G_{tr}^{o,\,o\rightarrow w}$ was also determined to be -35 kJ mol^{-1}.

For the transfer of α-$[Mo_8O_{26}]^{4-}$, it was rather difficult to obtain a reproducible voltammogram at ordinary scan rates, due to the appearance of a maximum which might be related to a quite rapid decomposition or transformation of the complex anion (possibly, into β-isomer) in the W-phase. Nevertheless, a well-defined cyclic voltammogram (not shown) could be obtained most readily by using higher scan rates (e.g., 1.0 V s-1). As shown in Fig. 1-4, E_{mid} is virtually constant (0.183 ± 0.004 V) over the pH range 1.6-3.8, indicating no participation of protonation in the transfer process. In a similar manner as $[VMoO_{19}]^{3-}$ mentioned above, $\Delta_{o}^{w}\phi^{o}$ and $\Delta G_{tr}^{o,\,o\rightarrow w}$ for α-$[Mo_8O_{26}]^{4-}$ were evaluated based on pH-independent E_{mid}.

As illustrated by the transfer of the two polyanions, the values of $\Delta_{o}^{w}\phi^{o}$ and $\Delta G_{tr}^{o,\,o\rightarrow w}$ for other kinds of polyanions were likewise determined. The results are summarized in Table 1-1. For further details, see each reference noted in the table.

In Table 1-2 the values of $\Delta_{o}^{w}\phi^{o}$ determined using different supporting-electrolyte systems are compared for some typical polyanions. The divergences are almost within the experimental errors (±0.005 V), except for $[P_2Mo_{18}O_{62}]^{6-}$, which shows a slight deviation. This result implies that the ion, association either in NB or in W has no significant influence on the transfer potential of a polyanion. It should also be noted that the $\Delta_{o}^{w}\phi^{o}$-values given in Table 1-1 were determined using some different supporting-electrolyte systems. If the effect of ion association was not negligible, such a clear correlation as shown below (Fig. 1-5) could not been obtained.

Table 1-1.

Standard Potentials and Standard Gibbs Free Energy of Transfer of Heteropoly- and Isopolyanions at the Nitrobenzene/Water Interface (25℃)

No.	Anion	Form	$\lvert z\rvert/n^{2/3}$	$\Delta_o^w \phi^\circ$ / V	$\Delta G_{tr}^{\circ,\, o\to w}$ / kJmol^{-1}	Ref.
1a	$[SiMo_{12}O_{40}]^{4-}$	α	0.342	0.066	26	30,31
1b	$[SiMo_{12}O_{40}]^{4-}$	β	0.342	0.067	27	31
2a	$[GeMo_{12}O_{40}]^{4-}$	α	0.342	0.064	26	31
2b	$[GeMo_{12}O_{40}]^{4-}$	β	0.342	0.066	26	31
3a	$[PMo_{12}O_{40}]^{3-}$	α	0.256	0.248[a)]	72[a)]	31
3b	$[PMo_{12}O_{40}]^{3-}$	β	0.256	0.248[a)]	72[a)]	31
4	$[AsMo_{12}O_{40}]^{3-}$	α	0.256	0.243[a)]	71[a)]	31
5	$[SiW_{12}O_{40}]^{4-}$	α	0.342	0.071	28	31
6	$[PW_{12}O_{40}]^{3-}$	α	0.256	0.243[a)]	74[a)]	31
7	$[P_2Mo_{18}O_{62}]^{6-}$	α	0.383	0.005	3	33
8	$[As_2Mo_{18}O_{62}]^{6-}$	α	0.383	0.005	3	33
9	$[S_2Mo_{18}O_{62}]^{4-}$	α	0.255	0.269[a)]	104[a)]	33
10	$[S_2VMo_{17}O_{62}]^{5-}$		0.319	0.085	41	33
11	$[P_2Mo_{18}O_{61}]^{4-}$		0.258	0.239	92	33
12	$[Mo_8O_{19}]^{2-}$		0.281	0.164	32	32
13	$[VMo_5O_{19}]^{3-}$		0.421	-0.119	-35	This study
14	$[Mo_8O_{26}]^{4-}$	α	0.460	-0.137	-53	This study

a) Approximate values estimated from the foot of voltammetric wave

Table 1-2.

Standard Ion-Transfer Potentials of Some Typical Polyanions at the Nitrobenzene/Water Interface Determined Using Three Different Supporting-Electrolyte Systems (25℃)

Anion	$\Delta_o^w \phi^\circ$ /V		
	System 1 cell A	System 2 cell B	System 3 cell C
α-$[SiMo_{12}O_{40}]^{4-}$	0.071	0.066[30,31]	0.073
α-$[GeMo_{12}O_{40}]^{4-}$	0.068	0.064[31]	0.072
α-$[P_2Mo_{18}O_{62}]^{6-}$	0.005	0.005	0.023
$[Mo_6O_{19}]^{2-}$	0.172	0.164[32]	0.170

1.4 Discussion

In table 1-1, anions **1-6** have the Keggin-type structure (see Fig. 3-2), whereas anions **7-11** have the Dawson-type structure (or a related structure for **11**) (see Fig. 3-29).

In either structure, anions of the same ionic charge have nearly equal values of $\Delta_o^w \phi^\circ$ and $\Delta G_{tr}^{o,o\to w}$, independent of the central heteroatoms. Further, there is no difference in the transfer potential between the α- and β-isomers, in which one M_3O_{13} (M = Mo or W) group is rotated by 60°. (see Fig. 3-2) These results seem to support the hypothesis that the surface charge of such a polyanion is nonlocalized.

In the following, the author discusses the dependence of $\Delta_o^w \phi^\circ$ on the surface charge density of a polyanion. Unfortunately, however, there is only one available value of the ionic radii, viz., r = 0.56 nm for $[SiW_{12}O_{40}]^{4-}$ [43]. Accordingly, the surface charge density of a polyanion was estimated as follows: Because all of the space of the polyanion structure is taken up by the bulky oxygen atoms, which are virtually close-packed [1], the ionic volume can be determined solely based on the number of oxygen atoms (n). If the polyanion is assumed to be a hard sphere with a uniform surface charge, r should be proportional to $n^{1/3}$. Consequently, the surface charge density, $ze/4\pi r^2$ (e, the elementary charge), can be regarded as being proportional to $|z|/n^{2/3}$. Against this quantity, the $\Delta_o^w \phi^\circ$-values for the polyanions are plotted in Fig. 1-5. Despite the large difference in sizes, charges, and even structures, all of the data surprisingly lay on a straight line.

$$\Delta_o^w \phi^\circ(V) = -1.981(|z|/n^{2/3}) + 0.749. \qquad (1.4.)$$

Such a simple relationship was not observed between $\Delta G_{tr}^{o,o\to w}$ and $|z|/n^{2/3}$. It should be also noted that a similar linear plot was obtained for polyanion transfer at another ITIES, viz., 1,2-dichloroethane/water interface. (see Chapter II)

The standard ion transfer potentials of ions provide useful criteria for predicting their "hydrophobic" behaviors in such processes as

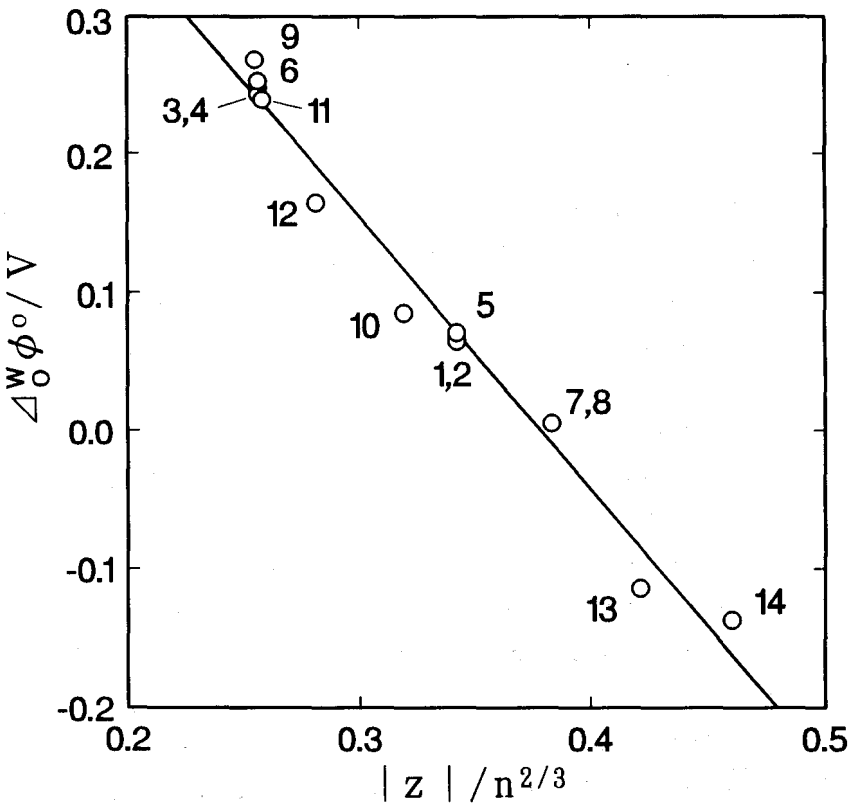

Fig. 1-5. Plot of the standard ion-transfer potentials of heteropoly- and isopolyanions at the NB/W interface against $|z|/n^{2/3}$ (z, ionic valence ; n, number of oxygen atoms). Numbers 1-14 correspond to the polyanion listed in Table 1-1.

liquid-liquid extraction [23-27] and liquid-membrane transport. [28] Thus, the transfer potentials can be used as a scale for the hydrophobicity of ions. For the polyanions of interest, however, the quantity $|z|/n^{2/3}$ (the values being shown in Table 1-1) may be conveniently employed as an alternative to $\Delta {}^{W}_{O}\phi^{\circ}$, since a linear relationship exists between the two quantities (Fig. 1-5).

According to the $|z|/n^{2/3}$-values, polyanions may be classified as being either hydrophobic or hydrophilic. As a whole, polyanions with $|z|/n^{2/3}$-values smaller than 0.3 (e.g., the anions 3, 4, 6, 9, 11, and 12) are unstable in aqueous solutions, and are classified as being "hydrophobic"; they are known to be highly stabilized by the addition of water-miscible organic solvents. Most of the new heteropolyanions prepared from mixed aqueous solvents [12-17] belong to this class. On the other hand, "hydrophilic" polyanions with $|z|/n^{2/3}$-values larger than 0.3 are relatively stable in aqueous solutions. Thus, the values of $|z|/n^{2/3}$ are useful for evaluating the stability of polyanions in solutions. As described in Chapter III, the Keggin-type molybdophosphate anion $[PMo_{12}O_{40}]^{3-}$, being classified as hydrophobic ($|z|/n^{2/3}$ = 0.256), does not exist stably in an aqueous solution; as a result relatively hydrophilic anions such as $[H_3PMo_{11}O_{39}]^{4-}$ ($|z|/n^{2/3}$ = 0.348) are formed.

Furthermore, the $|z|/n^{2/3}$ value may provide useful criteria for evaluting the extractability of polyanions into organic solvents. It appears that polyanions with smaller $|z|/n^{2/3}$-values are preferentially extracted into organic solvents. For the Keggin-type molybdates, the trivalent anions (3 and 4 with $|z|/n^{2/3}$ = 0.256) tend to be extracted more readily, i.e., at lower acid concentrations than the tetravalent anions (1 and 2 with $|z|/n^{2/3}$ = 0.342). [44-46]

In conclusion, the value of $|z|/n^{2/3}$ seems to be promising for a hydrophobicity scale of polyanions.

Finally, the author would like to add that the linear plot of $\Delta {}^{W}_{O}\phi^{\circ}$ vs. $|z|/n^{2/3}$ in Fig. 1-4 is of interest concerning a study of ion solvation [47,48] as well. The plot means that the standard transfer energy ($\Delta G_{tr}^{0,\,O\to W}$), namely the difference in the solvation energies of the polyanion in O and W, depends linearly on $1/n^{2/3}$ (cf. Eq. 1-3),

which is proportional to $1/r^2$. Note that this dependence cannot be accounted for by the Born-type electrostatic solvation energy [49], which should depend on $1/r$. Such a non-Bornian solvation energy may be interpreted by taking into account the so-called short-range interaction [50] of an ion with solvent molecules in its immediate vicinity (i.e., donor-acceptor effects or hydrogen bonds). However, it seems that a new basic theory would be necessary for a thorough understanding of the present result.

CHAPTER II

Solvation Energy of Heteropoly- and Isopolyanions[b,c)]

2.1. Introduction

The Gibbs energy of ion transfer at the ITIES is a key concept intimately related to ion transfer processes taking place in biomembrane systems, solvent extraction, liquid membrane type ion-selective electrodes, etc [47]. The Gibbs transfer energies of various ions have been evaluated from solubility data [51,52] and extraction data [53,54] and recently from electrochemical data obtained using ion-transfer voltammetry [20-22].

In the theoretical treatment, it has become customary to divide the Gibbs transfer energy into electrostatic and non-electrostatic parts:

$$\Delta G_{tr}^{o,\,o\to w} = \Delta G_{tr}^{o,\,o\to w}(el) + \Delta G_{tr}^{o,\,o\to w}(non\text{-}el) \qquad (2\text{-}1)$$

The electrostatic contribution has frequently been evaluated using the simple Born model [49] in which the ion is considered as a hard sphere of a given radius r immersed in a continuous medium of constant permittivity. In this model, the electrostatic solvation (or resolvation) energy is proportional to 1/r. However, the defects of the Born model have been well known for a long time and a variety of modifications have been proposed [47,55-57]. As mentioned in Chapter I, the standard ion transfer potentials $\Delta_o^w \phi^\circ$ of heteropoly- and isopolyanions at the NB/W interface depended linearly on the surface charge densities of the polyanions. Since $\Delta_o^w \phi^\circ$ is related to the standard Gibbs transfer energy by Eq. 1-3, the result means that $\Delta G_{tr}^{o,\,o\to w}$ depends not on 1/r (the simple Born model) but on $1/r^2$. This non-Bornian dependence suggests that short-range interactions of the ion with the solvent molecules play a significant role [48]. In order to know whether such a dependence also exists for other ITIES, experiments have been extended to the 1,2-dichloroethane(DCE)/W interface.

2.2. Experimental

The preparation of the TBA^+ salts of (1) α-$[PMo_{12}O_{40}]^{3-}$ [31], (2) α-$[SiMo_{12}O_{40}]^{4-}$ [31], (3) α-$[P_2Mo_{18}O_{62}]^{6-}$ [33], (4) $[Mo_8O_{16}]^{2-}$ [32], and (5) $[VMo_5O_{19}]^{3-}$ (section 1.2) has been described previously. Analytical grade DCE was purified by shaking with distilled water. The other chemicals are as described in section 1.2.

The voltammetric measurements were performed in a manner similar to that described in section 1.2. The following electrochemical cell was used:

	I	II	III	IV	V	
	0.02 M TPnACl	0.02-0.2 M	0.1 M TPnATPB,	0.05 M $MgCl_2$,	0.05 M $MgCl_2$,	
Ag/AgCl	0.1 M $MgSO_4$	TPnATPB	x mM polyanion	0.5 M $MgSO_4$,	0.5 M $MgSO_4$	AgCl/Ag
	(W)	(DCE)	(DCE)	(W)	(W)	

For further details, see section 1.2.

2.3. Results

Figure 2-1 shows representative cyclic voltammograms for the transfer of the anions **1**-**5** at the DCE/W interface. In each voltammetric wave, the anodic peak corresponds to the transfer of a polyanion from DCE to W, whereas the cathodic peak corresponds to its transfer back to DCE. Anions **2** and **3** gave well-defined reversible waves; however, the other three anions showed irreversible behaviour because of their decomposition in W [32]; when the scan rate was reduced, the cathodic peaks became less prominent (the voltammograms for anions **1**, **4**, and **5** shown in Fig. 2-1 were recorded at higher scan rates). Nevertheless, the values of E_{mid} for these anions as well as for anions **2** and **3** were almost independent of the scan rate. As shown in Fig. 2-2, the values of E_{mid} were almost invariant at higher pH values, although they shifted to positive potentials at lower pH because of their protonation in the organic solvent phase [31].

In the NB-W system mentioned in Chapter I, it was apparent that ion pairing in either NB or W has no significant influence on the transfer potential of a polyanion. In such a case, $E_{1/2}^{rev}$ is expressed by Eqs. 1-1 and 1-2. However, in the DCE-W system studied here, ion pairing between the polyanion A^z and cation B^+ of the organic base electrolyte may occur in O because of the lower value of the dielectric constant (i.e. ε = 10.36; cf. ε = 34.82 for NB). If A^z and B^+ form a 1:1 ion pair (AB^{z+1}), $\Delta_o^w\phi_{1/2}^{rev}$ in Eq. 1-1 can be written as [58-60].

$$\Delta_o^w\phi_{1/2}^{rev} = \Delta_o^w\phi_{app}^{\circ} + \frac{RT}{zF}\ln\frac{\gamma_A^{\circ}\sqrt{D_A^w}}{\gamma_A^w\sqrt{D_A^{\circ}}} \qquad (2\text{-}2)$$

where

$$\Delta_o^w\phi_{app}^{\circ} = \Delta_o^w\phi^{\circ} - \frac{RT}{zF}\ln\left[1 + K_a^{\circ}\,a\,C^{\circ}\frac{\gamma_A^{\circ}\gamma_B^{\circ}\sqrt{D_{AB}^{\circ}}}{\gamma_{AB}^{\circ}\sqrt{D_A^{\circ}}}\right] \qquad (2\text{-}3)$$

where γ_j^{α} and D_j^{α} are the activity coefficient and the diffusion coefficient of ion j(= A^z, B^+, or AB^{z+1}) in phase α(= O or W), K_a° is the association constant of the ion pair AB^{z+1}, c° is the bulk concentration

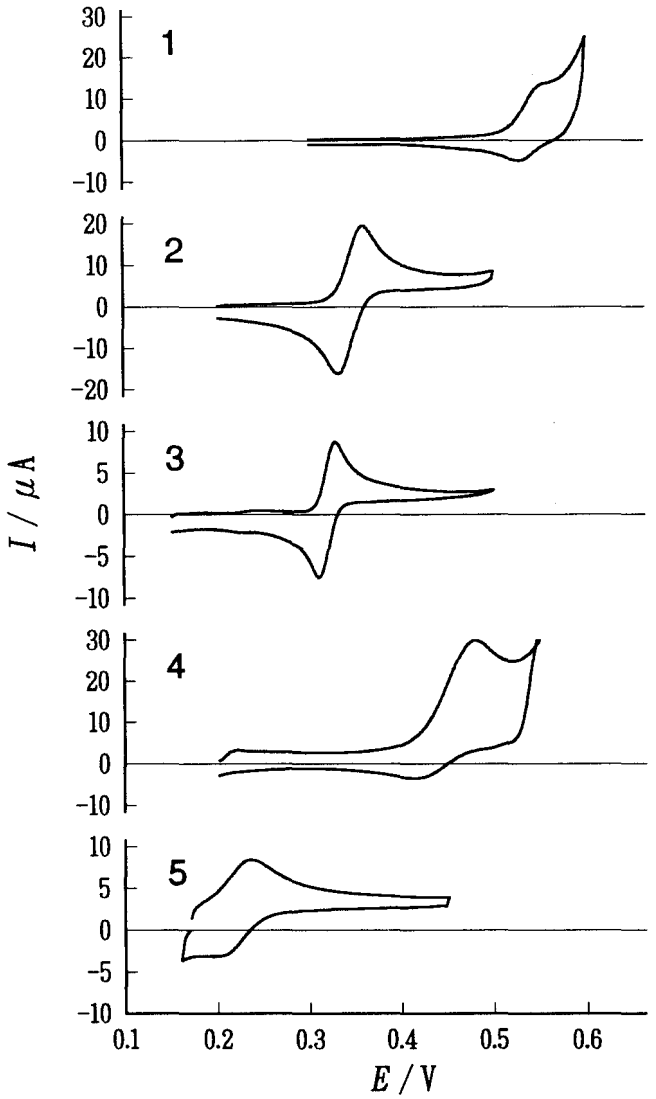

Fig. 2-1. Cyclic voltammograms of the transfer of (1) α-$[PMo_{12}O_{40}]^{3-}$, (2) α-$[SiMo_{12}O_{40}]^{4-}$, (3) α-$[P_2Mo_{18}O_{62}]^{6-}$, (4) $[Mo_6O_{19}]^{2-}$, and (5) $[VMo_5O_{19}]^{3-}$ at the DCE/W(pH 2.8) interface. The polyanion concentrations added to DCE phase as the TBA^+ salt were as follows : (1) 0.2, (2) 0.2, (3) 0.1, (4) 0.2, and (5) 0.1 mM. Scan rates : (1) 0.05, (2) 0.02, (3) 0.02, (4) 0.5, and (5) 0.1 V s^{-1}. Supporting electrolytes : 0.1 M TPnATPB in DCE ; 0.05 M $MgCl_2$ + 0.5 M $MgSO_4$ in W.

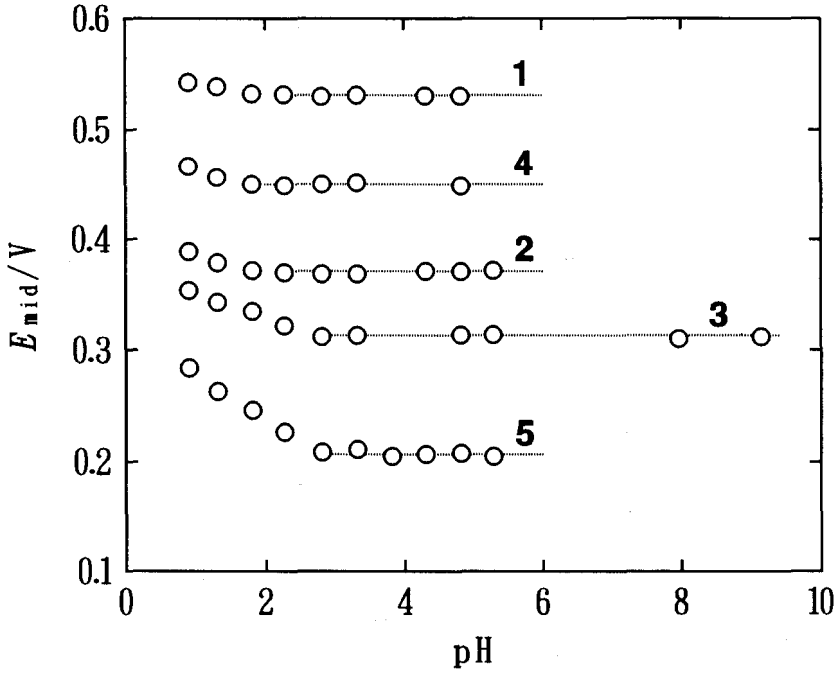

Fig. 2-2. pH dependences of the midpoint potentials for the transfer of (1) α-$[PMo_{12}O_{40}]^{3-}$, (2) α-$[SiMo_{12}O_{40}]^{4-}$, (3) α-$[P_2Mo_{18}O_{62}]^{6-}$, (4) $[Mo_6O_{19}]^{2-}$, and (5) $[VMo_5O_{19}]^{3-}$ at the DCE/W interface. Supporting electrolytes : 0.1 M TPnATPB in DCE ; 0.05 M $MgCl_2$ + 0.5 M $MgSO_4$ in W.

of the organic base electrolyte, and α the degree of dissociation.

In order to examine the effect of ion pairing, cyclic voltammetric measurements for the polyanion transfer were performed for several concentrations c° of the organic base electrolyte, namely 0.02, 0.05, 0.1, and 0.2 M. The observed values of $E_{1/2}^{rev}$ are shown in Table 2-1. Further, the author measured the values of $E_{1/2}^{rev}$ for the transfer of the tetramethylammonium ion (TMA^+), for which the value of the standard potential is known: $\Delta_o^w \phi^{\circ}$ = 0.160 V [60]. By applying Eqs. 1-1, 2-2, and 2-3 to the transfer of TMA^+, ΔE_{ref} was estimated for each concentration of the organic base electrolyte; its values are also shown in Table 2-1.

Table 2-1.
Reversible half-wave potentials for polyanion transfer at the DCE/W interface for several concentrations of the organic base electrolyte

No.	Ion	$E_{1/2}^{rev}$/V			
		0.02 M	0.05 M	0.1 M	0.2 M
1	α-$[PMo_{12}O_{40}]^{3-}$	0.520	0.529	0.531	0.534
2	α-$[SiMo_{12}O_{40}]^{4-}$	0.357	0.367	0.371	0.373
3	α-$[P_2Mo_{18}O_{62}]^{6-}$	0.310	0.311	0.313	0.312
4	$[Mo_6O_{19}]^{2-}$	0.435	0.444	0.450	0.454
5	$[VMo_5O_{19}]^{3-}$	0.196	0.205	0.207	0.208
	TMA^+	0.432	0.418	0.390	0.372
	ΔE_{ref}/V	0.303	0.284	0.253	0.232

In this estimation, it was assumed that $\gamma_A^{\circ} = \gamma_B^{\circ} = \gamma^{\circ}$ and $\gamma_{AB}^{\circ} = 1$, and the parameters γ° and α were evaluated by solving the following system of equations [59]:

$$-\log \gamma^{\circ} = A\sqrt{c^{\circ}\alpha} / (1 + Ba\sqrt{c^{\circ}\alpha}) \quad (2\text{-}4)$$

$$K_{ab}^{\circ} = (1 - \alpha)/(\gamma^{\circ})^2 c^{\circ}\alpha^2 \quad (2\text{-}5)$$

where A, B, and $\mathring{a}$ are the parameters of the Debye-Hückel theory and K^{o}_{ab} is the association constant of the base electrolyte in O (K^{o}_{ab} = 1.5×10^{3} $dm^{3}mol^{-1}$ for TPnATPB in DCE [61]). The activity coefficient in W was calculated directly from Eq. 2-4 because the ion pairing is negligible in W. The following assumptions were also used;

$$D^{W}_{A}/D^{O}_{A} = 0.87 \text{ (Walden rule)},$$

$$K^{o}_{a} = 1.24\times10^{4}\ dm^{3}mol^{-1} \text{ [51]},$$

and

$$D^{O}_{AB}/D^{O}_{A} = \gamma_{B}/(\gamma_{B}+\gamma_{A}) \simeq 0.4.$$

Equations 1-1 and 2-2 were then applied to the polyanion transfer. Since there is no available method for evaluating the activity coefficients of multivalent polyanions (z = -2 to -6), it was tentatively assumed that $\gamma^{O}/\gamma^{W} = 1$. Using this and another assumption, i.e. $D^{W}/D^{O} = 0.87$, together with the estimated values of ΔE_{ref} (Table 2-1), the author evaluated the "apparent" ion transfer potential $\Delta^{W}_{O}\phi^{o}_{app}$; the result is shown in Table 2-2. With increasing base electrolyte concentration, $\Delta^{W}_{O}\phi^{o}_{app}$ for each polyanion shifted to positive potentials in accord with Eq. 2-3, showing that the transfer potentials of the polyanions were influenced to some extent by the ion pairing.

Table 2-2.
Apparent standard ion transfer potentials for the polyanion transfer at the DCE/W interface for several concentrations of the organic base electrolyte

No.	Ion	$\lvert z\rvert/n^{2/3}$	$\Delta^{W}_{O}\phi^{o}_{app}$/V			
			0.02 M	0.05 M	0.1 M	0.2 M
1	α-$[PMo_{12}O_{40}]^{3-}$	0.256	0.520	0.529	0.531	0.534
2	α-$[SiMo_{12}O_{40}]^{4-}$	0.342	0.357	0.367	0.371	0.373
3	α-$[P_2Mo_{18}O_{62}]^{6-}$	0.383	0.310	0.311	0.313	0.312
4	$[Mo_6O_{19}]^{2-}$	0.281	0.435	0.444	0.450	0.454
5	$[VMo_5O_{19}]^{3-}$	0.421	0.196	0.205	0.207	0.208

2.4. Discussion

In Fig. 2-3 the values of $\Delta_o^w \phi^\circ_{app}$ obtained for the DCE/W system are plotted against the quantity $|z|/n^{2/3}$ mentioned in Chapter I at various concentrations of the organic base electrolyte. As can be seen in the figure, despite the large differences in size, charges, and even structures, the plot gave a straight line at each base electrolyte concentration. It should be noted that the slope of each straight line was almost the same. This means that there were no marked differences in the effect of ion pairing between the polyanions tested. Accordingly, it can be assumed that the change in $\Delta_o^w \phi^\circ_{app}$ with $|z|/n^{2/3}$ corresponds to that in the "true" ion transfer potential, i.e. $\Delta_o^w \phi^\circ$. Thus a linear dependence of $\Delta_o^w \phi^\circ$ on $|z|/n^{2/3}$, i.e.

$$\Delta_o^w \phi^\circ = -(1.781\pm0.023)|z|/n^{2/3} + \text{const} \qquad (2\text{-}6)$$

is confirmed in the DCE-W system. As mentioned in Chapter I, a similar dependence was found in the NB-W system.

Using Eq. 2-1 and 1-3, the following equation is obtained:

$$\Delta_o^w \phi^\circ = \Delta_o^w \phi^\circ(\text{el}) + \Delta_o^w \phi^\circ(\text{non-el}) \qquad (2\text{-}7)$$

with

$$\Delta_o^w \phi^\circ(\text{el}) = -\Delta G_{tr}^{\circ,\, o\to w}(\text{el})/zF \qquad (2\text{-}8)$$

$$\Delta_o^w \phi^\circ(\text{non-el}) = -\Delta G_{tr}^{\circ,\, o\to w}(\text{non-el})/zF. \qquad (2\text{-}9)$$

Thus $\Delta_o^w \phi^\circ$ must involve the non-electrostatic contribution $\Delta_o^w \phi^\circ(\text{non-el})$. The non-electrostatic term of the resolvation energy $\Delta G_{tr}^{\circ,\, o\to w}(\text{non-el})$ is generally recognized as a solvophobic interaction or the energy of a cavity formation in solvent. Several formulae have been proposed for the theoretical calculation of the cavity formation energy [55,62]. Volkov and coworkers [47,57] successfully employed the semiempirical Uhlig formula [62]

$$\Delta G_{tr}^{\circ,\, o\to w}(\text{non-el}) = 4\pi N_A r^2 \sigma_{o,w} \text{sgn}(\sigma_o - \sigma_w) \qquad (2\text{-}10)$$

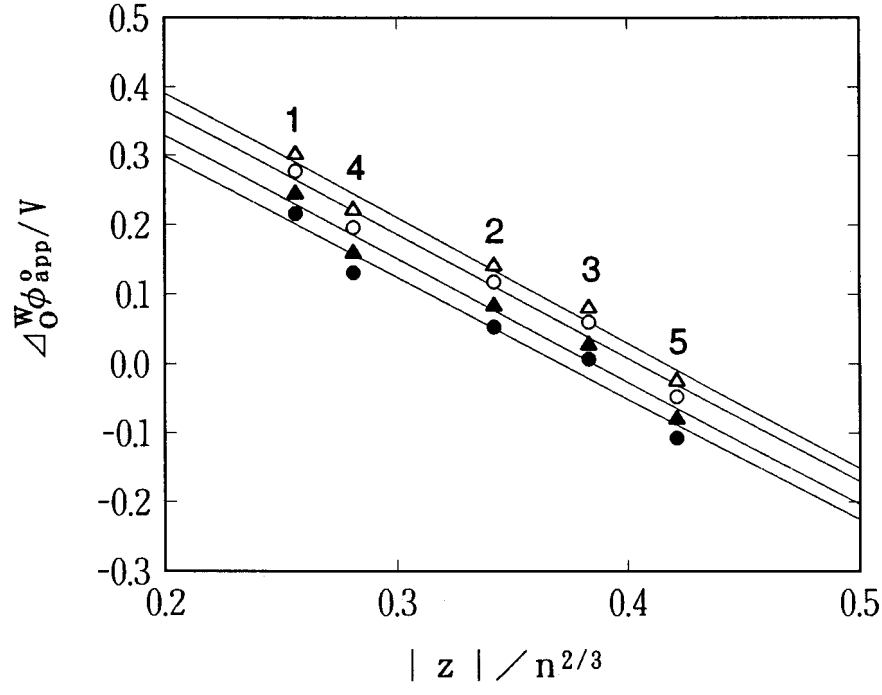

Fig. 2-3. Plots of $\Delta_O^W\phi^0_{app}$ for (1) α-$[PMo_{12}O_{40}]^{3-}$, (2) α-$[SiMo_{12}O_{40}]^{4-}$, (3) α-$[P_2Mo_{18}O_{62}]^{6-}$, (4) $[Mo_6O_{19}]^{2-}$, and (5) $[VMo_5O_{19}]^{3-}$ at the DCE/W interface against $|z|/n^{2/3}$ for several concentrations c^O of the organic base electrolyte : ● 0.02 M ; ▲ 0.05 M ; ○ 0.1 M ; △ 0.2 M.

to evaluate the solvophobic contribution to the resolvation energy of large cations. In this formula, $\sigma_{o,w}$ is the interfacial tension at the plane interface between two solvents, σ_o and σ_w are the surface tensions at the boundaries of solvents O and W respectively with air, and

$$\mathrm{sgn}(\sigma_o - \sigma_w) = \begin{cases} +1 & \sigma_o > \sigma_w \\ -1 & \sigma_o < \sigma_w \end{cases}$$

The Uhlig formula may be valid for $\sigma_{o,w} > 10$ mN m^{-1} and $r > 0.2$ nm [47,57,62]. Since the present system satisfies these requirements, the author tentatively employed the Uhlig formula with 27.9 mN m^{-1} [63] to estimate $\Delta_o^w \phi^\circ$(non-el) expressed by Eq. 2-9. In the application of this formula, the values of r were obtained using the simple relation r(in nm) = $0.164n^{1/3}$, as the value of r for $[SiW_{12}O_{40}]^{4-}$ with n=40 is known to be 0.56 nm [43]. In Fig. 2-4, together with linear plot of $\Delta_o^w \phi^\circ$ against $|z|/n^{2/3}$ (represented by $\Delta_o^w \phi^\circ_{app}$ at c° = 0.1 M), the "relative" change of $\Delta_o^w \phi^\circ$(el) is shown by plotting the values of $\Delta_o^w \phi^\circ_{app} - \Delta_o^w \phi^\circ$(non-el). As can be seen, both $\Delta_o^w \phi^\circ$(el) and $\Delta_o^w \phi^\circ$(non-el) depend linearly on $|z|/n^{2/3}$.

$$\Delta_o^w \phi^\circ(\mathrm{el}) = -1.241(|z|/n^{2/3}) + \mathrm{const'}$$

Although the data are not shown here, a similar conclusion has been confirmed for the NB-W system (see Chapter I).

Thus it is apparent that the "electrostatic" part of $\Delta_o^w \phi^\circ$ for the polyanion transfer depends linearly on $|z|/n^{2/3}$:

$$\Delta_o^w \phi^\circ(\mathrm{el}) = -a(|z|/n^{2/3}) + b \qquad (2\text{-}11)$$

where a and b are constants which are independent of z and n (or r). By using relation 1-3, $\Delta G_{tr}^{o;\, o\to w}$(el) can be expressed as

$$\Delta G_{tr}^{o;\, o\to w}(\mathrm{el}) = -aF(z^2/n^{2/3}) + bzF \qquad (2\text{-}12)$$

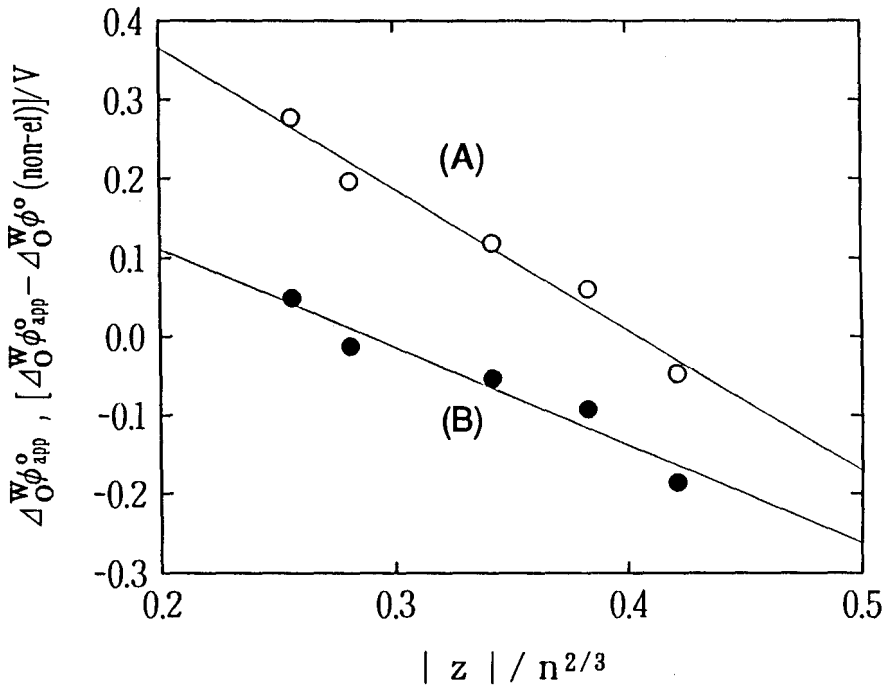

Fig. 2-4. Plots of (A) $\Delta_O^W\phi^o_{app}$ and (B) $\Delta_O^W\phi^o_{app} - \Delta_O^W\phi^o$(non-el) against $|z|/n^{2/3}$ at c^o = 0.1 M: (1) α-$[PMo_{12}O_{40}]^{3-}$, (2) α-$[SiMo_{12}O_{40}]^{4-}$, (3) α-$[P_2Mo_{18}O_{62}]^{6-}$, (4) $[Mo_8O_{19}]^{2-}$, and (5) $[VMo_5O_{19}]^{3-}$.

In this way $\Delta G^{o}_{tr}{}^{o\rightarrow w}$(el) depends linearly on $1/n^{2/3}$ and, consequently, on $1/r^2$. Such a dependence on ion size conflicts with the Bornian (long-range) electrostatic solvation energy which should depend on 1/r [49]. In the author's opinion, such a non-Bornian solvation energy can be explained in terms of the short-range interactions of an ion with solvent molecules in its immediate vicinity (i.e. donor-acceptor effects or hydrogen bonds) (see Chapter I). It follows that $\Delta G^{o}_{tr}{}^{o\rightarrow w}$(el) or $\Delta {}^{w}_{o}\phi^{o}$(el) should be recognized, not as an "electrostatic" interaction, but as a "chemical" interaction.

CHAPTER III

Formation Equilibrium of Heteropolymolybdates in Aqueous Solutions[d)]

3.1. Introduction

A variety of heteropoly- and isopolyoxometalates have been prepared from aqueous solutions, and accordingly their formation equilibrium has been studied by various spectrophotometric and electrochemical techniques. [1,2] However, solution equilibria are rather complex, since more than one complex is mostly present in equilibrium, and complexes may undergo rapid (or slow) exchange, particularly in aqueous solutions. Moreover, the solute species do not necessarily bear a structural relationship to materials that can be crystallized from such solutions. In spite of a wide variety of available techniques, such complexity of polyoxometalate solutions makes it difficult to identify solute species. Consequently, further development of the techniques seems still desirable.

For the case of heteropolymolybdate anions containing pentavalent heteroatoms, viz., X = P or As, the aqueous P-Mo system has been most extensively studied using various techniques; polarography [64], voltammetry [14], equilibrium analysis by combined potentiometric-spectrophotometric titration [65-69], large-angle X-ray scattering [70], Raman [71,72], UV [73,74], and ^{31}P NMR [75-77] spectroscopies, etc. The existence of some major species, viz., $[P_2Mo_5O_{23}]^{6-}$, $[P_2Mo_{18}O_{62}]^{6-}$, $[PMo_{12}O_{40}]^{3-}$, has been confirmed by many authors, however, their formation conditions are still not fully understood. The existence of lacunary (defect) Keggin anions, $[PMo_{11}O_{39}]^{7-}$ and $[PMo_9O_{34}]^{9-}$, and their formation conditions are controversial. Furthermore, only little is known about the ill-defined species, e.g. $[PMo_{10}O_{34}]^{3-}$ and $[P_2Mo_2O_{13}]^{4-}$.

There have been only two reports on aqueous As-Mo solutions. On the basis of spectrophotometric, polarographic, and potentiometric studies, Contant [66,67] has concluded that the major species are

$[As_2Mo_6O_{26}]^{6-}$, $[As_2Mo_{17}O_{61}]^{10-}$, $[As_2Mo_{18}O_{62}]^{6-}$, and $[H_4As_4Mo_{12}O_{48}]^{4-}$. Pettersson [68,69], using emf and spectrophotometric measurements, proposed the different species, $[As_2Mo_5O_{23}]^{6-}$, $[As_2Mo_6O_{26}]^{9-}$, and $[AsMo_6O_{34}]^{9-}$.

For the case of aqueous molybdate systems containing tetravalent heteroatoms, X=Si and Ge, it is well known that the $XMo_{12}O_{40}^{4-}$ anions are quite stable in the aqueous solution [78-82]. Regarding heteropolyanions other than the Keggin anions, however, their formation equilibria have not been established. Although some authors [83,84] have suggested the existence of a lacunary Keggin anion XMo_{11} at higher pH(>4) values, there is only one report [85] describing neither of satisfactory synthetic procedures and identification.

Thus many questions about the aqueous heteropolymolybdate equilibria have remained unanswered. This may be attributed not only to the complexity of the equilibria but also to the difference in the conditions (primarily, heteroanion and molybdate concentrations); some spectroscopic methods including Raman and NMR, though promising for the identification of the complex species existing in higher concentrations (usually $\geq$ 0.01 M), are somewhat difficult to apply to dilute solutions, with which such electrochemical methods as voltammetry can treat.

As mentioned in Chapter I, the transfer of certain heteropoly- and isopoly anions across the NB/W interface can be examined by ion-transfer voltammetry. A moderately hydrophobic or semi-hydrophobic (or hydrophilic) polyanion in Table 1-1 (Chapter I) gives a voltammetric wave owing to the transfer across on ITIES. The voltammetric current is proportional to the concentration of the polyanion in aqueous (or nonaqueous) phase, while the potential at which the voltammetric wave appears is characteristic of the nature of the polyanion. Here, the author has applied this technique to the identification of polyanions formed in dilute X-Mo (X = Si, Ge, P, and As) solutions, and the results have been discussed on the basis of the hydrophobicity scale of polyanions proposed in Chapter I.

3.2. Experimental

Chemicals

Stock solutions of 0.1 M $NaH_2PO_4 \cdot 2H_2O$, 0.1 M $Na_2HAsO_4 \cdot 7H_2O$, and 0.2 M $Na_2MoO_4 \cdot 2H_2O$, and standard silicon and germanium solutions (Wako) (1000 ppm each) were used to prepare test aqueous solutions, which also contained 0.05 M $MgCl_2$ and 0.5 M $MgSO_4$ as supporting electrolytes. The pH of each test solution was adjusted as a manner similar to that described in Chapter I. Unless otherwise noted, test aqueous solutions were prepared within 1 day before use.

TBA^+ salt of 11-molybdogermanate(IV)

The TBA^+ salt of $[H_4GeMo_{11}O_{39}]^{4-}$ was prepared and characterized as follows:

A 0.9 g quantity of GeO_2 was suspended in a 200 ml solution of 7.2 g $Na_2MoO_4 \cdot 2H_2O$. Conc. HCl was added slowly with stirring at 80 ℃ until complete dissolution. After cooling, the solution was diluted to about 300 ml and the pH of the solution was adjusted to 5.7 with solid Li_2CO_3. The solution was stored at 4 ℃ for 1 day, and then a pale yellow precipitate was formed by adding 3.5 g of TBABr to the solution with vigorous stirring. These precipitates were collected by filtration, washed successively with H_2O, ethanol, and acetone and then dried at 50 ℃. The result of elemental analysis was:

Calcd for $(TBA)_4[H_4GeMo_{11}O_{39}]$:

Mo, 38.72; Ge, 2.66; C, 28.20; H, 5.47; N, 2.06%.

Found:

Mo, 38.79; Ge, 2.67; C, 28.92; H, 5.56; N, 2.05%.

In Fig. 3-1, the IR spectrum is shown together with those of the crystals of α-$(TBA)_4[GeMo_{12}O_{40}]$ [86] and β-$(TBA)_4[GeMo_{12}O_{40}]$ [87], prepared according to the reported methods. Their prominent bands(cm^{-1}) were as follows:

$(TBA)_4[H_4GeMo_{11}O_{39}]$:

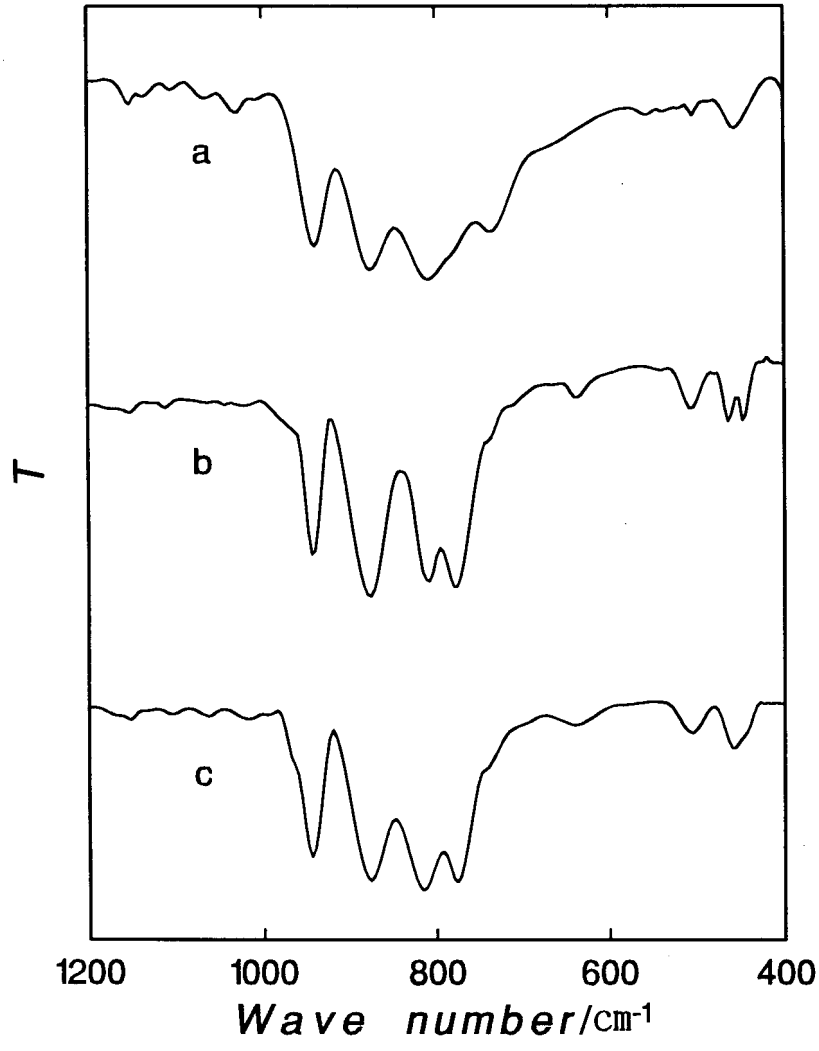

Fig. 3-1. IR spectra of (a) $TBA_4H_4[GeMo_{11}O_{39}]$, (b) α-$TBA_4[GeMo_{12}O_{40}]$, and (C) β-$TBA_4[GeMo_{12}O_{40}]$ in the KBr pellets.

939(vs), 878(vs), 812(vs), 775(sh), 737(s), 505(vw), 458(w)

α-$(TBA)_4[GeMo_{12}O_{40}]$:

943(vs), 873(vs), 810(vs), 780(vs), 640(vw), 506(w), 464(w), 449(w)

β-$(TBA)_4[GeMo_{12}O_{40}]$:

944(vs), 875(vs), 814(vs), 777(vs), 639(vw), 504(w), 460(w)

Except for the the characteristic band at 737 cm^{-1}, the IR spectrum of $(TBA)_4[H_4GeMo_{11}O_{39}]$ was similar to those of the Keggin anions (especially to the β-type isomer). This seems that the isolated $[H_4GeMo_{11}O_{39}]^{4-}$ anion has a structure related to the Keggin anion [88,89] (for example, see Fig. 3-2).

In contrast to the similarity of the IR spectra, the redox behavior was quite different from those of the Keggin anions as shown in Fig. 3-3. Cyclic voltammograms of the Keggin anions in CH_3CN {(b) and (c)} give a two-step reversible wave [e] as shown in Fig. 3-3. However, successive irreversible waves similar to those of $[H_3PMo_{11}O_{39}]^{4-}$ [77] were observed for $[H_4GeMo_{11}O_{39}]^{4-}$ {curve (a)}. The voltammogram of $[H_4GeMo_{11}O_{39}]^{4-}$ was found to change gradually with time in CH_3CN. Since voltammogram (b) shown in Fig. 3-4 is somewhat similar to that of α-$[GeMo_{12}O_{40}]^{4-}$, it can be considered that $[H_4GeMo_{11}O_{39}]^{4-}$ is converted into an α-Keggin anion in CH_3CN. This is supported by the fact that α-$(TBA)_4[GeMo_{12}O_{40}]$ is precipitated upon recrystallization of $(TBA)_4[H_4GeMo_{11}O_{39}]$ from CH_3CN.

Sodium salt of 9-molybdophosphate(V)

The crystals of $Na_3H_6PMo_9O_{34}\cdot xH_2O$ were obtained as follows:

A solution of 0.69 g $NaH_2PO_4\cdot 2H_2O$ and 9.7 g $Na_2MoO_4\cdot 2H_2O$ in 200 ml water was acidified with conc. HCl so that the pH became 1.0, and then kept for crystallization at room temperature. After two weeks of evaporation, yellowish crystals were obtained; during the evaporation (until the crystals started to form), the pH of the solution was held at 1.0 by dropping conc. NaOH solution sometimes. The crystals obtained were washed with ethanol and air-dried at room temperature. The content of water was determined by TG-DTA; the result found here was x =

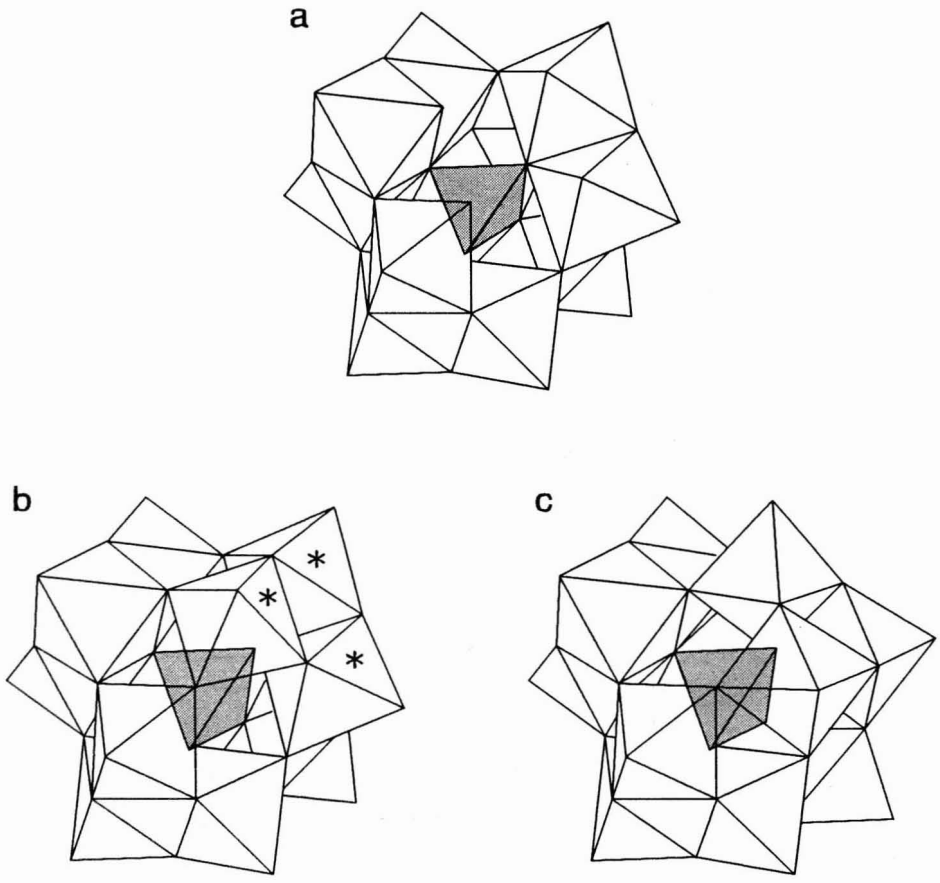

Fig. 3-2. Polyhedral representations of the structure, (a) α-XM_{11}, (b) α-XM_{12}, and (C) β-XM_{12}.

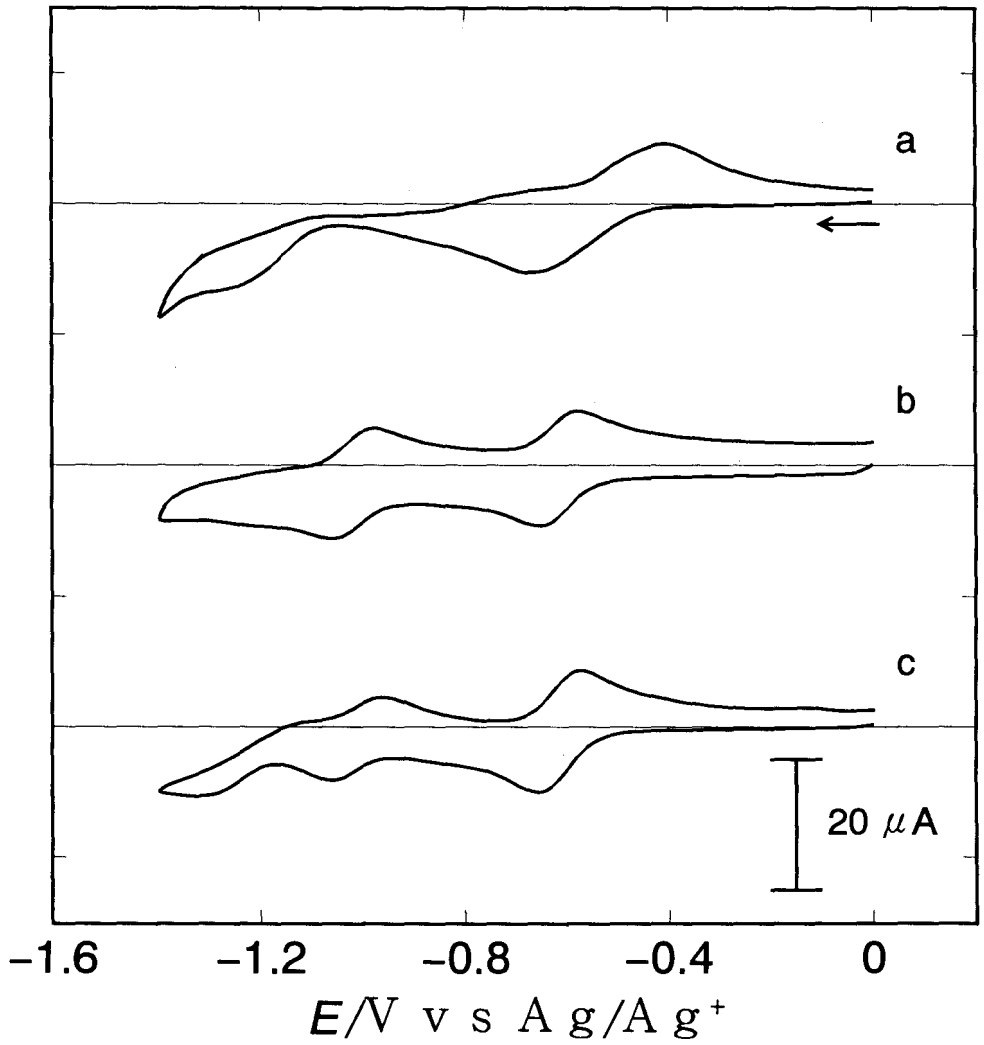

Fig. 3-3. Conventional cyclic voltammograms at a GC electrode of 1mM of (a) $[H_4GeMo_{11}O_{39}]^{4-}$, (b) α-$[GeMo_{12}O_{40}]^{4-}$, and (c) β-$[GeMo_{12}O_{40}]^{4-}$ in CH_3CN. Scan rate : 0.1 V s^{-1}. Supporting electrolyte : 0.05 M $TBAClO_4$.

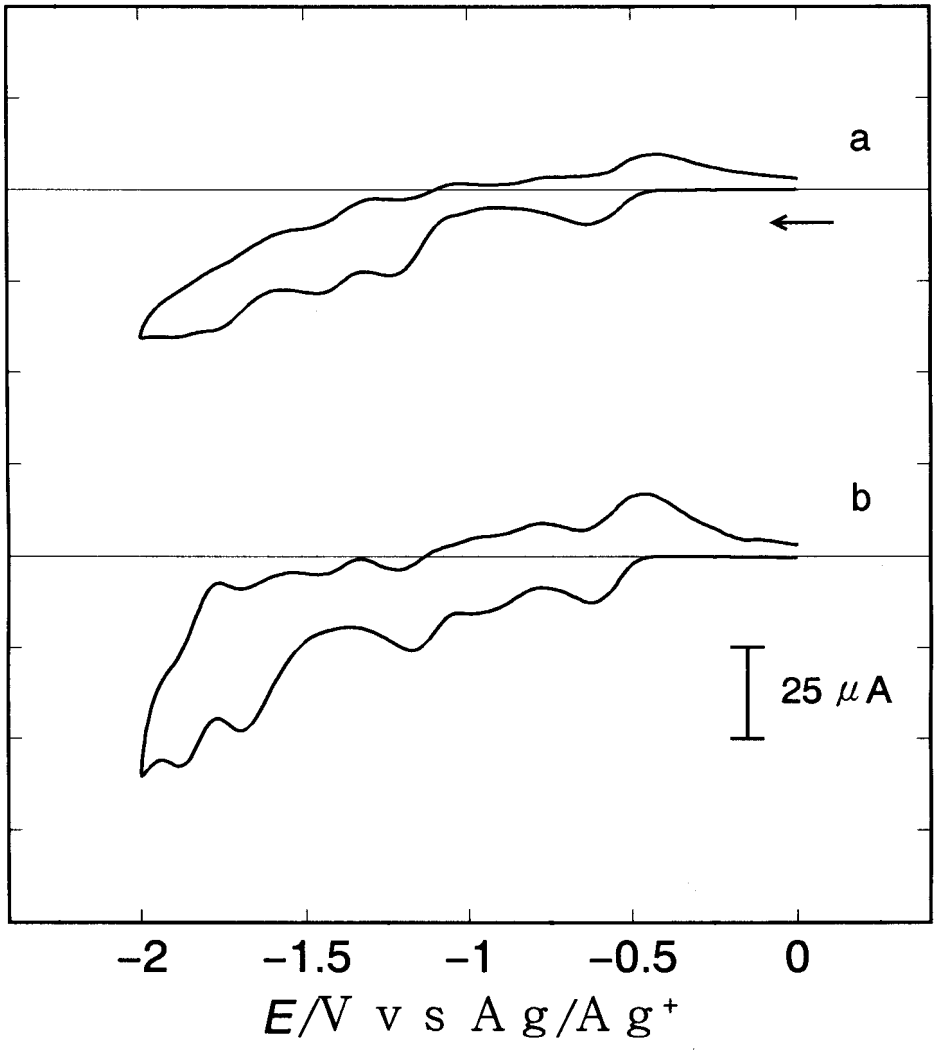

Fig. 3-4. Conventional cyclic voltammograms recorded (a) immediately after addition of TBA^+ salt of $[H_4GeMo_{11}O_{39}]^{4-}$ to the CH_3CN solution so that the concentration became 1 mM and (b) after one day. Scan rate : 0.1 V s^{-1}. Supporting electrolyte : 0.05 M $TBAClO_4$.

11.2 (lit. [90], x = 12-13). The result of elemental analysis was:

Calcd for $Na_3H_6PMo_6O_{34}\cdot 11.2H_2O$: Na, 4.0; P, 1.8; Mo, 50.3%.

Found: Na, 4.0; P, 1.8; Mo, 50.7%.

The IR spectrum of the crystals was in agreement with that of the crystals prepared according to Strandberg's method [90], 1062(vs), 1009(s), 963(vs), 940(vs), 927(vs), 910(vs), 854(vs), 786(vs), 721(s), 597(w), 519(w) cm^{-1}.

The preparation and characterization of the TBA^+ salt of 11-molybdophosphate, $(TBA)_4[H_3PMo_{11}O_{39}]$, were described previously. [32]

TBA+ salt of dodecamolybdotetraarsenate(V)

The TBA^+ salt of $[H_4As_4Mo_{12}O_{50}]^{4-}$ was prepared according a procedure similar to the reported method [91].

A 4.2 g quantity of MoO_3 was added to a solution of 5 g of a 60%(w/w) H_3AsO_4 solution and 5 ml of 13 M HNO_3 in 50 ml water. The suspension was heated to 50 ℃. Fifty ml of an aqueous 30% H_2O_2 solution was added slowly with stirring to yield a yellow supernatant solution. In order to achieve the decomposition of the peroxo compounds formed, the solution was stored on a water bath (~ 80 ℃) until no further O_2 evolution was observed. The entire reaction mixture was then cooled to 0 ℃ and filtered. To the pale yellow filtrate, 3.5 g of TBABr was added. The resulting white precipitate was filtered off and washed successively with water, ethanol, and acetone.

As shown in Fig 3-5, the IR spectrum of the salt was in agreement with that of tetraammonium dodecamolybdotetraarsenate(V) tetrahydrate prepared according to Sasaki's [92] method :

$(NH_4)_4[H_4As_4Mo_{12}O_{52}]\cdot 4H_2O$:

985(m) , 957(vs), 926(vs), 871(vs), 799(s), 581(vs), 488(w) /cm^{-1}.

$(TBA)_4[H_4As_4Mo_{12}O_{52}]\cdot 4H_2O$:

980(sh), 949(s), 920(sh), 876(vs), 788(s), 581(s), 475(w) /cm^{-1}.

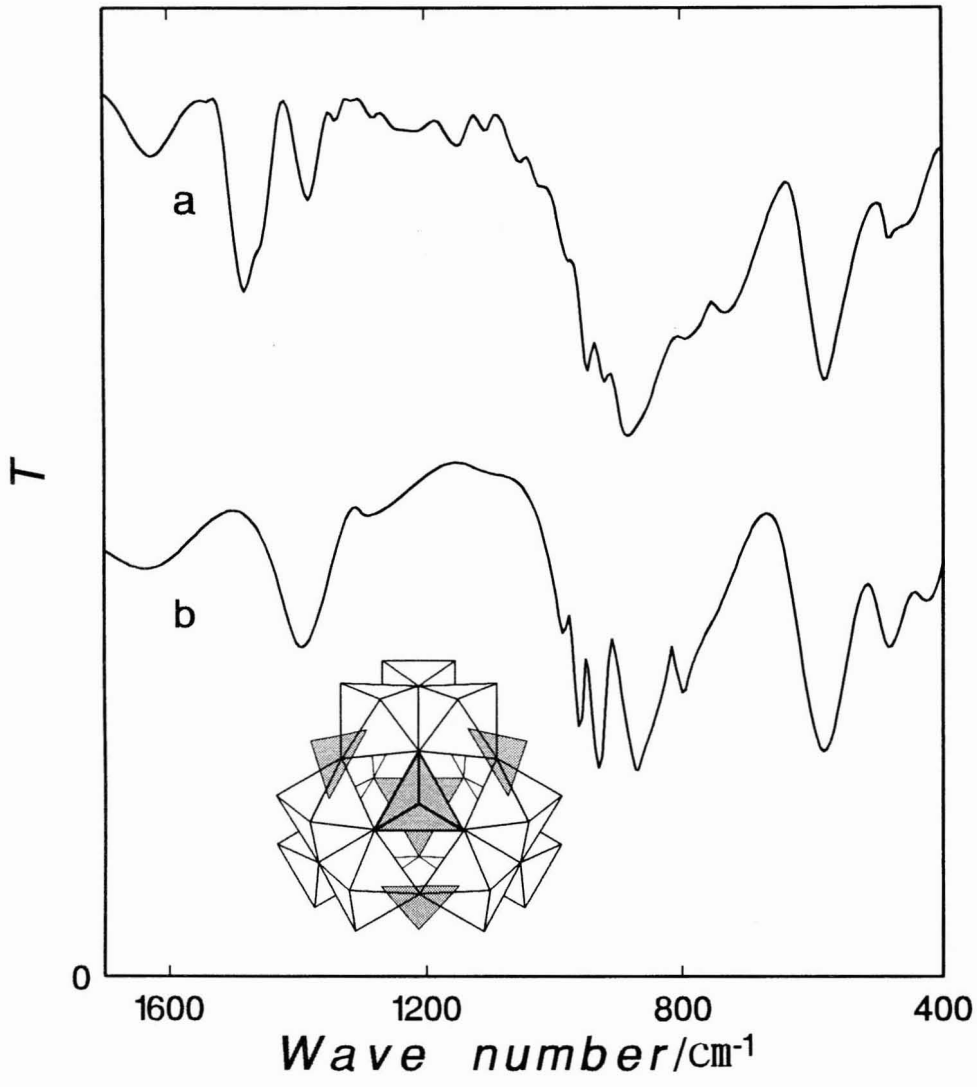

Fig. 3-5. IR spectra of (a) $TBA_4H_4As_4Mo_{12}O_{50}$ and (b) $(NH_4)_4H_4As_4Mo_{12}O_{50}$ in the KBr pellets.

TBA$^+$ salt of 10-molybdoarsenate(V)

A solution of 0.62 g $Na_2HAsO_4 \cdot 7H_2O$ and 4.8 g $Na_2MoO_4 \cdot 2H_2O$ in 100 ml water was acidified with conc. HCl so that the pH became 3.0, and then a pale yellow precipitate was formed by adding 2.7 g of TBABr to the solution with vigorous stirring. These precipitates were collected by filtration, washed successively with H_2O, ethanol, and acetone, and then dried at 50 ℃. The result of elemental analysis was:

Calcd for $(TBA)_4[H_5AsMo_{10}O_{37}]$:

Mo, 36.65; As, 2.86; C, 29.37; H, 5.74; N, 2.14%.

Found:

Mo, 36.52; As, 2.80; C, 30.24; H, 5.95; N, 2.14%.

Ion-transfer voltammetric measurements

In studying the transfer of the heteropolymolybdate complexes formed in aqueous solutions, the following electrochemical cell was used:

with

I: 0.02 M TPnACl + 0.1 M $MgSO_4$ (W)

II: 0.1 M TPnATPB (NB)

III: 0.1 M TPnATPB (NB)

IV: test solution containing X and Mo (see above) (W)

V: 0.05 M $MgCl_2$ + 0.5 M $MgSO_4$ (W)

More details were mentioned above (section 1.2).

In the electrochemical measurements for the transfer of the isolated heteropolyanions, $[H_4GeMo_{11}O_{39}]^{4-}$, $[H_3PMo_{11}O_{39}]^{4-}$, $[H_2As_4Mo_{12}O_{50}]^{6-}$, and $[AsMo_{10}O_{38}]^{4-}$, the procedure described in section 1.2 was employed.

Conventional voltammetric measurements

Conventional voltammetric measurements with a glassy carbon(GC) electrode were also made by using the microcomputer-controlled system [39]. A Tokai glassy carbon rod (GC-30S) with a surface area of 7.1 mm^2 was used as a working electrode and a platinum wire served as the counter. The reference electrode was an Ag/AgCl electrode. The electrochemical cell was as follows:

Ag/AgCl (RE)	internal solution (same as phase V) (W)	test solution (same as phase IV) (W)	GC electrode (WE)

Before each measurement, the GC electrode was freshly polished with 0.25 μm diamond slurry and washed with distilled water in an ultrasonic field.

Measurements

UV spectra were recorded on a Hitachi 220-A spectrometer equipped with a constant temperature housing for the cell (path length, 1 mm). The contents of Na, Ge, and Mo were determined using a Shimadzu model ICPS-5000 inductively coupled argon plasma emission spectrometer. The determination of P was made by flow injection analysis. Arsenic was determined with a Hitachi high-performance liquid chromatograph (a Model L-6000 pump, a Model L-3720 conductivity detector, and a Model D-2500); the separation was performed with a Tosoh TSKgel IC-Anion-PW_{XL} column.

Unless otherwise noted, the electrochemical and spectrophotometric measurements were carried out at 25±0.1 ℃.

3.3 Results

3.3.1 Molybdosilicates(IV)

First the author will show the results obtained for [Mo] = 4.0 mM. Figure 3-6 represents the cyclic voltammograms at [Si] = 1.0 mM for the solutions of several pH values. Four cathodic (negative current) peaks marked I_c, II_c, A_c, and B_c were observed on the initial potential scan from 0.45 to 0.10 V. This means that four different polyanions transferred across the test interface from W to NB, according to the variation of interfacial potential difference. As seen in the figure, respective cathodic peaks were accompanied by anodic (positive current) peaks (I_a, II_a, A_a, and B_a) on the reversed potential scan, indicating that the polyanions returned to W reversibly. In the range of [Si] = 0.33 - 2.0 mM, no other voltammetric wave were observed.

The four voltammetric waves, each comprising a pair of cathodic and anodic peaks, may be treated as common reversible waves, although a few waves were distorted to some extent, possibly because of interconversion of polyanions in NB or at the NB/W interface [32].

In Fig. 3-7, the cathodic peak currents are plotted against pH and [Si] at [Mo] = 4.0 mM. According to a formal application of the theory of a reversible wave for an electron transfer at a stationary electrode, the cathodic peak currents should be proportional to the bulk concentrations of polyanions in W [38]. For this reason, the cathodic peak currents in Fig. 3-7 represent the distribution diagrams for species I and II. The curve at [Si] = 1.0 mM shows that almost all Mo(VI) take part in the formation of species I in the pH range 1.2 - 3.6, whereas species II is a minor species existing at around pH 4.5.

The pH dependence of the E_{mid}-value for the wave of species I in Fig. 3-6 is shown in Fig. 3-8 together with that of α-$[SiMo_{12}O_{40}]^{4-}$ [31], being obtained in the manner similar to that mentioned in Chapter I (note that α-$[SiMo_{12}O_{40}]^{4-}$ anion was dissolved in NB phase and the water phase contained neither germanate nor molybdate). Their plots coincided well with each other within experimental errors, which clearly demonstrates that species I is identified to be a Keggin anion.

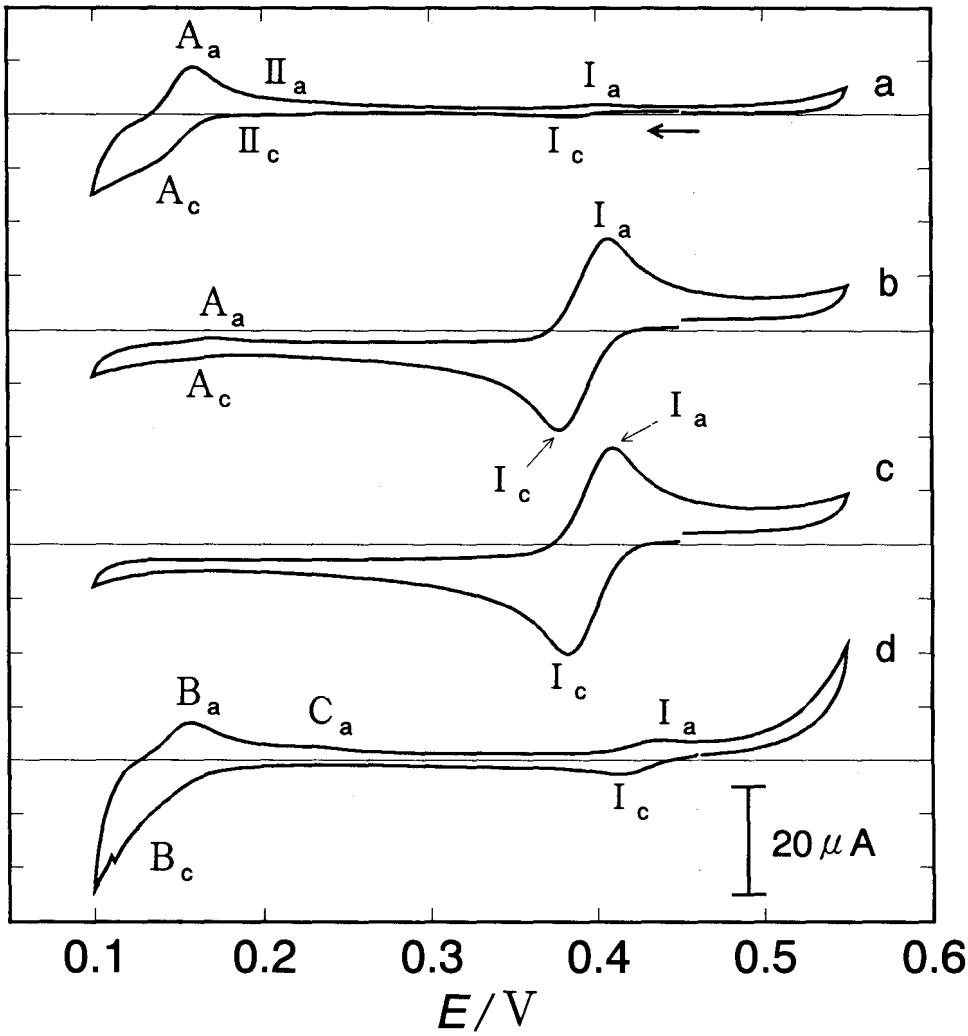

Fig. 3-6. Cyclic voltammograms for the transfer across the NB/W interface of the heteropoly- and isopolyanions formed in the W phase ([Si] = 1.0 mM and [Mo] = 4.0 mM). pH 4.5(a), 3.7(b), 2.3(c), and 1.0(d). Supporting electrolytes : 0.1 M TPnATPB in NB ; 0.05 M $MgCl_2$ + 0.5 M $MgSO_4$ in W. Scan rate : 0.02 V s^{-1}.

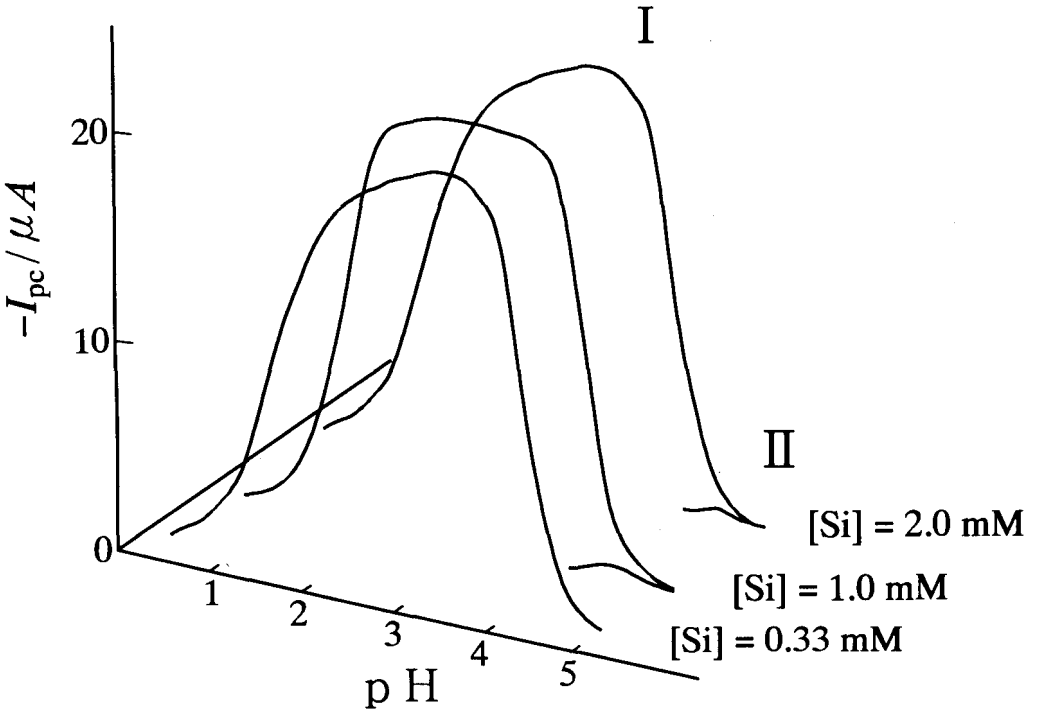

Fig. 3-7. Distribution diagrams for species I and II at [Mo] = 4.0 mM as a function of pH and [Si] using cathodic peak currents of the cyclic voltammograms as shown in Fig. 3-6.

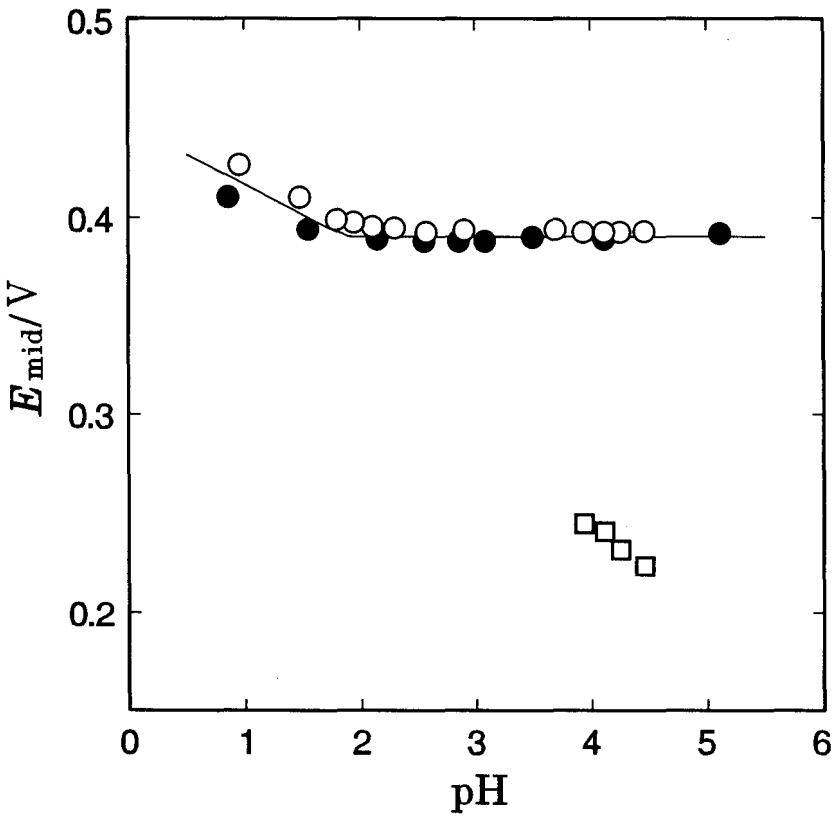

Fig. 3-8. pH dependences of the midpoint potentials for the transfer of (○) species Ⅰ, (●) $[SiMo_{12}O_{40}]^{4-}$, and (□) species Ⅱ.

The isolation of species II from the aqueous solutions was unsuccessful due to its poor stability. However, species II can be reasonably assumed to be a 11-molybdosilicate complex, $[H_3SiMo_{11}O_{39}]^{5-}$, since its ion-transfer potential in Fig 3-8 and the pH region in which it formed are accord with those of $[H_3GeMo_{11}O_{39}]^{5-}$ (see below, section 3.3.2), which is further supported by a similarity of kinetic behavior (mentioned below, Chapter IV).

Species A and B were found to be certain isopolyanions, because the waves owing to their transfer were observed even in the absence of the heteroanions as shown in Fig. 3-9. In the pH range 1.9-4.6, a well-developed reversible wave with cathodic and anodic peaks(A_c and A_a) was obtained. In Fig. 3-10, the currents for A_c are plotted against pH. The cathodic peak current was largest at pH 3.0. It is generally agreed that the dominant isopoly species at the pH is the heptamolybdate anion $[Mo_7O_{24}]^{6-}$ (Fig. 3-11) with protonated forms [93-96]. Figure 3-12 shows the pH dependence of the E_{mid}-value for the wave of species A. The E_{mid}-value was almost constant (0.173±0.003 V) in the pH range 1.9-3.3, whereas it shifted to more negative potentials at pH > 3.3. This shift can be elucidated by the protonation-deprotonation reaction of some protonated forms {the slope(V/pH) in such a pH range in Fig. 3-12 (= 0.025) is smaller than the theoretical value (= 0.059), since the buffer condition ($[H^+] \ll [HMo_7O_{24}]^{5-}$ or $[H^+] \gg [HMo_7O_{24}]^{5-}$) was not accomplished.};

$$[H_2Mo_7O_{24}]^{4-} \qquad \text{NB}$$

$$\text{——— } \Updownarrow \text{ ———————————————————————}$$

$$[H_2Mo_7O_{24}]^{4-} \rightleftharpoons [HMo_7O_{24}]^{5-} + H^+ \ (pKa = \sim 3.7). \ [93a] \qquad \text{W}$$

Consequently, it can be concluded that species A transfers across the interface as a diprotonated form: $[H_2Mo_7O_{24}]^{4-}$ in the pH range 1.9-3.3. The standard potential ${}^{W}_{NB}\Delta\phi^{\circ}$ and the standard Gibbs energy ΔG for the transfer of $[H_2Mo_7O_{24}]^{4-}$ at the NB/W interface were estimated to be -0.147 V and -57 kJ mol^{-1}, respectively, from the pH-independent E_{mid}-value. [30,31] The value of ${}^{W}_{NB}\Delta\phi^{\circ}$ was consistent with the value of -0.201 V calculated by Eq. 1.4.

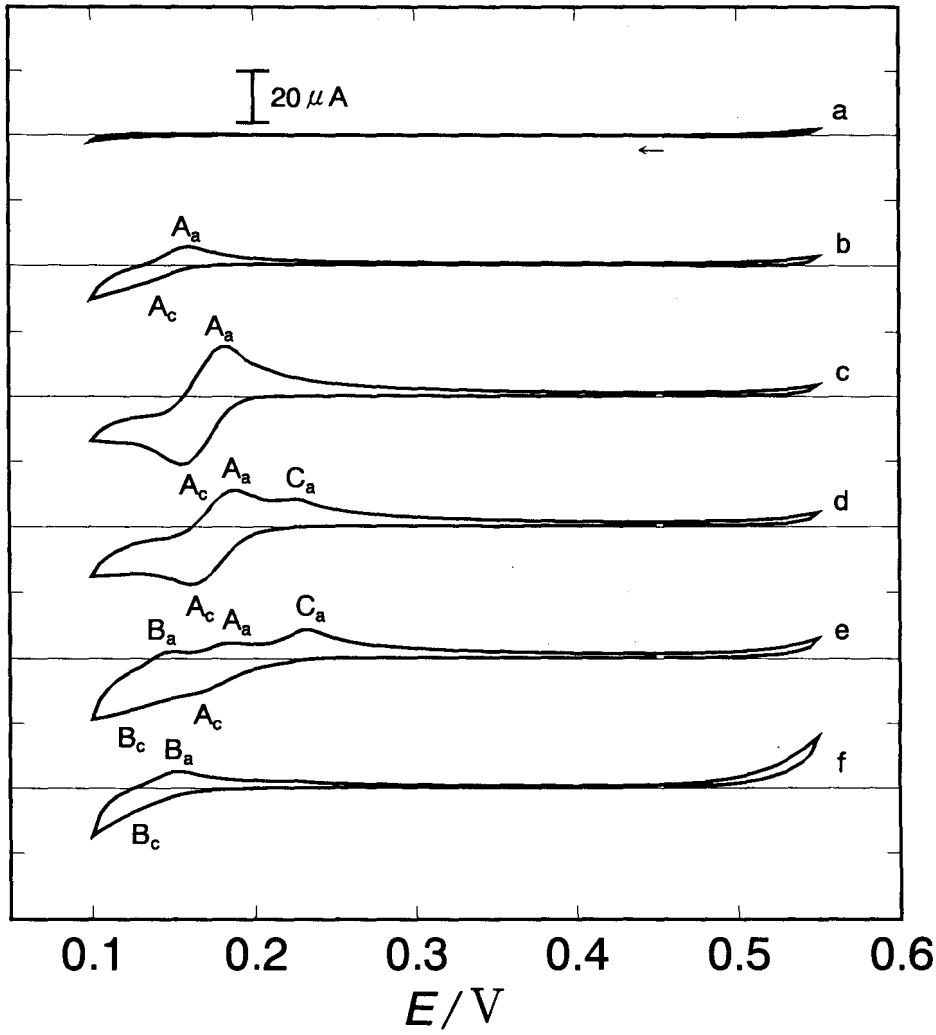

Fig. 3-9. Cyclic voltammograms for the transfer across the NB/W interface of the isopolyanions formed in the W phase ([Mo] = 4.0 mM). pH 5.3(a), 4.6(b), 3.0(c), 2.2(d), 1.7(e), and 0.9(f). Scan rate : 0.02 V s^{-1}.

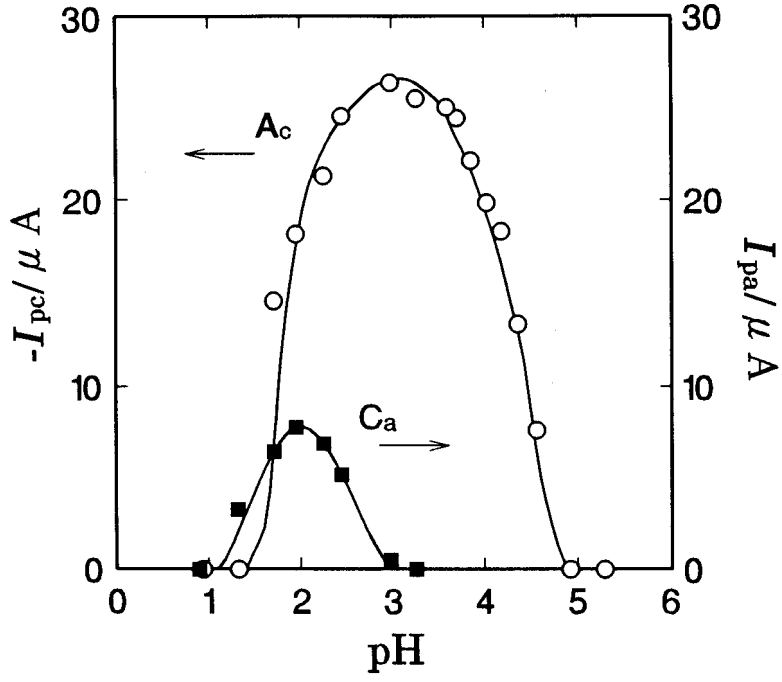

Fig. 3-10. pH dependences of (○) the cathodic peak current for the transfer of species A (A_c) and of (●) the anodic peak current of species C (C_a).

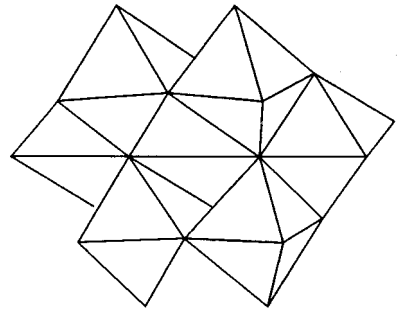

Fig. 3-11. Structure of heptamolybdate.

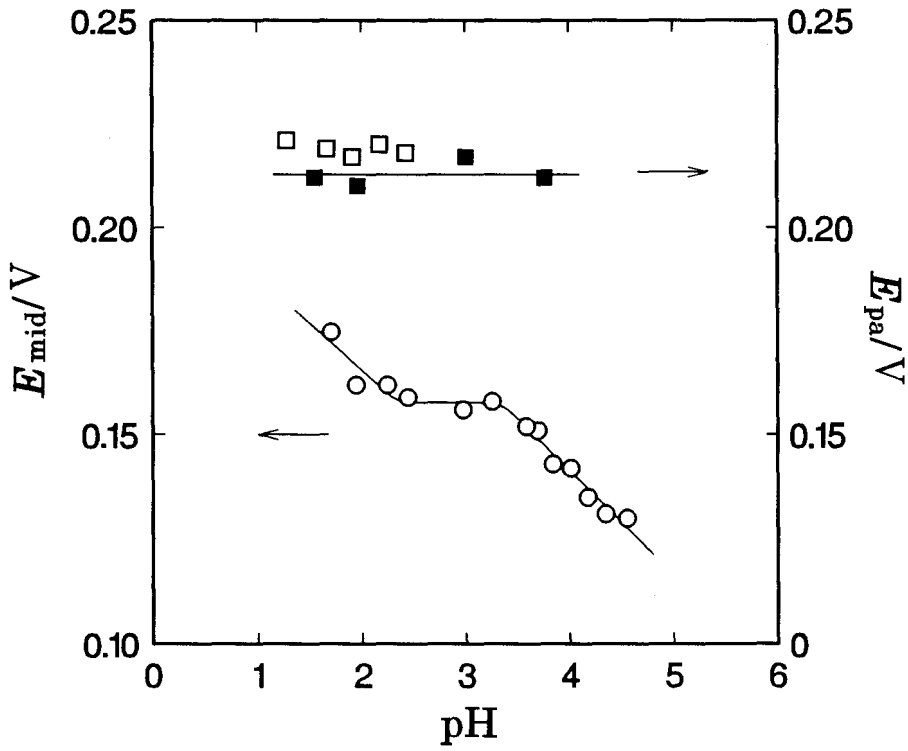

Fig. 3-12. pH dependences of the midpoint potential for the transfer of (○) species A and of the anodic peak potentials of (□) species C and (■) α-$[Mo_8O_{26}]^{4-}$ (cf. Capter Ⅰ).

When pH was lowered below 1.5, the wave of species A disappeared and another wave with cathodic and anodic peaks (B_c and B_a) was instead developed at a somewhat negative potential (~0.150 V; see Fig. 3-9), demonstrating the presence of another isopolyanion (species B) in the pH range 0.9-1.7. This species is not yet identified, but the author favours β-$[Mo_8O_{26}]^{4-}$ [95,97,98] or its related anion $[H_3Mo_8O_{28}]^{5-}$ [95,99], which has been claimed to exist in more acidic solutions than the heptamolybdate anion.

In the pH range of 0.9-2.2, there also appeared another anodic peak (C_a) at around 0.220 V on the reverse potential scan. Since no corresponding cathodic peak appeared on the initial potential scan, the anodic peak seemed to be ascribed to the transfer of a certain isopolyanion (species C) possibly generated by the rapid conversion of the species A and/or B in the NB phase or at the interface. Because the potential (0.215±0.008 V) of the anodic peak owing to the transfer of α-$[Mo_8O_{26}]^{4-}$ from NB to W (see Chapter I) coincides well with that of peak C_a, species C is supposed to be α-$[Mo_8O_{26}]^{4-}$. This may be supported by Klemperer and Shum's observation [37] that β-$[Mo_8O_{26}]^{4-}$ is transformed into the α-type in organic solvents.

Furthermore, another set of ion-transfer voltammetric measurements at [Si] = 0.33 mM was performed. No voltammetric waves other than those observed at [Mo] = 4.0 mM series were found. As a result of these measurements, the distribution diagram against pH and [Mo] is shown in Fig. 3-13. As seen in the distribution diagrams shown in Fig. 3-7 and Fig. 3-13, the peak height of species II (at around pH 4.5) is much less than that of species I (at around pH 2.3) at any [Si] and [Mo] conditions. It can be said that pH is a dominant factor for the formation of molybdosilicate complexes in the aqueous Si-Mo system.

In the present study, the presence of two heteropolyanions, $[H_3SiMo_{11}O_{39}]^{5-}$ and $[SiMo_{12}O_{40}]^{4-}$, as well as two isopolyanions $[H_2Mo_7O_{24}]^{4-}$ and β-$[Mo_8O_{26}]^{4-}$(?), has been confirmed in acidic aqueous solutions and described on the following scheme.

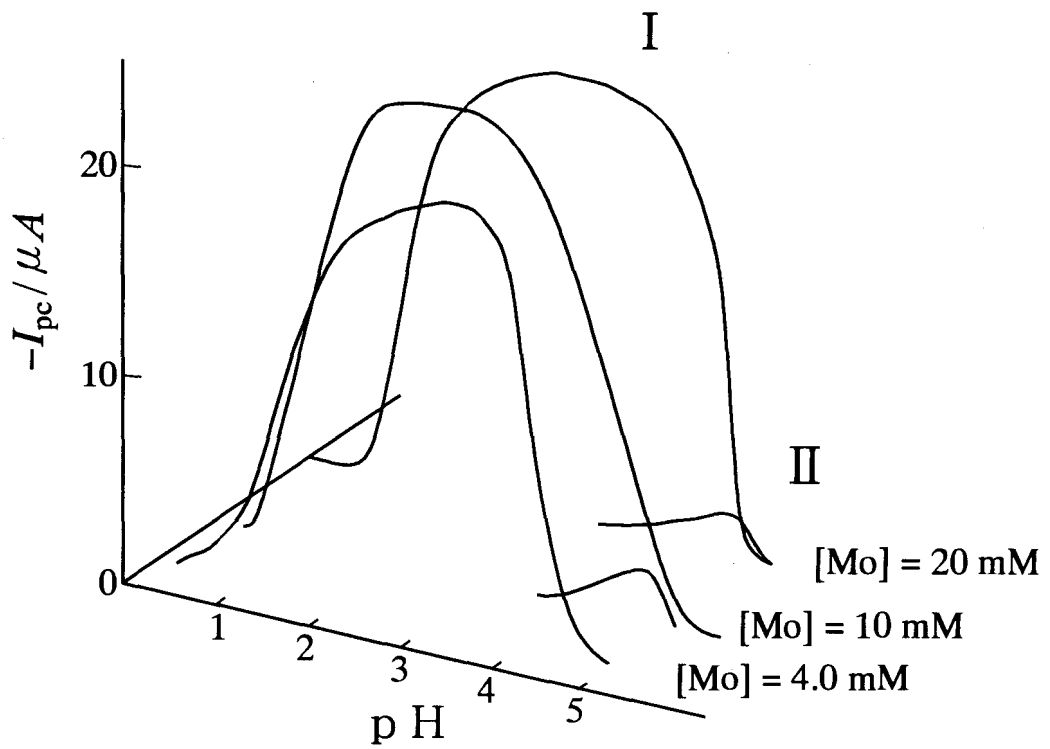

Fig. 3-13. Distribution diagrams for species I and II at [Si] = 0.33 mM as a function of pH and [Mo].

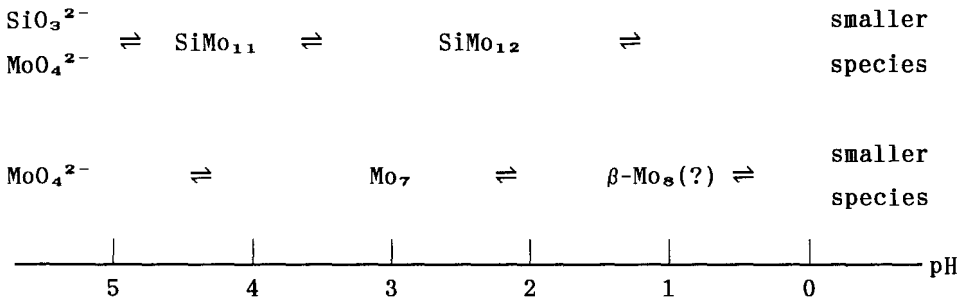

Scheme 3-1. Scheme for the formation of heteropoly- and isopolyanions in the aqueous silicate-molybdate system. $SiMo_{11}$, $SiMo_{12}$, Mo_7, and β-Mo_8 represent 11-molybdosilicate, 12-molybdosilicate, heptamolybdate and β-octamolybdate, respectively.

3.3.2 Molybdogermanates(IV)

Figure. 3-14 shows the cyclic voltammograms at [Ge] = 1.0 mM and [Mo] = 4.0 mM. Under certain conditions {for example, see curve (b)}, three voltammetric waves, each comprising a pair of cathodic (I_c, II_c, and A_c) and anodic (I_a, II_a, and A_a) peaks, were obtained, indicating that at least three complex species (I, II, and A) were formed in W phase. With a lowering of scan rate, IIa became smaller compared with II_c, and simultaneously Ia became larger. This can be elucidated by the transformation from species II into species I at the NB/W interface. (cf. Chapter IV) Since species A is the isopolyanion , $[H_2Mo_7O_{24}]^{4-}$ (cf. section 3.3.1), species I and II may be heteropolyanions. No voltammetric waves due to the transfer of other heteropoly species were observed at any set of [Ge] and [Mo]. Figure. 3-15 shows the pH dependence of the E_{mid} for the wave of species I together with that of α-$[GeMo_{12}O_{40}]^{4-}$ [31], which clearly demonstrates that species I is the Keggin anion.

The distribution diagram against pH and [Ge] at [Mo] = 4.0 mM is shown in Fig. 3-16, whereas the distribution diagram against pH and [Mo] at [Ge] = 0.33 mM is also shown in Fig. 3-17. From these diagrams, the formations of these species were found to be optimum at pH 2.2 and pH 3.4 for species I and species II respectively.

By consulting the diagrams, the heteropolymolybdate complex responsible for species II was isolated as the TBA^+ salt, which was identified to be $TBA_4[H_4GeMo_{11}O_{39}]$. (see Experimental.) Immediately after adding the salt to the NB phase, cyclic voltammograms at the NB/W interface (note that the W-phase contained neither germanate nor molybdate) were recorded at various pH values ($[H_4GeMo_{11}O_{39}]^{4-}$ anion transformed into the keggin-type anion even in the bulk of NB). As a typical example, a cyclic voltammogram obtained at pH 3.5 is shown in Fig. 3-18. In Fig. 3-15, the E_{mid} for 11-molybdogermanate is plotted against pH together with that for species II obtained from the voltammograms in Fig 3-14. Their plots coincided well with each other within the experimental errors. The E_{mid}-value was almost constant (0.235±0.005 V) in the pH range 2.4-3.6. The value of $\Delta_{NB}^{W}\phi^{\circ}$, being

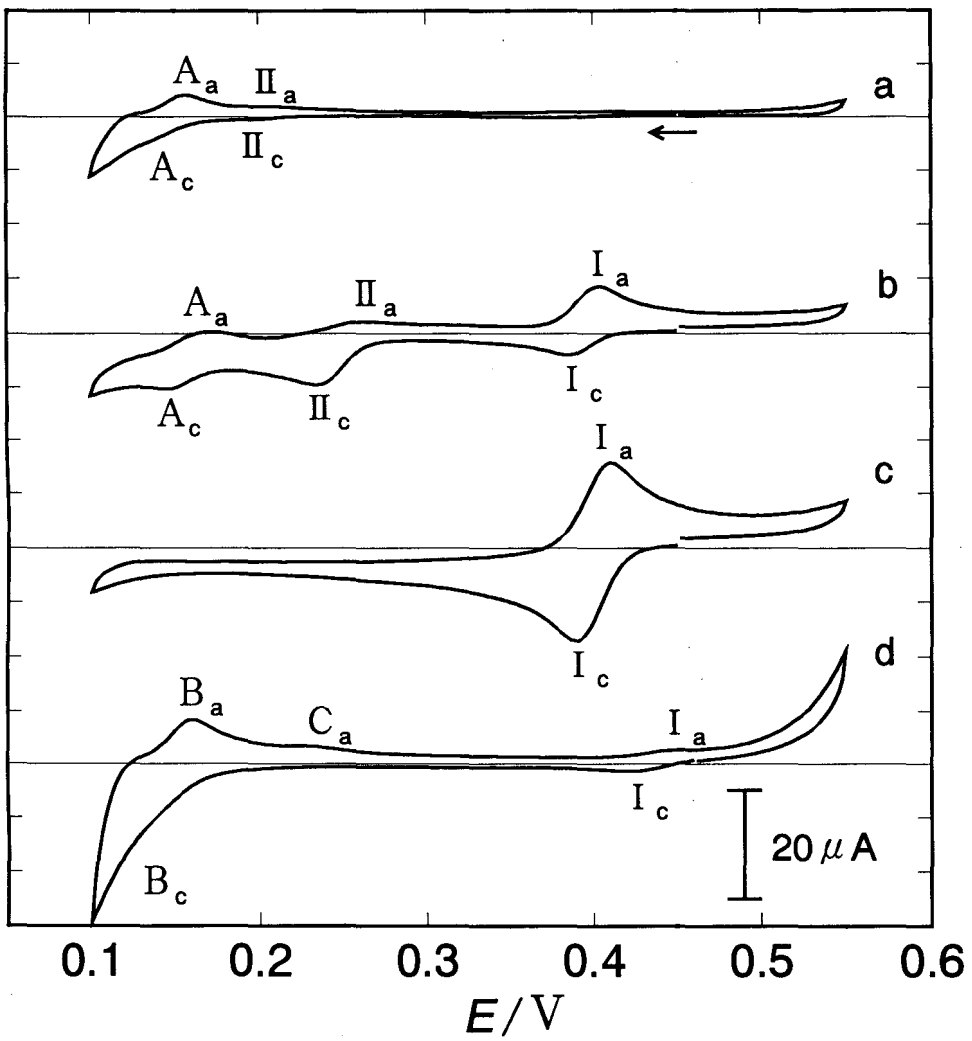

Fig. 3-14. Cyclic voltammograms for the transfer across the NB/W interface of the heteropoly- and isopolyanions formed in the W phase ([Ge] = 1.0 mM and [Mo] = 4.0 mM). pH 4.4(a), 3.6(b), 2.1(c), and 1.0(d). Scan rate : 0.02 V s^{-1}.

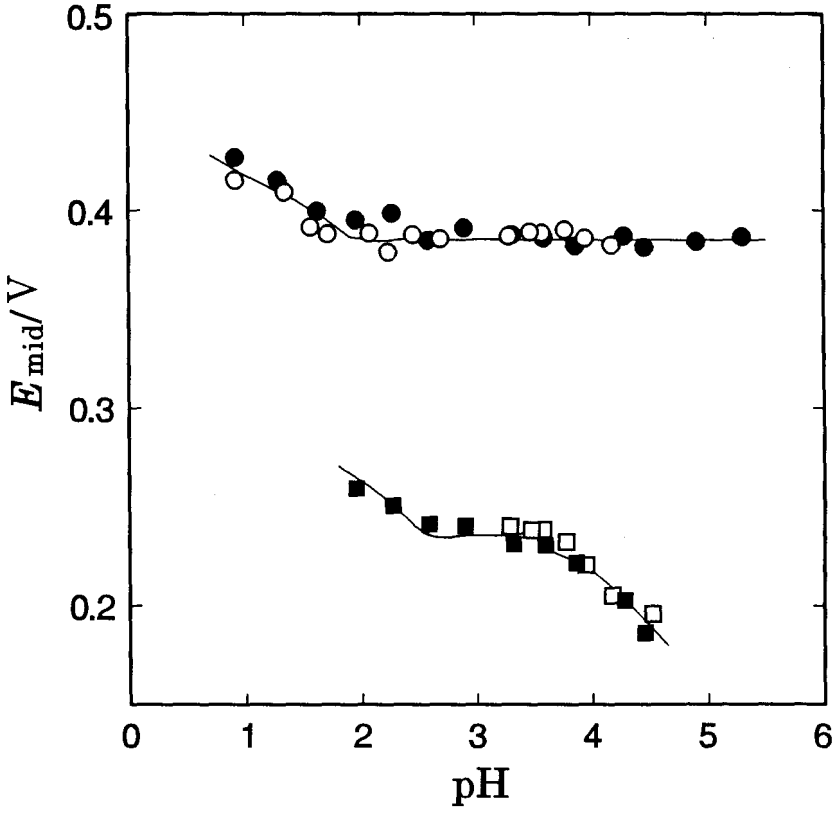

Fig. 3-15. pH dependences of the midpoint potentials for the transfer of (○) species Ⅰ, (□) species Ⅱ, (●) $[GeMo_{12}O_{40}]^{4-}$, and (■) $[H_3GeMo_{11}O_{39}]^{5-}$.

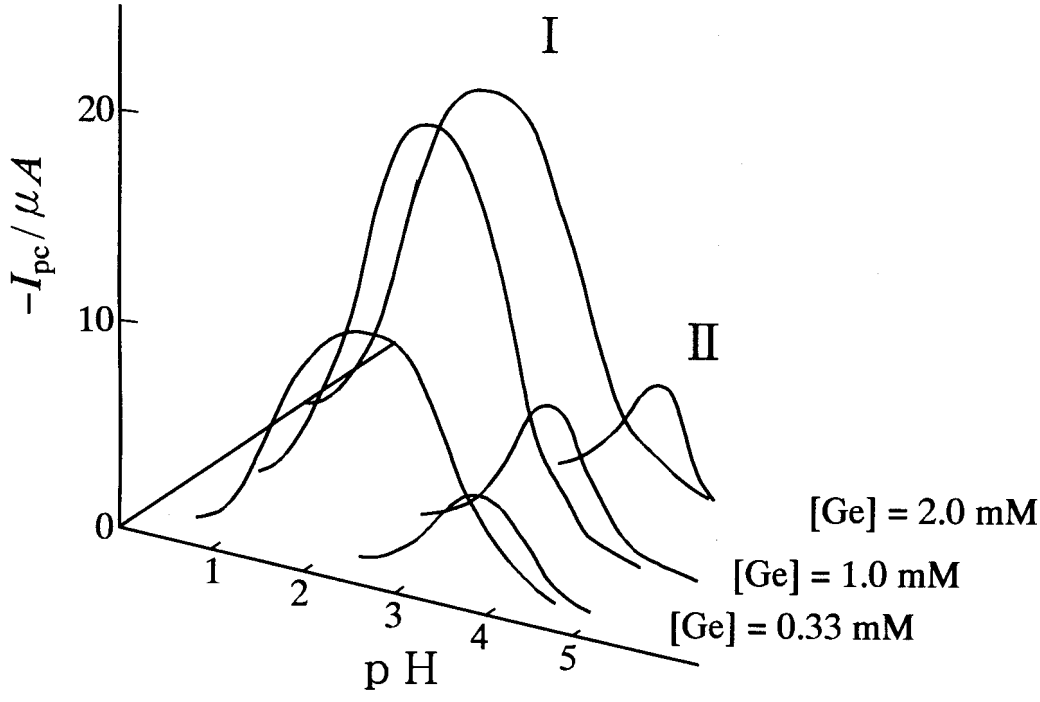

Fig. 3-16. Distribution diagrams for species I and II at [Mo] = 4.0 mM as a function of pH and [Ge].

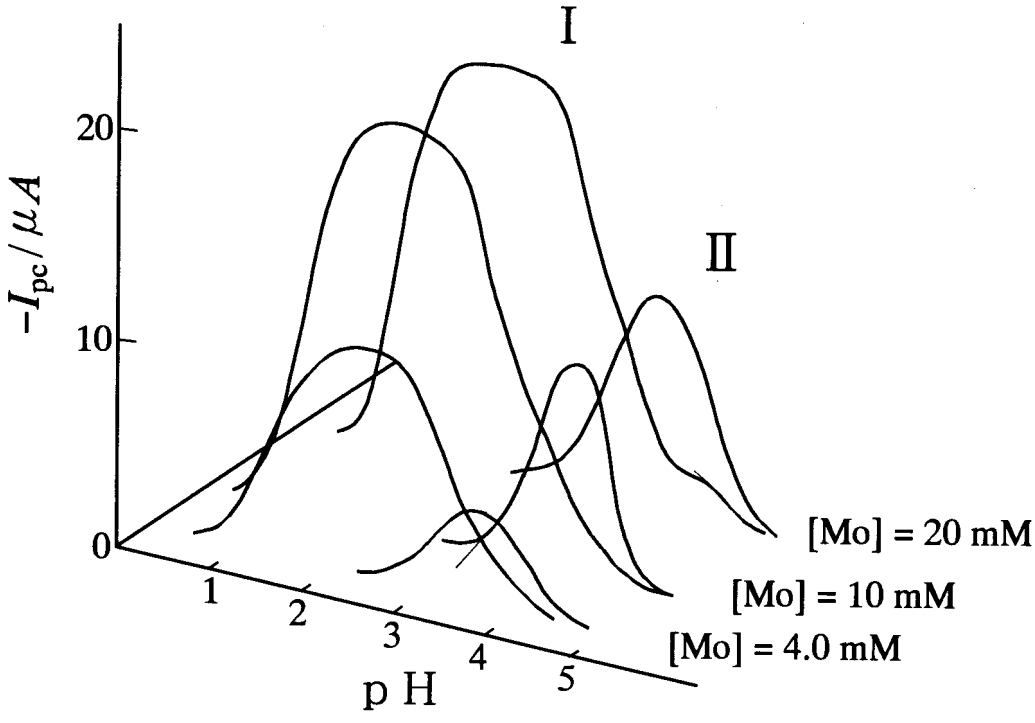

Fig. 3-17. Distribution diagrams for species I and II at [Ge] = 0.33 mM as a function of pH and [Mo].

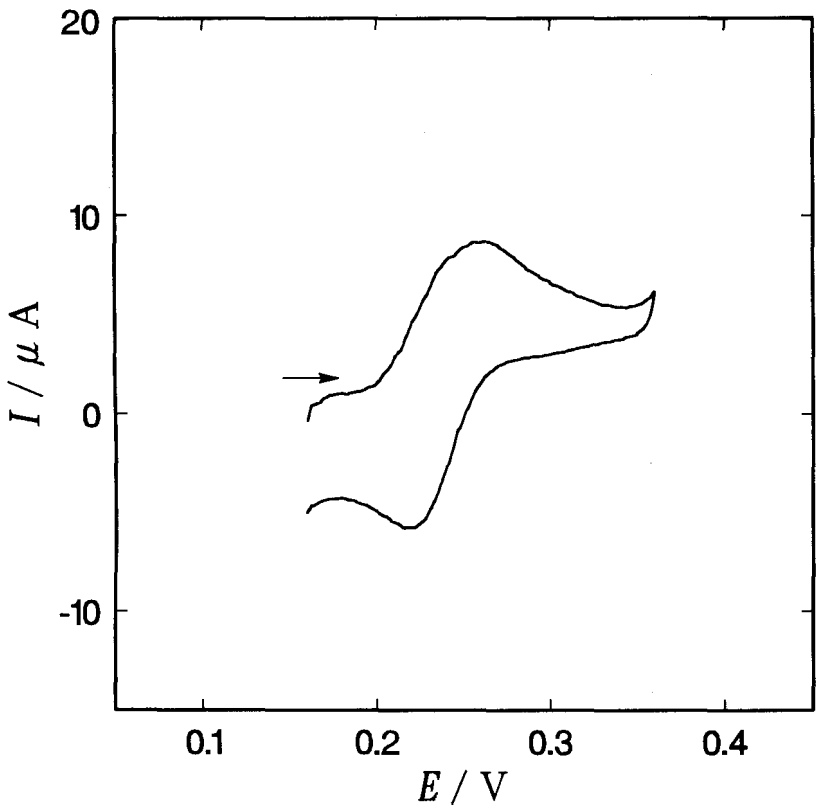

Fig. 3-18. Cyclic voltammograms of the NB/W(pH 3.5) interface in the presence of 0.5 mM $TBA_4[H_4GeMo_{11}O_{39}]$ in NB. Scan rate : 0.02 V s^{-1}.

estimated to be -0.086 V from the pH-independent E_{mid}, was consistent with the value of -0.112 V calculated for $[H_3GeMo_{11}O_{39}]^{5-}$ using Eq. 1.4. These facts illustrate that species II in the aqueous solution is identified to be a lacunary Keggin anion, $[H_3GeMo_{11}O_{39}]^{5-}$, in the pH range 2.4-3.6. On the other hand, the E_{mid}-value shifted to more negative potentials at pH > 3.6. This shift is due to the protonation preceding a transfer of species II (cf. 3.3.1).

$[H_3GeMo_{11}O_{39}]^{5-}$ NB

$\Downarrow$

$[H_3GeMo_{11}O_{39}]^{5-} \rightleftharpoons [H_2GeMo_{11}O_{39}]^{6-} + H^+$ W(pH > 3.6)

In the present study, the presence of two heteropolyanions, $[H_3GeMo_{11}O_{39}]^{5-}$ and $[GeMo_{12}O_{40}]^{4-}$, has been confirmed in acidic aqueous solutions and described on the following scheme.

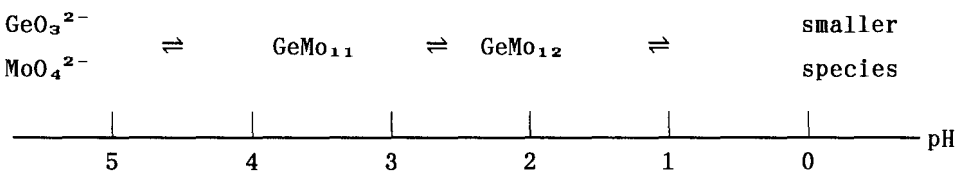

Scheme 3-2.

Scheme for the formation of heteropolyanions in the aqueous germanate-molybdate system. $GeMo_{11}$ and $GeMo_{12}$, represent 11-molybdogermanate and 12-molybdogermanate, respectively.

3.3.3 Molybdophosphates(V)

In Figures 3-19 and 3-20 are shown cyclic voltammograms at [P] = 1.0 mM and [Mo] = 4.0 mM and the distribution diagrams against pH and [P] at [Mo] = 4.0 mM, respectively. Species A and B were found to be isopolyanions as mentioned above (cf. 3.3.1.).

In order to identify species I, the following experiment was performed: First, a yellow heteropolyanion $[H_3PMo_{11}O_{39}]^{4-}$, which formed in an aqueous solution at pH 3.1 as shown in Fig. 3-20, was isolated as the TBA^+ salt [32]. By adding the salt to the NB phase, cyclic voltammograms were recorded at various pH values. Cyclic voltammograms obtained at three different pH values are shown in Fig. 3-21. On the initial potential scan, a well-developed anodic peak due to the transfer of the heteropolyanion from NB to W was observed at any scan rate. However, the cathodic peak on the reverse potential scan was small compared with the anodic peak, especially at lower scan rates. This can be explained by a partial decomposition of the anion in W. The previous study [32] showed that the anion transfers across the interface as a tetravalent anion, i.e. $[H_3PMo_{11}O_{39}]^{4-}$, at pH 3.1. However, the transfer process seems to be affected by protonation (or deprotonation) reactions of the anion in W and/or NB, since the transfer potential was changed by pH as seen in Fig. 3-19. In Fig. 3-22 is plotted against pH the midpoint potential E_{mid} together with that for species I in Fig. 3-19. Their plots coincided well with each other within the experimental errors, which clearly demonstrates that species I is a lacunary Keggin anion $[H_3PMo_{11}O_{39}]^{4-}$.

In contrast to species I, the identification of species II was unsuccessful because the species could not be isolated. Nevertheless, it can be said that species II is neither of the Keggin anion $[PMo_{12}O_{40}]^{3-}$ and the Dawson anion $[P_2Mo_{18}O_{62}]^{6-}$, because the Keggin anion gives a voltammetric wave in the polarizable potential range [31], and the Dawson anion gives a voltammetric wave at more positive potential than species II [33].

As seen in the results at a lower [P]/[Mo] ratio([P] = 0.33 mM and [Mo] = 20 mM) in Fig. 3-23 and Fig. 3-24 , no distinct wave for species

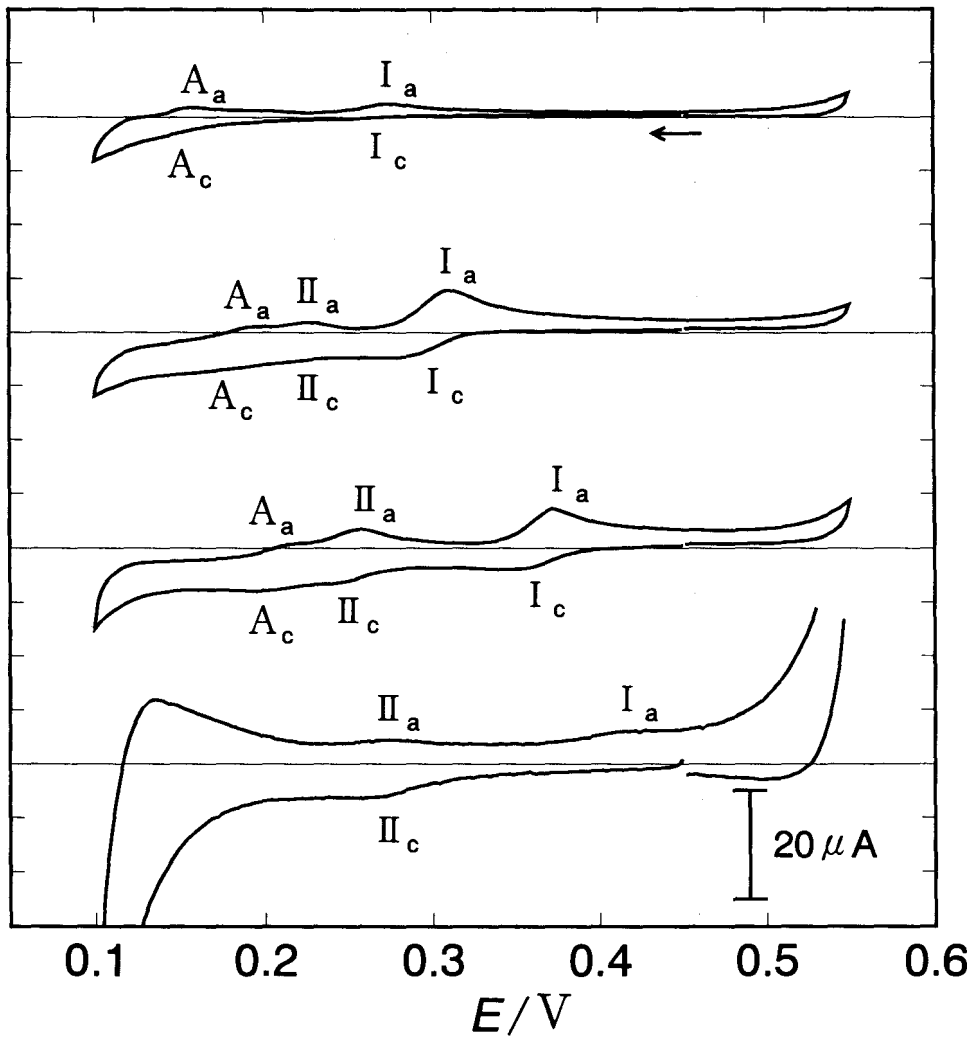

Fig. 3-19. Cyclic voltammograms for the transfer across the NB/W interface of the heteropoly- and isopolyanions formed in the W phase ([P] = 1.0 mM and [Mo] = 4.0 mM). pH 4.3(a), 3.4(b), 2.1(c), and 0.9(d). Scan rate : 0.02 V s^{-1}.

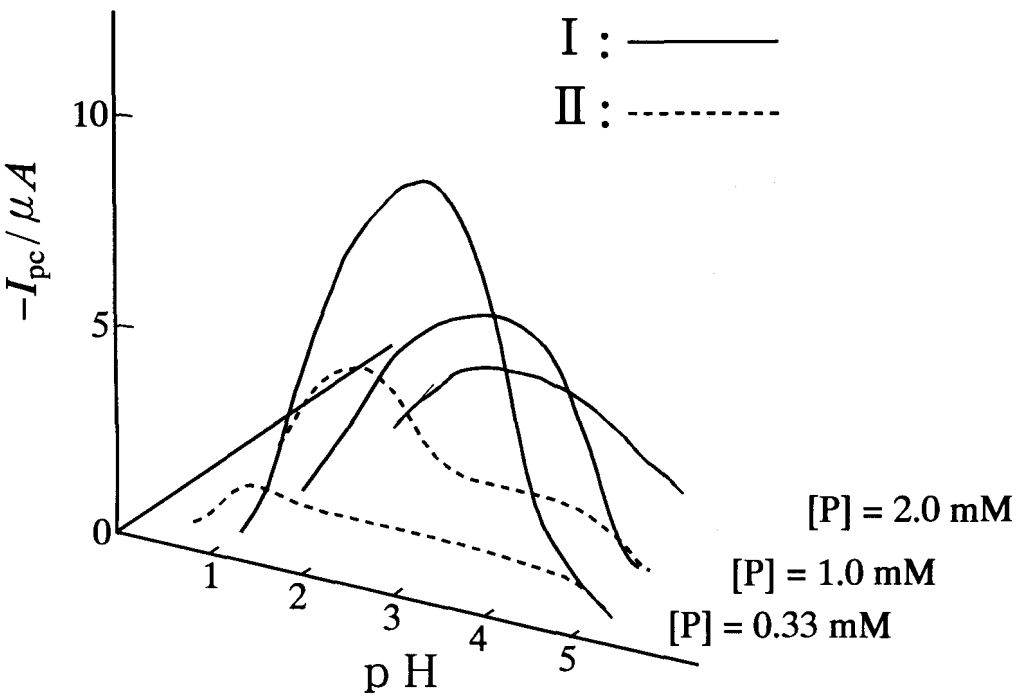

Fig. 3-20. Distribution diagrams for species I and II at [Mo] = 4.0 mM as a function of pH and [P].

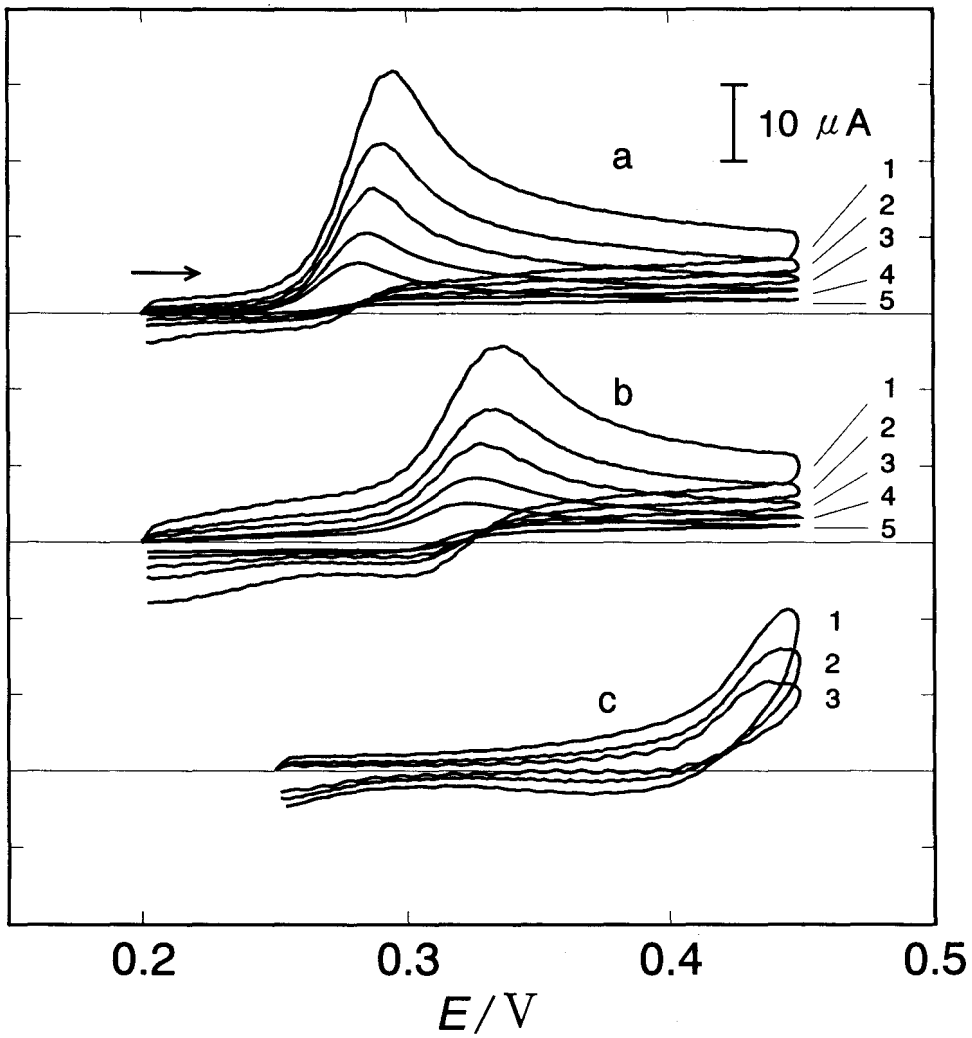

Fig. 3-21. Cyclic voltammograms for the transfer of $[H_3PMo_{11}O_{39}]^{4-}$ across the NB/W interface at pH 4.2(a), 3.3(b), and 0.5(c). The NB phase contained 0.2 mM $TBA_4[H_4PMo_{11}O_{39}]$. Scan rates : (1) 0.4, (2) 0.2, (3) 0.1, (4) 0.05, and (5) 0.02 V s^{-1}.

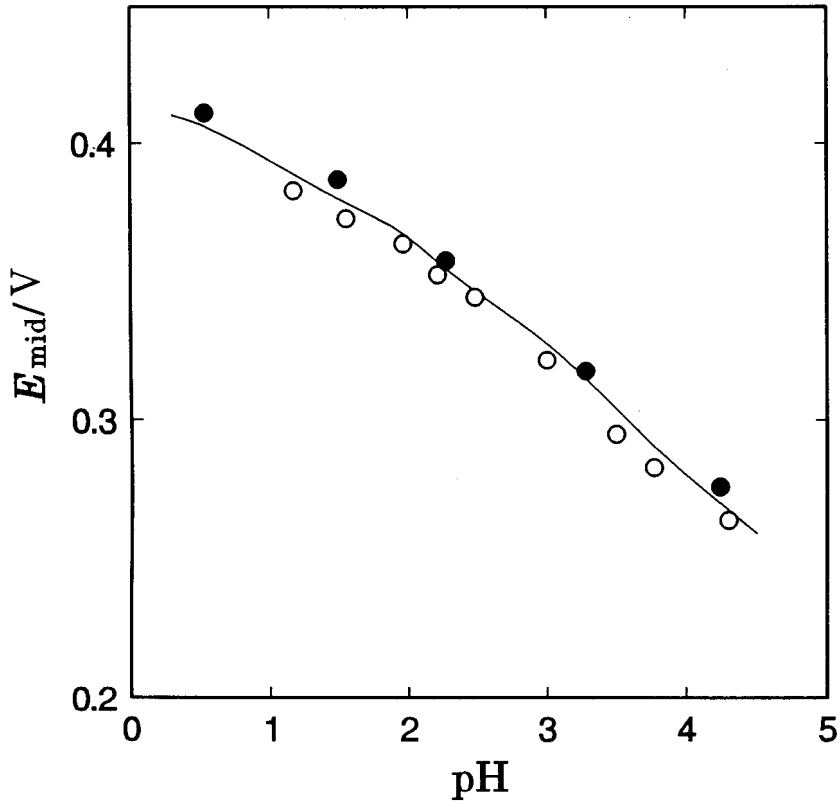

Fig. 3-22. pH dependences of the midpoint potentials for the transfer of (○) species I and (●) $[H_3PMo_{11}O_{39}]^{4-}$.

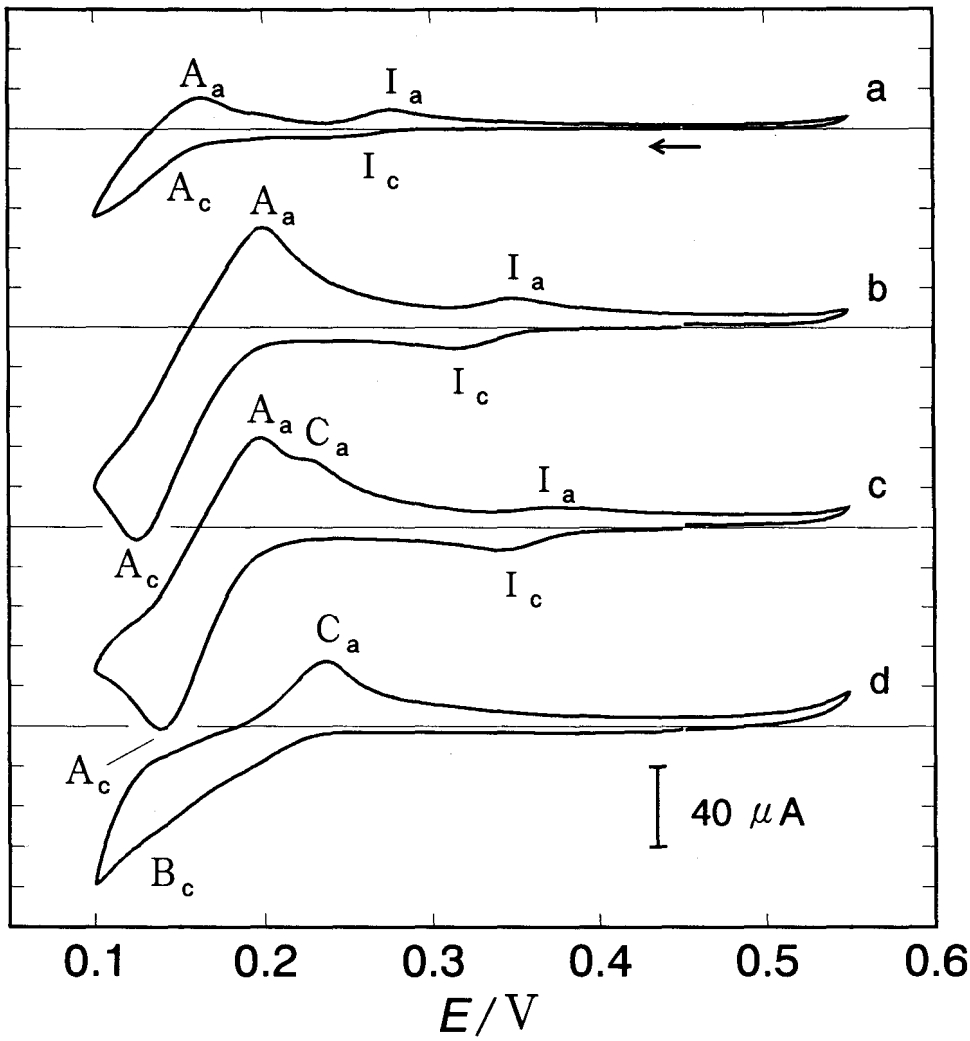

Fig. 3-23. Cyclic voltammograms for the transfer across the NB/W interface of the heteropoly- and isopolyanions formed in the W phase ([P] = 0.33 mM and [Mo] = 20 mM). pH 4.7(a), 2.9(b), 2.2(c), and 1.2(d). Scan rate : 0.02 V s^{-1}.

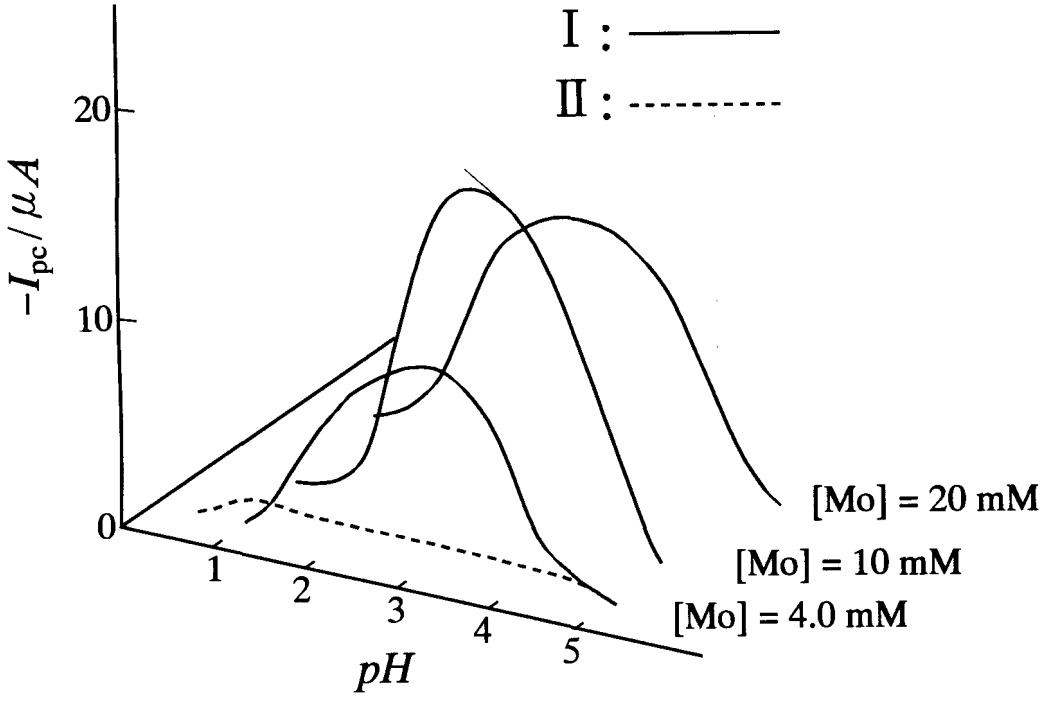

Fig. 3-24. Distribution diagrams for species I and II at [P] = 0.33 mM as a function of pH and [Mo].

II was observed in the whole pH range. Instead, the presence of another heteropolyanion was anticipated from additional measurements by UV spectroscopy and conventional voltammetry with a GC electrode. In Fig. 3-25 are shown cyclic voltammograms recorded at various pH values. Note that the voltammetric waves are due to the redox reactions of molybdophosphate anions at the GC electrode surface. With a lowering pH, the first reduction (cathodic) peak, shown by asterisk in each voltammogram, shifted to more positive potentials accompanying a change in the peak height [denoted by I_{pc}(GC)]. In Fig. 3-26 is shown the pH dependence of I_{pc}(GC) together with those of the absorbance at 340 nm and I_{pc}(NB/W) which represents the value of I_c in Fig. 3-23. By comparison of the pH dependence, it can be concluded that the first cathodic peak in Fig. 3-25 is assigned to species I, i.e. $[H_3PMo_{11}O_{39}]^{4-}$ at pH > 2.5, but to another yellow heteropolyanion (denoted by species III) at lower pH values; the latter anion seems too hydrophilic to give a wave due to its transfer from W to NB in the polarizable potential range. The presence of two heteropolyanions responsible for the reduction wave can be also seen from a plot of the first cathodic peak potential E_{pc} against pH (Fig. 3-27); the plot gives two straight lines with an inflection point at pH 2.5.

In order to know the nature of species III existing at around pH 1.0, the species was isolated from the aqueous solution. As mentioned in Experimental, the salt of $Na_3H_6PMo_9O_{34}\cdot xH_2O$ could be crystallized from the solution of [P] = 0.022 M and [Mo] = 0.2 M (pH 1.0). This result strongly suggests that species III is an α-A-type 9-molybdophosphate anion (its structure is shown in Fig. 3-28). The presence of 9-molybdophosphate anion at low pH has been frequently claimed. [65,68,70,75,76] However, it seems that the formation conditions of the anion are still not fully understood. The pK_a values for

$$[H_6PMo_9O_{34}]^{3-} \rightleftharpoons \cdots \rightleftharpoons [H_3PMo_9O_{34}]^{6-}, \text{ viz. } 1.01, 3.04, \text{ and } 4.41$$

have been reported [68], but they are not acceptable. According to the pK_a values, $[H_6PMo_9O_{34}]^{3-}$ and $[H_6PMo_9O_{34}]^{3-}$ anions must occur at

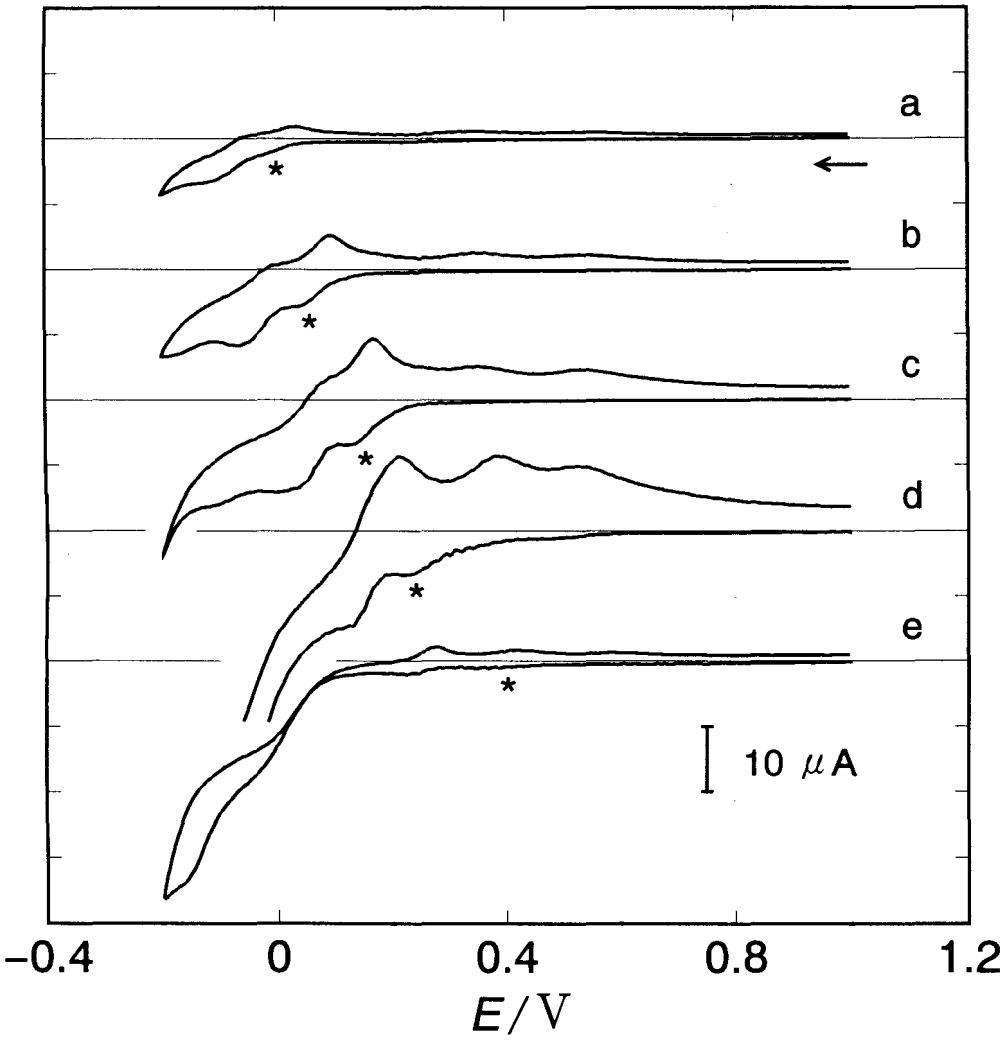

Fig. 3-25. Conventional cyclic voltammograms at a GC electrode in the test solutions with [P] = 0.33 mM and [Mo] = 20 mM. pH 4.1(a), 2.9(b), 2.2(c), 1.2(d), and 0.1(e). Scan rate : 0.1 V s^{-1}. The first reduction (cathodic) peak is shown by an asterisk in each voltammogram.

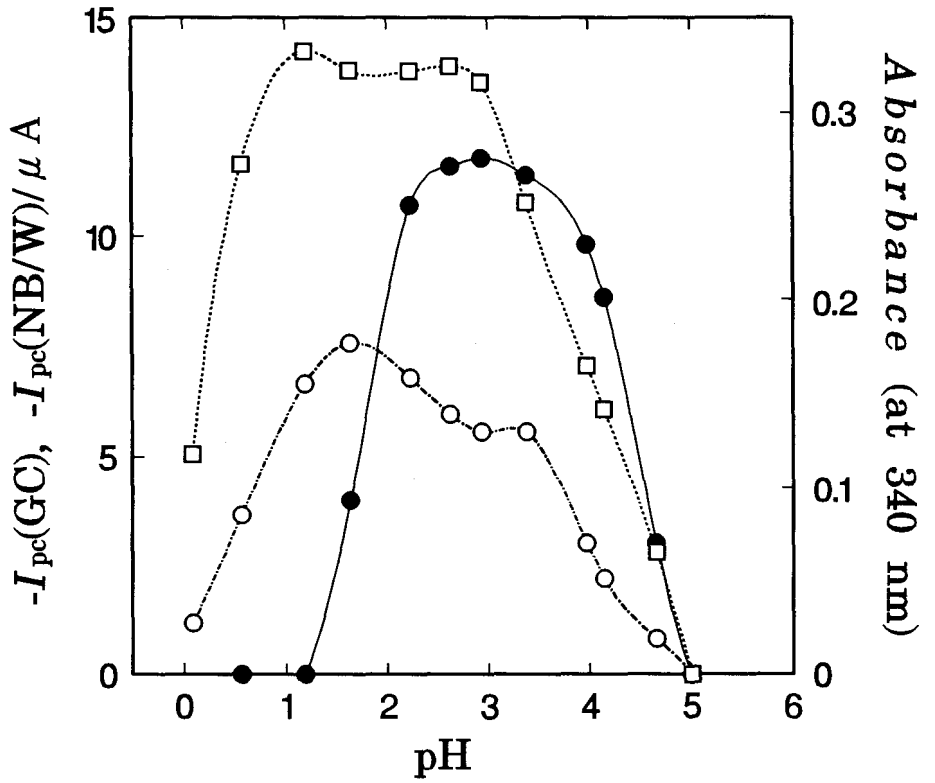

Fig. 3-26. pH dependences of the first reduction peak current I_{pc}(GC), the cathodic peak current I_c(NB/W) for the transfer of species I, and absorbance at 340 nm of the test solutions with [P] = 0.33 mM and [Mo] = 20 mM.

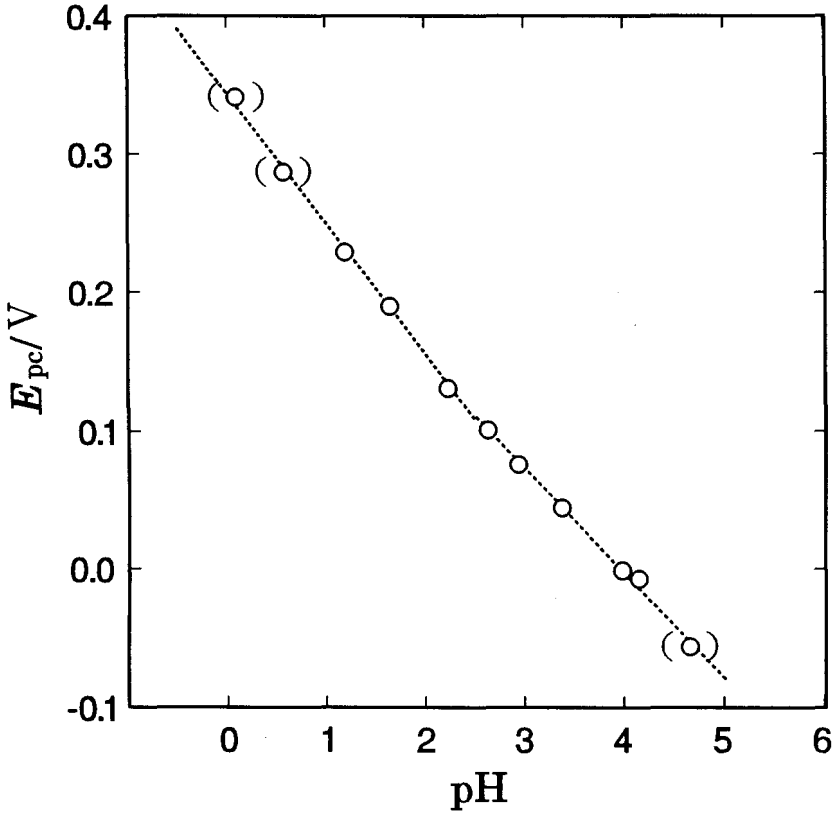

Fig. 3-27. pH dependence of the first reduction peak potential for the cyclic voltammograms shown in Fig. 3-25.

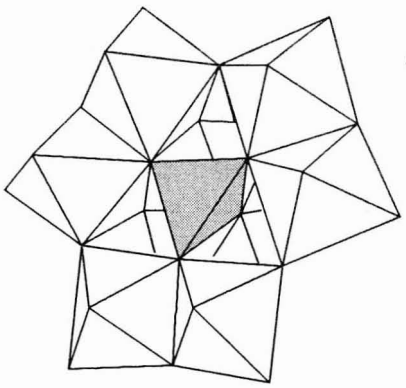

Fig. 3-28. Structure of the α-A-XM_9 anion.

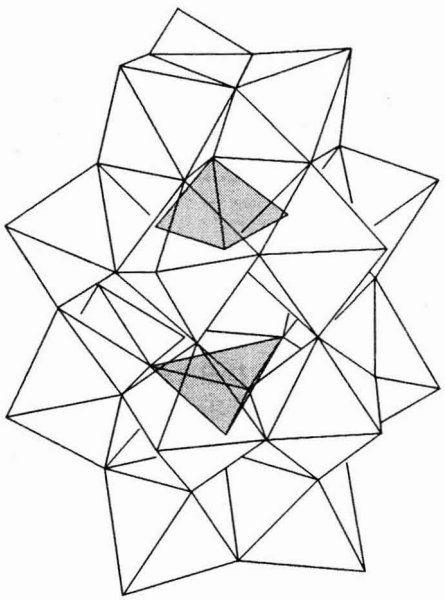

Fig. 3-29. Structure of α-$[P_2Mo_{18}O_{62}]^{6-}$.

around pH 1.0. Since the trivalent and tetravalent anions are rather hydrophobic owing to their lower ionic charges (based on Eq. 1.4, their $\Delta_{NB}^{W}\phi^{\circ}$-values are calculated to be +0.181 V and -0.006 V, respectively), these anions should give voltammetric waves for their transfer in the polarizable potential range. However, this is not the fact, as seen in Fig. 3-19 or Fig. 3-23. It appears likely that the 9-molybdophosphate anion exists in solutions as a pentavalent anion $[H_4PMo_9O_{34}]^{5-}$ and/or a hexavalent anion $[H_3PMo_9O_{34}]^{6-}$.

Until a major comprehensive paper [100] was published in 1986, there was no explicit description of the formation conditions of the Dawson anion (an example of its structure is shown in Fig. 3-29). According to the paper[100], 9-molybdophosphate anions (α-A-type) dimerize very slowly as:

$$2[H_6PMo_9O_{34}]^{3-} \rightleftharpoons [P_2Mo_{18}O_{62}]^{6-} + 6H_2O.$$

It takes 1 month for the Dawson anion to form at 25 ℃ in full amount. No sign of the anion was found in "fresh" solutions prepared within 24 h. This finding is in harmony with the present results. In the ion-transfer voltammetric measurement, if $[P_2Mo_{18}O_{62}]^{6-}$ had been formed in a certain amount in the fresh solutions tested, a voltammetric wave for its transfer [33] would have appeared in the polarizable potential range {e.g., on curve (d) in Fig. 3-23}. A preliminary study has revealed that the formation of $[P_2Mo_{18}O_{62}]^{6-}$ is accelerated by heating of solutions under suitable conditions: pH = 1 and [Mo] $\geq$ 0.02 M([P]/[Mo] = 2/18). Thus, $[P_2Mo_{18}O_{62}]^{6-}$ can be considered a thermodynamically stable species in such solutions.

In a ^{31}P NMR study [76], one of the minor signals was tentatively assigned to $[PMo_{10}O_{34}]^{3-}$. In this study also, species II has been tentatively assumed to the 10-molybdophosphate anion; the author favours $[H_5PMo_{10}O_{37}]^{4-}$ or $[H_4PMo_{10}O_{37}]^{5-}$ for the formula, known as 10-tungstophosphate [101], rather than $[PMo_{10}O_{34}]^{3-}$ in view of the relatively negative transfer potential (the estimated $\Delta_{NB}^{W}\phi^{\circ}$-values for $[PMo_{10}O_{34}]^{3-}$, $[H_5PMo_{10}O_{37}]^{4-}$ and $[H_4PMo_{10}O_{37}]^{5-}$ are +0.182 V, +0.182, and -0.143 V by Eq. 1-4, respectively). The fact that species II is

more prominent at higher [P]/[Mo] ratios than species I (Figs. 3-19 and 3-23) is worth paying particular attention because of its implications on the validity of the above assumption. Nevertheless, further investigation is needed for the clarification of the presence of the 10-molybdophosphate anion.

The 5-molybdodiphosphate anion $[P_2Mo_5O_{23}]^{6-}$ (colorless) is generally believed to form at higher pH values and higher [P]/[Mo] ratios. [65,68,70a,72,73,76,100] In the present study, no wave for the transfer of the anion could be obtained even under the conditions suitable for its formation, but this result never denies the presence of the 5-molybdodiphosphate anion. According to the pK_a values [100] of 5.10 and 3.65, the anion should exist in solutions as $[P_2Mo_5O_{23}]^{6-}$ (higher pH), $[HP_2Mo_5O_{23}]^{5-}$ (medium pH) and $[H_2P_2Mo_5O_{23}]^{4-}$ (lower pH). It seems that these species, even if they exist, give no waves in the polarizable potential range, because of their hydrophilic characters owing to high ionic charges per ionic sizes.

In the present study, the presence of four heteropolyanions, $[H_3PMo_{11}O_{39}]^{4-}$, $[H_pPMo_{10}O_{37}]^{(9-p)-}$(p=4,5)(?), $[H_qPMo_9O_{34}]^{(9-p)-}$(p=3,4), and $[P_2Mo_{18}O_{62}]^{6-}$, as well as two isopolyanions $[H_2Mo_7O_{24}]^{4-}$ and β-$[Mo_8O_{26}]^{4-}$(?), has been confirmed in acidic aqueous solutions and described on the following scheme.

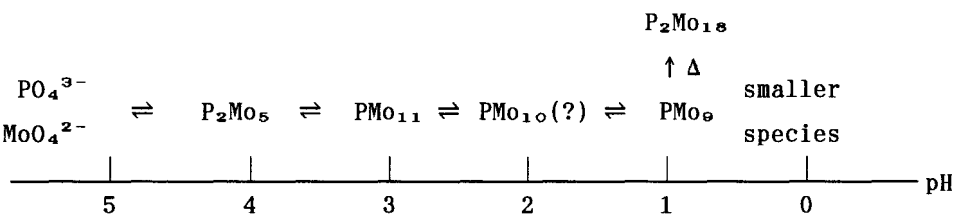

Scheme 3-3.

Scheme for the formation of heteropoly- and isopolyanions in the aqueous phosphate-molybdate system. PMo_9, PMo_{10}, PMo_{11}, P_2Mo_5, P_2Mo_{18}, Mo_7, and β-Mo_8 represent 9-molybdophosphate, 10-molybdophosphate, 11-molybdophosphate, 5-molybdodiphosphate, 18-molybdodiphosphate, respectively.

3.3.4 Molybdoarsenates(V)

In Fig. 3-30 are shown cyclic voltammograms at [As] = 1.0 mM and [Mo] = 4.0 mM. Two cathodic peaks (II_c and A_c) were observed on the initial potential scan, although their anodic peaks (I_a, II_a, and A_a) were well-developed. The cathodic peak responsible for the transfer of species I (I_c) is not seen clearly in Fig. 3-30, however, I_c became a well-developed peak at higher [Mo](= 20 mM) value, as shown in Fig. 3-31. As shown in Fig 3-32, the value of I_c in Fig. 3-31 was increased with lowering pH. It seem likely that species I, which was quite minor species or not present in the aqueous solutions, was produced by a chemical reaction preceding a reversible charge transfer [102].

Species I was isolated as the TBA^+ salt in order to identify. The result of elemental analysis showed that the salt was $(TBA)_4[H_5AsMo_{10}O_{38}]$. By adding the salt to the NB phase, cyclic voltammograms were recorded at various pH values. In Fig. 3-33 are shown cyclic voltammograms obtained at four different pH values. On the initial potential scan, a well-developed anodic peak due to the transfer of the heteropolyanion from NB to W was observed at any scan rate. However, the cathodic peak on the reversed potential scan was quite small compared with the anodic peak, especially at lower scan rate. This can be accounted for by a decomposition of the anion in W phase because of its quite low stability in the aqueous solutions. Because the cathodic waves in Fig. 3-33 are not recognizable, the values of E_{pa} were used to characterize species I, instead of the E_{mid}-values. The E_{pa} for the $[H_pAsMo_{10}O_{38}]^{(8-p)-}$ anion against pH is shown in Fig. 3-34 together with that for species I in Fig. 3-31. Their plots coincided well with each other within experimental errors, which clearly demonstrates that species I is identified to be the $[H_pAsMo_{10}O_{38}]^{(8-p)-}$ anion. The estimated $\Delta^{W}_{NB}\phi^{\circ}$ values (+0.035 V for $[H_5AsMo_{10}O_{38}]^{4-}$ and -0.112 for $[H_4AsMo_{10}O_{37}]^{5-}$) were in line with the result of Fig. 3-31.

In contrast to species I, species II was found to be quite stable in the aqueous solution at higher pH values and to be a semi-hydrophobic anion [$\Delta^{W}_{NB}\phi^{\circ}$ = -0.120 V for curve (c) in Fig. 3-30]. Since Sasaki et. al. [92] suggested the existence of $[H_4As_4Mo_{12}O_{50}]^{4-}$ in the

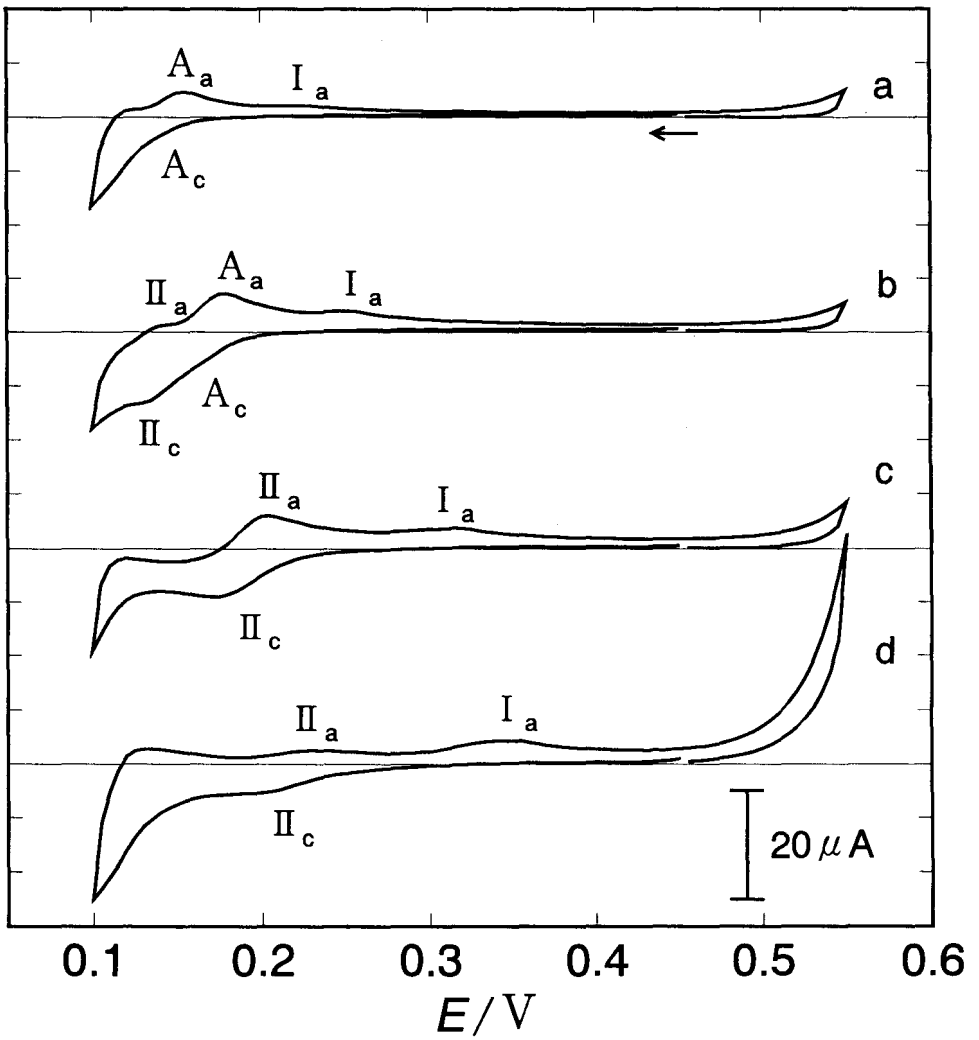

Fig. 3-30. Cyclic voltammograms for the transfer across the NB/W interface of the heteropoly- and isopolyanions formed in the W phase ([As] = 1.0 mM and [Mo] = 4.0 mM). pH 4.4(a), 3.6(b), 2.1(c), and 0.9(d). Scan rate : 0.02 V s^{-1}.

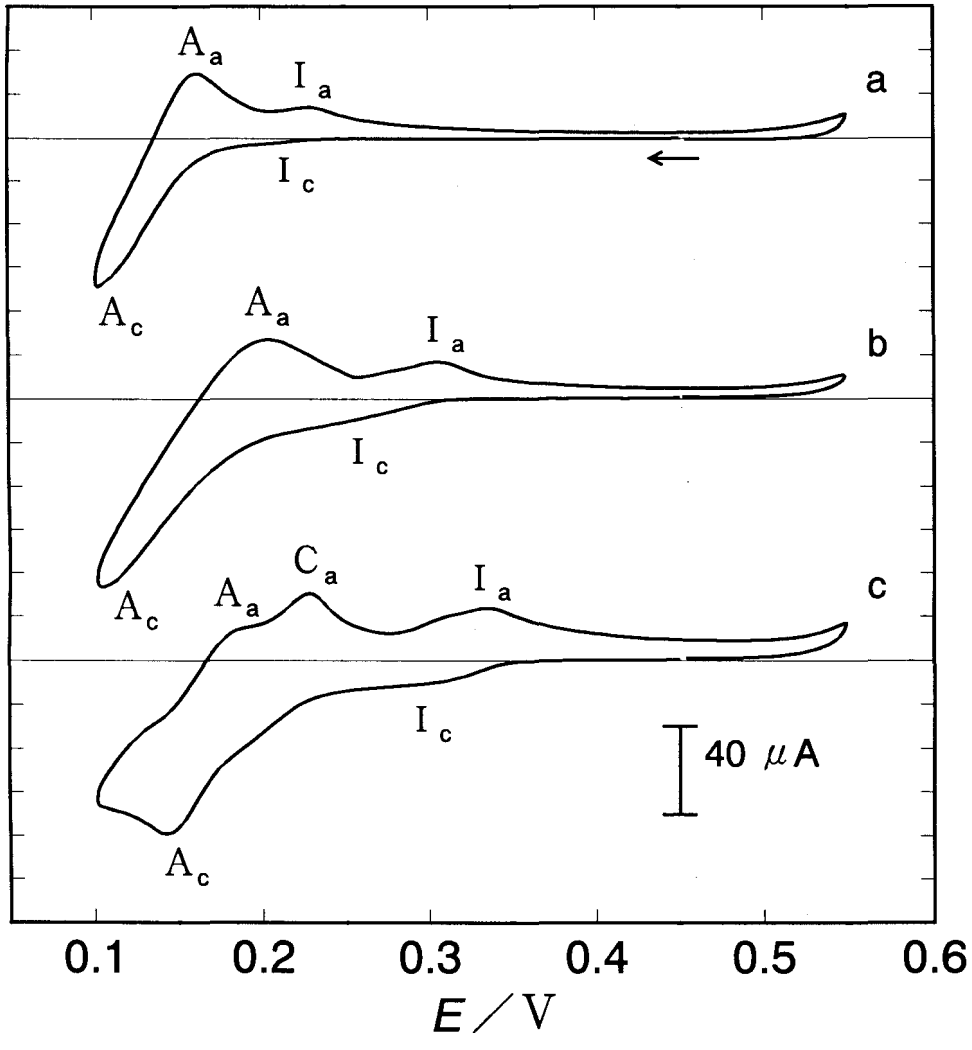

Fig. 3-31. Cyclic voltammograms for the transfer across the NB/W interface of the heteropoly- and isopolyanions formed in the W phase ([As] = 1.0 mM and [Mo] = 20 mM). pH 4.1(a), 2.8(b), and 1.6(c). Scan rate : 0.02 V s^{-1}.

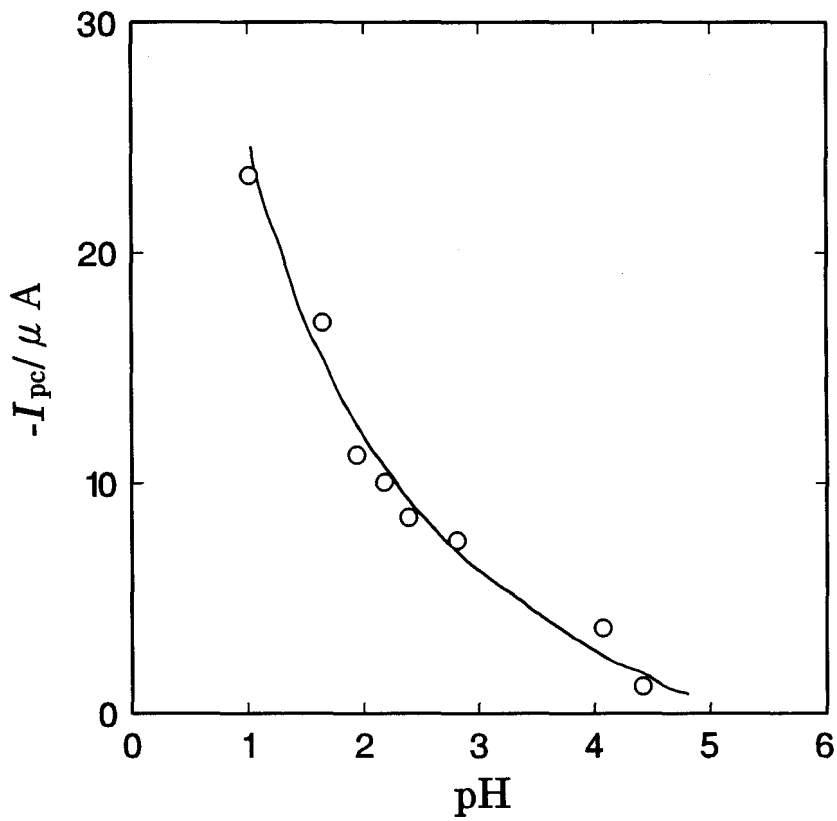

Fig. 3-32. pH dependence of the cathodic peak current I_c for the transfer of species I shown in Fig. 3-31.

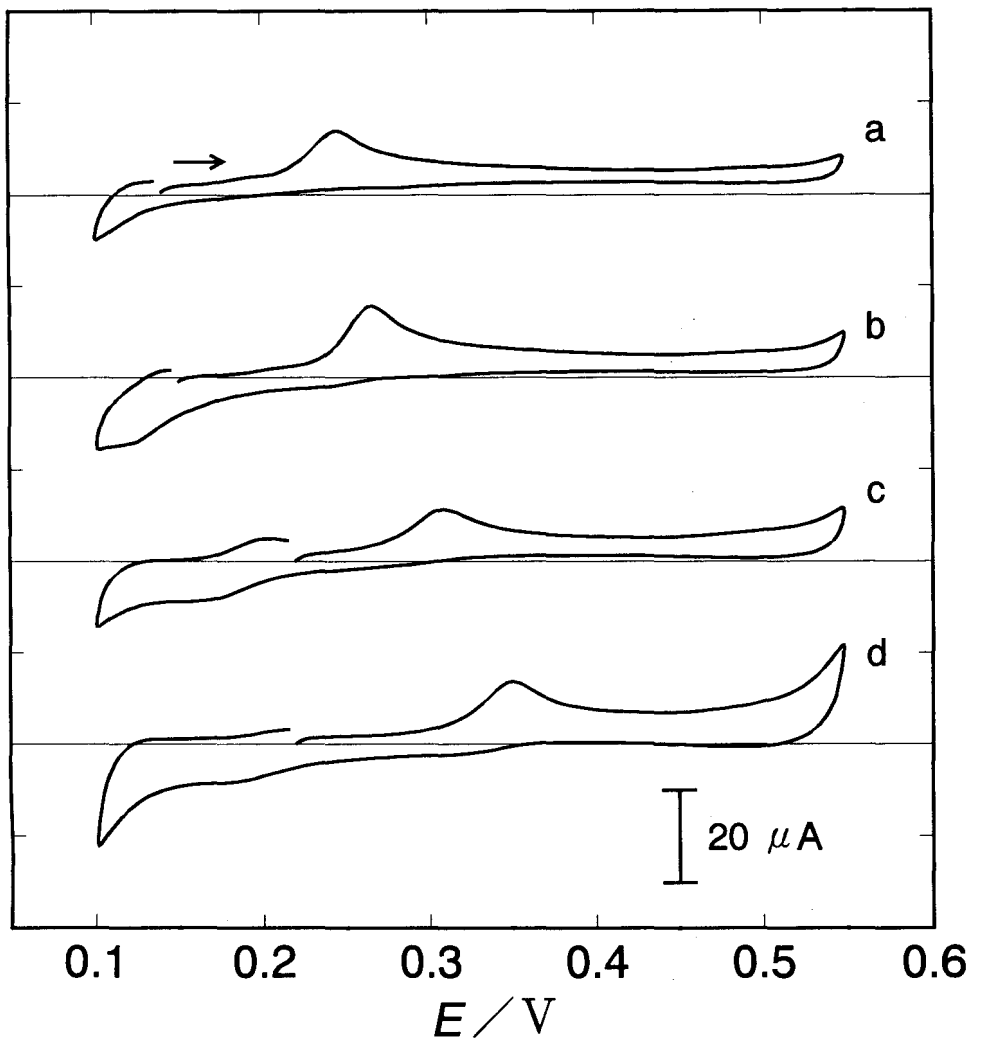

Fig. 3-33. Cyclic voltammograms for the transfer of 10-molybdoarsenate across the NB/W interface at pH 4.5(a), 3.6(b), 2.6(c), and 1.6(d). The NB phase contained 0.5 mM $TBA_4[H_5AsMo_{10}O_{37}]$. Scan rate : 0.02 V s^{-1}.

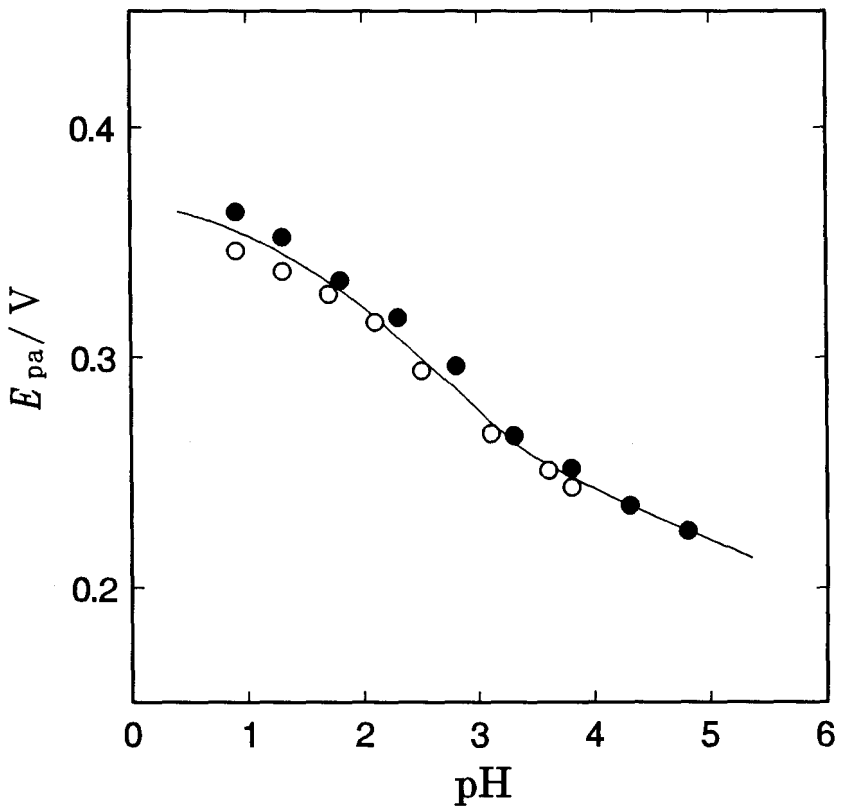

Fig. 3-34. pH dependences of the anodic peak potentials for the transfer of (○) species I (Fig. 3-30) and (●) 10-molybdoarsenate (Fig. 3-33) across the NB/W interface.

aqueous solution, the TBA^+ salt of $[H_4As_4Mo_{12}O_{50}]^{4-}$ was prepared (see Experimental.). Owing to rapid transformation of the heteropolyanion in the NB phase, cyclic voltammograms were recorded immediately after the addition of the salt to NB. A typical example is shown in Fig. 3-35, showing that the $\Delta^{W}_{NB}\phi^{\circ}$-value of the $[H_pAs_4Mo_{12}O_{50}]^{(8-p)-}$ anion was consistent with that of species II. The $\Delta^{W}_{NB}\phi^{\circ}$-value of species II was in accord with the value of -0.127 V calculated as $[H_2As_4Mo_{12}O_{50}]^{6-}$ by Eq. 1.4. This fact suggests that species II transferred as the hexavalent anion, $[H_2As_4Mo_{12}O_{50}]^{6-}$.

The lacunary Keggin anion, 11-molybdoarsenate, was never observed at any conditions. Although the additional measurements by UV spectroscopy and conventional voltammetry with GC electrode were performed (cf. 3.3.3), a 9-molybdoarsenate complex was not also detected.

In analogy with the P-Mo system, the existence of the Dawson anion [33] was not also observed in "fresh" solutions tested.

Species A and B were found to be isopolyanions as mentioned above in section 3.3.1.

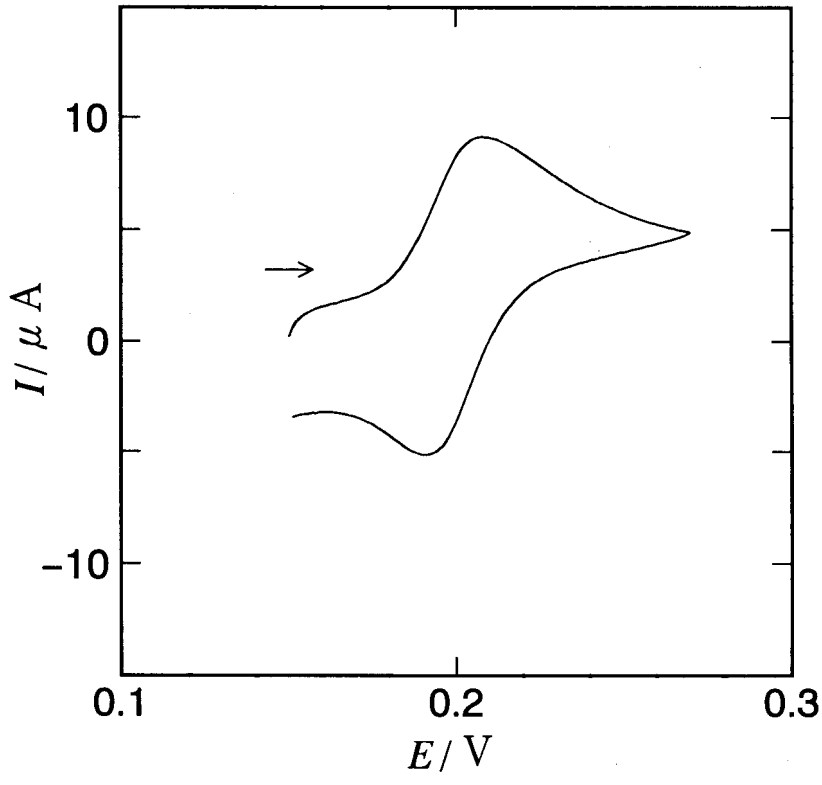

Fig. 3-35. Cyclic voltammograms of the NB/W(pH 2.1) interface in the presence of 0.2 mM $TBA_4[H_4As_4Mo_{12}O_{50}]$ in NB. Scan rate : 0.02 V s^{-1}.

3.4 Discussion

On the basis of the linear dependence of $\Delta^{W}_{O}\phi^{\circ}$ on $|z|/n^{2/3}$ (Eq. 1-4) observed for a variety of polyanions, the author has proposed that the quantity $|z|/n^{2/3}$ can be employed as a hydrophobicity (or hydrophilicity) scale of polyanions. As mentioned in Chapter I, the value of $|z|/n^{2/3}$ can be regarded as being proportional to the surface charge density of the polyanion. The smaller the $|z|/n^{2/3}$-value is, the more hydrophobic (or the less hydrophilic) the polyanion becomes. In Table 3-1 are shown the $|z|/n^{2/3}$-values for the heteropoly- and isopolyanions associated with the present study.

It should be stressed that the yellow Keggin anions with pentavalent heteroatoms, $[PMo_{12}O_{40}]^{3-}$ and $[AsMo_{12}O_{40}]^{3-}$, being labile in aqueous solutions, have a relatively small value of $|z|/n^{2/3}$ (= 0.248). On the other hand, the Keggin anions with tetravalent heteroatoms, $[SiMo_{12}O_{40}]^{4-}$ and $[GeMo_{12}O_{40}]^{4-}$, having less hydrophobicity ($[SiMo_{12}O_{40}]^{4-}$ and $[GeMo_{12}O_{40}]^{4-}$ with $|z|/n^{2/3}$ = 0.342), tend to be more stable in aqueous solutions at lower acid concentrations.

11-heteropolymolybdate anions, $[H_3SiMo_{11}O_{39}]^{5-}$, $[H_3GeMo_{11}O_{39}]^{5-}$, and $[H_3PMo_{11}O_{39}]^{4-}$ were observed in all systems except for the As-Mo system. These anions are more stable in aqueous solutions than their corresponding Keggin anions from the standpoint of their hydrophilicity ($[H_3SiMo_{11}O_{39}]^{5-}$ and $[H_3GeMo_{11}O_{39}]^{5-}$, with $|z|/n^{2/3}$ = 0.435, $[H_3PMo_{11}O_{39}]^{4-}$ with $|z|/n^{2/3}$ = 0.348). As a result, relatively hydrophilic, lacunary Keggin anions, as well as some hydrophilic isopolyanions, seem to be formed preferentially at the case of the P-Mo system. It should be noted that the lacunary structures (see Fig. 3-2) can accommodate their ionic charges to their environments by protnation or deprotonation, in such a way as

$$\cdots \rightleftharpoons [H_4PMo_{11}O_{39}]^{3-} \overset{-H^+}{\rightleftharpoons} [H_3PMo_{11}O_{39}]^{4-} \overset{-H^+}{\rightleftharpoons} [H_2PMo_{11}O_{39}]^{5-} \rightleftharpoons \cdots$$

$$\cdots \rightleftharpoons [H_4GeMo_{11}O_{39}]^{4-} \overset{-H^+}{\rightleftharpoons} [H_3GeMo_{11}O_{39}]^{5-} \overset{-H^+}{\rightleftharpoons} [H_2GeMo_{11}O_{39}]^{6-} \rightleftharpoons \cdots$$

Only in the As-Mo system, however, the so-called "reversed" Keggin anion, $[H_2As_4Mo_{12}O_{50}]^{6-}$ (cf. the polyhedral representaion in Fig. 3-5), existed in stead of 11-molybdoarsenate. The $|z|/n^{2/3}$-value(= +0.442 for $[H_2As_4Mo_{12}O_{50}]^{6-}$) was found to be higher than the $|z|/n^{2/3}$-value(= +0.348) for the tetravalent 11-molybdoarsenate anion, $[H_3AsMo_{11}O_{39}]^{4-}$.

In the case that the heteroatoms were tetravalent, same solute species, XMo_{11} and XMo_{12}, were observed. The orders of the stabilities estimated form their distribution diagrams are given as

$$[SiMo_{12}O_{40}]^{4-} > [GeMo_{12}O_{40}]^{4-}$$
$$[H_3SiMo_{11}O_{39}]^{5-} < [H_3GeMo_{11}O_{39}]^{5-}$$

However, in the case of pentavalent heteroatoms, a variety of solute species were observed as shown in Table 4-1.

As shown above, ion-transfer voltammetry can only detect species that give voltammetric waves in the polarizable potential range. Extremely hydrophilic polyanions, such as 9-molybdophosphate (α-A-type) and 5-molybdodiphosphate, cannot be detected. In this respect, the present method is inferior to NMR or Raman spectroscopy which can detect almost species. Nevertheless, the author does conclude that the proposed method is of great value as a new tool for the study of solution chemistry of polyanions, because this method alone affords useful information concerning the ionic charge and solvation energy of solute species. For the clarification of the complicated equilibrium in polyanion solutions, it seems absolutely necessary to take into account the solvation (hydration) energies which rely heavily on the ionic charges (see Eq. 1-3 and 1-4). The author would like to add that the present method is applicable to more dilute solutions compared to NMR or Raman spectroscopy. However, in view of the clarification of the mechanism of polymerization, dilute solute systems appear to be more interesting.

Table 3-1. Heteropoly- and Isopolyanions associated with the present study and their $|z|/n^{2/3}$-values (hydrophobicity scale) and standard ion transfer potentials at the NB/W interface.

X/Mo	polyanion	$\|z\|n^{2/3}$	$\Delta_{NB}^{W}\phi$ °/V	
			Calcd	Found
1/12	$[SiMo_{12}O_{40}]^{4-}$	0.342	+0.072	+0.066[b]
	$[GeMo_{12}O_{40}]^{4-}$	0.342	+0.072	+0.066[b]
	$[PMo_{12}O_{40}]^{3-}$	0.256	+0.241	+0.248[b]
	$[AsMo_{12}O_{40}]^{3-}$	0.256	+0.241	+0.248[b]
1/11	$[H_3SiMo_{11}O_{39}]^{5-}$	0.435	-0.112	Fig. 3-8.
	$[H_3GeMo_{11}O_{39}]^{5-}$	0.435	-0.112	-0.086 (Fig. 3-15.)
	$[H_3PMo_{11}O_{39}]^{4-}$	0.348	+0.060	Fig. 3-22.
1/10	$[H_5PMo_{10}O_{37}]^{4-}$	0.360	+0.035	Fig. 3-31
	$[H_4PMo_{10}O_{37}]^{5-}$	0.450	-0.112	
	$[H_4AsMo_{10}O_{37}]^{4-}$	0.360	+0.035	
	$[H_4AsMo_{10}O_{37}]^{5-}$	0.450	-0.112	
1/9	$[H_3PMo_9O_{34}]^{5-}$	0.572	-0.384	
2/18	$[P_2Mo_{18}O_{62}]^{6-}$	0.383	-0.010	+0.005c
	$[As_3Mo_{18}O_{62}]^{6-}$	0.383	-0.010	+0.005c
4/12	$[H_2As_4Mo_{12}O_{52}]^{6-}$	0.442	-0.127	-0.120 (Fig. 3-35.)
2/5	$[H_2P_2Mo_5O_{23}]^{4-}$	0.495	-0.231	
	$[HP_2Mo_5O_{23}]^{5-}$	0.618	-0.476	
	$[P_2Mo_5O_{23}]^{6-}$	0.742	-0.721	
0/7	$[H_2Mo_7O_{24}]^{4-}$	0.481	-0.203	-0.147 (Fig. 3-10.)
0/8	α-$[Mo_8O_{26}]^{4-}$	0.456	-0.154	-0.137c
	β-$[Mo_8O_{26}]^{4-}$	0.456	-0.154	
	$[H_3Mo_8O_{28}]^{5-}$	0.542	-0.325	

a) By Eq. 1-4

b) Approximate value for α-isomer (see Chapter I)

c) From Table 1-1.

CHAPTER IV

Formation Kinetics of Heteropolymolybdates in Aqueous Solutions[f,g)]

4.1 Introduction

The clarification of formation mechanisms of heteropolyanions seems to shed light on analytical and catalytic processes [3] associated with them. Among the heteropolyanions, Keggin anions are mostly used on the analytical and catalytic processes.

Since the formation rates of heteropolytungstates are relatively slow, their formation processes are comparatively easy to follow, e.g. by the isolation of metastable species in the processes of formation or decomposition of the Keggin anions. Despite the differences of heteroatoms, all authors [88, 103-104] obtained an unified conclusion that the Keggin anion is produced via the lacunary anion, i.e., 11-heteropolytungstate.

On the other hand, since the formation rates of heteropolymolybdates are quite rapid compared with those of heteropolytungstates, it is not very easy to follow the formation processes. Hence, the formation of heteropolymolybdates has been the basis of the widely utilized methods for the determination of such oxoanions as orthophosphate and silicate. Nevertheless, their formation mechanisms have not been elucidated very well.

There have been a few reports on the formation kinetics of heteropolymolybdates in aqueous solutions [74b,105]. Using stopped-flow measurements, Kircher and Crouch [74b] concluded that 12-molybdophosphate formed from the lacunary species, 9-molybdophosphate, in quite high acidic solutions ($[H^+] \geq 0.3$ M). However, the analysis was based on a lot of uncertain assumptions; hence, the conclusion seems unreliable. Truesdale and coworkers [105] investigated the formation kinetics of molybdosilicates. They have proposed that the formation process of α-form of $[SiMo_{12}O_{40}]^{4-}$ involves a formation of another heteropoly species (e.g. Si → another heteropoly species → α-

$[SiMo_{12}O_{40}]^{4-}$), whereas that of the β-form obeys first-order kinetics with respect to only unreacted silicate (i.e. Si → β-$[SiMo_{12}O_{40}]^{4-}$). However, this analysis was on the basis of their spectrophotometric studies [81,82] which conflicted with those of most previous workers.

The above two works were in common that they were based on indirect determination of solute species by spectrophotometric methods. As mentioned above, ion-transfer voltammetry using the O/W interface can determine directly semi-hydrophobic or -hydrophilic ions. In this study, a novel technique based on the amperometric detection of polyanions has been developed to study the formation kinetics of 12-molybdosilicate and 12-molybdogermanate. Through the analyses of the formation curves obtained, reaction mechanisms were determined. The author has obtained a direct evidence that the lacunary Keggin anion, i.e., 11-heteropolymolybdate, is the intermediate for formation of the Keggin-type heteropolymolybdate.

4.2. Experimental

All chemicals are described in Chapter III.

In this study, the following electrochemical cell was used.

Ag/AgCl (RE2)	I	II	III	IV	V	AgCl/Ag (RE1)

with

I: 0.02 M TPnACl + 0.1 M $MgSO_4$ (W)

II: 0.1 M TPnATPB (NB)

III: 0.1 M TPnATPB (NB)

IV: 0.05 M $MgCl_2$ + 0.5 M $MgSO_4$ + 24 mM Na_2MoO_4 + buffer (W)

V: 0.05 M $MgCl_2$ + 0.5 M $MgSO_4$ (W)

An electrolytic cell assembly is shown in Fig. 4-1.

A standard solution of Si or Ge was syringed to phase IV with stirring so that its concentration became 100 μM. Immediately after the injection, amperometric measurement was started to follow the formation of heteropolyanions. The stirring was always stopped at 20 s after the injection of the standard solution (note that the amperometric data in the first 30 s were not used for analysis).

The electrochemical measurements were carried out at three different temperatures, T = 5, 15, and 25±0.1 ℃.

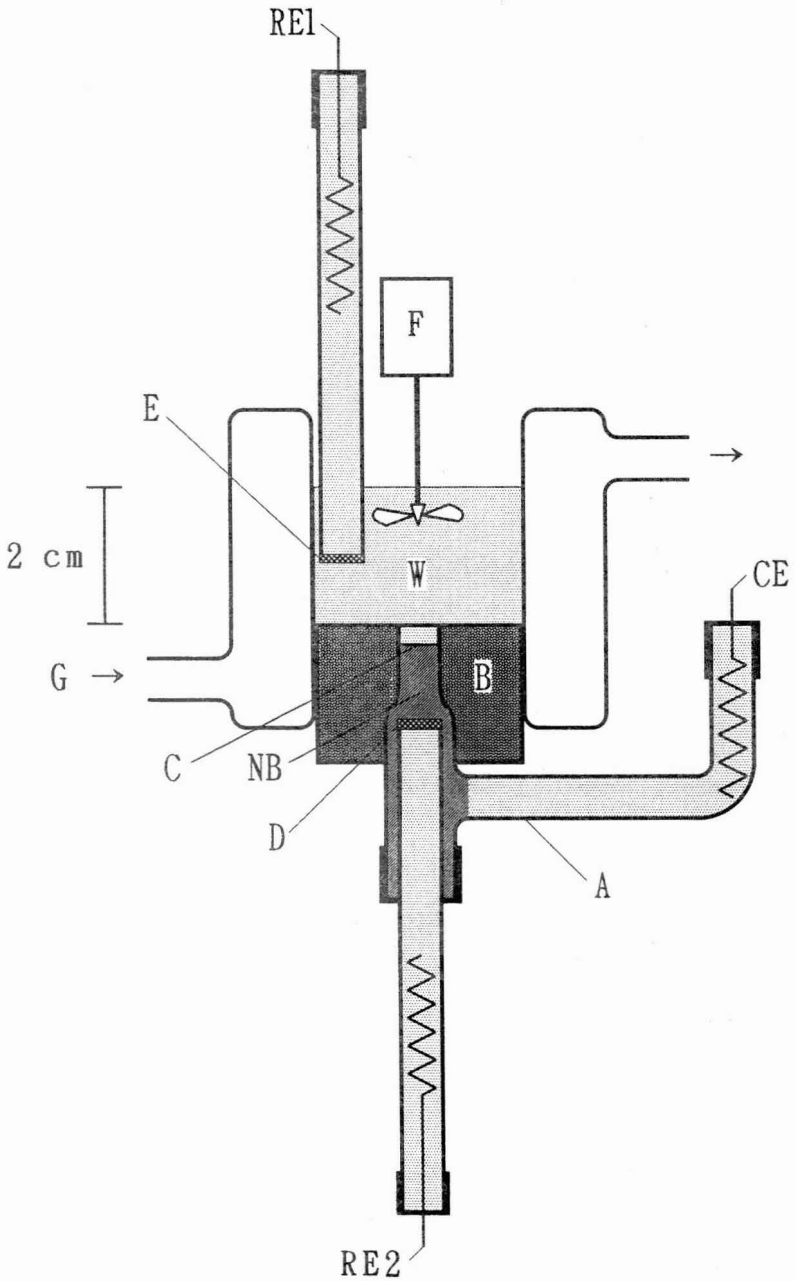

Fig. 4-1. Electrolytic cell : (W) water phase, (NB) nitrobenzene phase, (RE1, RE2) reference electrodes, (CE) counter electrode, (A) glass tube, (B) silicone rubber, (C) test interface, (D,E) sintered glass, (F) stirrer, and (G) thermostated water.

4.3. Theoretical

Here, let us derive theoretical equations which can explain concentration-time curves for the formation of species I ($[H_3XMo_{11}O_{39}]^{5-}$) and II ($[XMo_{12}O_{40}]^{4-}$) {X = silicate (Si) or germanate (Ge)} which are formed in aqueous solutions containing excess molybdate (Mo). When [Mo](= 24 mM) is much higher than the initial concentration of X, $[X]_o$ (typically, 100 μM), the variation of [Mo] is neglected during the reaction. Accordingly, we can assume that the above reaction process obeys first-order kinetics.

Case A: Two-step successive chemical reaction

Consider the case in which species II is formed via species I:

$$X + Mo(excess) \underset{k_2}{\overset{k_1}{\rightleftharpoons}} I \underset{k_4}{\overset{k_3}{\rightleftharpoons}} II \qquad \text{(scheme 1A)}$$

Here, k_n (n = 1, 2, 3, and 4) are rate constants. The differential first-order rate equations of species X, I, and II can be given:

$$\frac{d[X]}{dt} = k_2[I] - k_1[X] \qquad (4\text{-}1)$$

$$\frac{d[I]}{dt} = k_1[X] + k_4[II] - (k_2+k_3)[I] \qquad (4\text{-}2)$$

$$\frac{d[II]}{dt} = k_3[I] - k_4[II] \qquad (4\text{-}3)$$

For the sake of convenience, two parameters, α and β, are introduced, which are related to the rate constants by

$$\alpha + \beta = k_1 + k_2 + k_3 + k_4 \tag{4-4}$$

and

$$\alpha\beta = k_1k_3 + k_1k_4 + k_2k_4 \tag{4-5}$$

By solving the above differential equations [106], Eqs. 4-1 to 4-3, we obtain:

$$[I] = k_1[X]_o \left[\frac{k_4}{\alpha\beta} + \frac{k_4-\alpha}{\alpha(\alpha-\beta)} e^{-\alpha t} + \frac{k_4-\beta}{\beta(\beta-\alpha)} e^{-\beta t} \right] \tag{4-6}$$

$$[II] = k_1k_3[X]_o \left[\frac{1}{\alpha\beta} + \frac{1}{\alpha(\alpha-\beta)} e^{-\alpha t} + \frac{1}{\beta(\beta-\alpha)} e^{-\beta t} \right] \tag{4-7}$$

Equilibrium concentrations of species I and II are then given by

$$[I]_{eq} = \lim_{t\to\infty} [I] = \frac{k_1k_4}{\alpha\beta} \tag{4-8}$$

and

$$[II]_{eq} = \lim_{t\to\infty} [II] = \frac{k_1k_3}{\alpha\beta} \tag{4-9}$$

Using Eqs. 4-6, 4-7, 4-8, and 4-9, a simple relation:

$$[I] - [II]\frac{[I]_{eq}}{[II]_{eq}} = A(e^{-\alpha t} - e^{-\beta t}) \tag{4-10}$$

with

$$A = \frac{k_1[X]_o}{\beta-\alpha} \tag{4-11}$$

is obtained.

If the decomposition of species II can be neglected, i.e.,

$$X \underset{k_2}{\overset{k_1}{\rightleftharpoons}} I \xrightarrow{k_3} II \qquad \text{(scheme 1B)}$$

Eqs. 4-6 and 4-7 are simplified by introducing $k_4=0$:

$$[I] = A\,[\, e^{-\alpha t} - e^{-\beta t}\,] \tag{4-12}$$

and

$$[II] = k_1[X]_o \left[\frac{1}{\alpha\beta} + \frac{1}{\alpha(\alpha-\beta)} e^{-\alpha t} + \frac{1}{\beta(\beta-\alpha)} e^{-\beta t} \right] \tag{4-13}$$

where α, β, and A are given by

$$\alpha + \beta = k_1+k_2+k_3 \tag{4-14}$$

$$\alpha\beta = k_1k_3 \tag{4-15}$$

and Eq. 4-11.

Case B1: Competitive reaction

Let us consider the case in which species I and II are formed competitively:

$$X \underset{k_2}{\overset{k_1}{\rightleftharpoons}} I$$

$$X \underset{k_4}{\overset{k_3}{\rightleftharpoons}} II$$

(scheme 2A)

Under the assumption mentioned above, the differential first-order rate equations of species X, I, and II can be given:

$$\frac{d[X]}{dt} = k_2[I] + k_4[II] - (k_1+k_3)[X] \qquad (4\text{-}16)$$

$$\frac{d[I]}{dt} = k_1[X] - k_2[I] \qquad (4\text{-}17)$$

$$\frac{d[II]}{dt} = k_3[X] - k_4[II] \qquad (4\text{-}18)$$

where

$$[X]_o = [X] + [I] + [II] \qquad (4\text{-}19)$$

These differential equations can be solved using the method of the Laplace transformation. Under the initial conditions, $t = 0 : [X] = [X]_o$ and $[I] = [II] = 0$, the transforms of Eqs. 4-16 to 4-18 are given by

$$s[X]-s[X]_o = k_2[I] + k_4[II] - (k_1+k_3)[X] \qquad (4\text{-}20)$$

$$s[I] = k_1[X] - k_2[I] \qquad (4\text{-}21)$$

$$s[II] \quad k_3[X] - k_4[II] \qquad (4\text{-}22)$$

Equation 4-21 is also expressed as

$$[I] = \frac{k_1[X]}{s+k_2} \tag{4-23}$$

By substituting Eq. 4-19 and 4-23 into Eq. 4-20, we obtain

$$s[X]-s[X]_o = \frac{k_1(k_2-k_4)[X]}{s+k_2} - (k_1+k_3+k_4)[X]+k_4[X]_o$$

Thus, [X] is expressed by

$$[X] = \frac{(s+k_2)(s+k_4)[X]_o}{s^2+(k_1+k_2+k_3+k_4)s+k_1k_4+k_2k_3+k_2k_4} \tag{4-24}$$

Using the convenient parameters, α and β, which are related to the rate constants by

$$\alpha + \beta = k_1 + k_2 + k_3 + k_4 \tag{4-25}$$

and

$$\alpha\beta = k_1k_4 + k_2k_3 + k_2k_4, \tag{4-26}$$

the denominator of the right-hand side of Eq. 4-24 may be converted to the form of $(s+\alpha)(s+\beta)$. Thus, Eq. 4-24 and 4-23 can be written by

$$[X] = \frac{(s+k_2)(s+k_4)[X]_o}{(s+\alpha)(s+\beta)} \tag{4-27}$$

$$[I] = \frac{k_1(s+k_4)[X]_o}{(s+\alpha)(s+\beta)} \tag{4-28}$$

Upon reverse transformation, we obtain:

$$[X] = [X]_o \left[\frac{k_2 k_4}{\alpha\beta} + \frac{(k_2-\alpha)(k_4-\alpha)}{\alpha(\alpha-\beta)} e^{-\alpha t} + \frac{(k_2-\beta)(k_4-\beta)}{\beta(\beta-\alpha)} e^{-\beta t} \right] \quad (4\text{-}29)$$

$$[I] = k_1[X]_o \left[\frac{k_4}{\alpha\beta} + \frac{k_4-\alpha}{\alpha(\alpha-\beta)} e^{-\alpha t} + \frac{k_4-\beta}{\beta(\beta-\alpha)} e^{-\beta t} \right] \quad (4\text{-}30)$$

By substituting Eqs. 4-29 and 4-30 into Eq. 4-19, [II] is expressed by

$$[II] = [X]_o - [X] - [I]$$

$$= k_3[X]_o \left[\frac{k_2}{\alpha\beta} + \frac{k_2-\alpha}{\alpha(\alpha-\beta)} e^{-\alpha t} + \frac{k_2-\beta}{\beta(\beta-\alpha)} e^{-\beta t} \right] \quad (4\text{-}31)$$

Equilibrium concentrations of species I and II are then given by

$$[I]_{eq} = \lim_{t\to\infty} [I] = \frac{k_1 k_4}{\alpha\beta} \quad (4\text{-}32)$$

$$[II]_{eq} = \lim_{t\to\infty} [II] = \frac{k_2 k_3}{\alpha\beta} \quad (4\text{-}33)$$

Using Eqs. 4-30, 4-31, 4-32, and 4-33, a simple relation:

$$[I] - [II] \frac{[I]_{eq}}{[II]_{eq}} = A(e^{-\alpha t} - e^{-\beta t}) \quad (4\text{-}34)$$

with

$$A = \frac{k_1(k_4-k_2)[X]_o}{k_2(\beta-\alpha)} \quad (4\text{-}35)$$

is obtained.

If the decomposition of species II can be neglected, i.e.,

$$X \underset{k_2}{\overset{k_1}{\rightleftharpoons}} I \qquad \text{(scheme 2B)}$$

$$X \xrightarrow{k_3} II$$

the introduction at $k_4=0$ into Eqs. 4-30 and 4-31 yields the following simple equations:

$$[I] = A\,[\, e^{-\alpha t} - e^{-\beta t}\,] \tag{4-36}$$

and

$$[II] = k_3[X]_o \left[\frac{k_2}{\alpha\beta} + \frac{k_2-\alpha}{\alpha(\alpha-\beta)} e^{-\alpha t} + \frac{k_2-\beta}{\beta(\beta-\alpha)} e^{-\beta t} \right] \tag{4-37}$$

where α, β, and A are given

$$\alpha + \beta = k_1+k_2+k_3 \tag{4-38}$$

$$\alpha\beta = k_2k_3 \tag{4-39}$$

and Eq. 4-11.

4.4. Results

Figure 4-2(a) shows a normal pulse voltammogram (NPV) for the transfer of heteropolyanions formed in the W-phase (200 μM Ge, 24 mM Mo, pH 3.3). Two cathodic waves, I_c and II_c, correspond to the cathodic peaks, II_c and I_c, in cyclic voltammetry (see Fig. 3-14), being due to the transfer of $[H_3GeMo_{11}O_{39}]^{5-}$ and $[GeMo_{12}O_{40}]^{4-}$ (cf. Chapter III).

Since the potentials of the two cathodic waves are adequately separated, the concentrations of species I and II can be simultaneously determined by dual pulse amperometry (DPA) [107] with double potential pulses of different amplitudes {see Fig. 4-2(b)}. At the beginning, the potential E is held at a potential, E_1 = 0.45 V, where neither species I nor II transfers across the NB/W interface. On this initial potential, two voltage pulses of short duration (τ = 100 ms) and different amplitudes, ΔE_1 = -0.17 V and ΔE_2 = -0.27 V, are applied alternatively at an interval, Δt = 3 s. The first voltage pulse (ΔE_1) gives the limiting current, i_1, due to the transfer of species I, while the second pulse (ΔE_2) gives the limiting current, i_2, due to the transfer of both species I and II. As shown above (Fig. 3-15), species I and II (i.e. $[H_3GeMo_{11}O_{39}]^{5-}$ and $[GeMo_{12}O_{40}]^{4-}$) transfer across the NB/W interface with no protonation in the pH ranges, 2.4-3.6 and 2.0-5.3, respectively. In these pH ranges, the limiting currents [38], i_1 and i_2, may be given by

$$i_1 = \frac{FA}{\sqrt{\pi\tau}} z_{II}\sqrt{D_{II}^W}\,[II] \qquad (4\text{-}40)$$

and

$$i_2 = \frac{FA}{\sqrt{\pi\tau}} \left(z_{II}\sqrt{D_{II}^W}\,[II] + z_I\sqrt{D_I^W}\,[I] \right) \qquad (4\text{-}41)$$

where z_j(j=I or II) is the ionic valence of species j, D_j^W(cm^2s^{-1}) the diffusion coefficient of j in W-phase, A the surface area (0.127 cm^2) of a test interface, and F the Faraday constant. As described in Chapter III, z_I and z_{II} are -4 and -5, respectively. Since there is little difference in size between species I and II, it seems reasonable to use

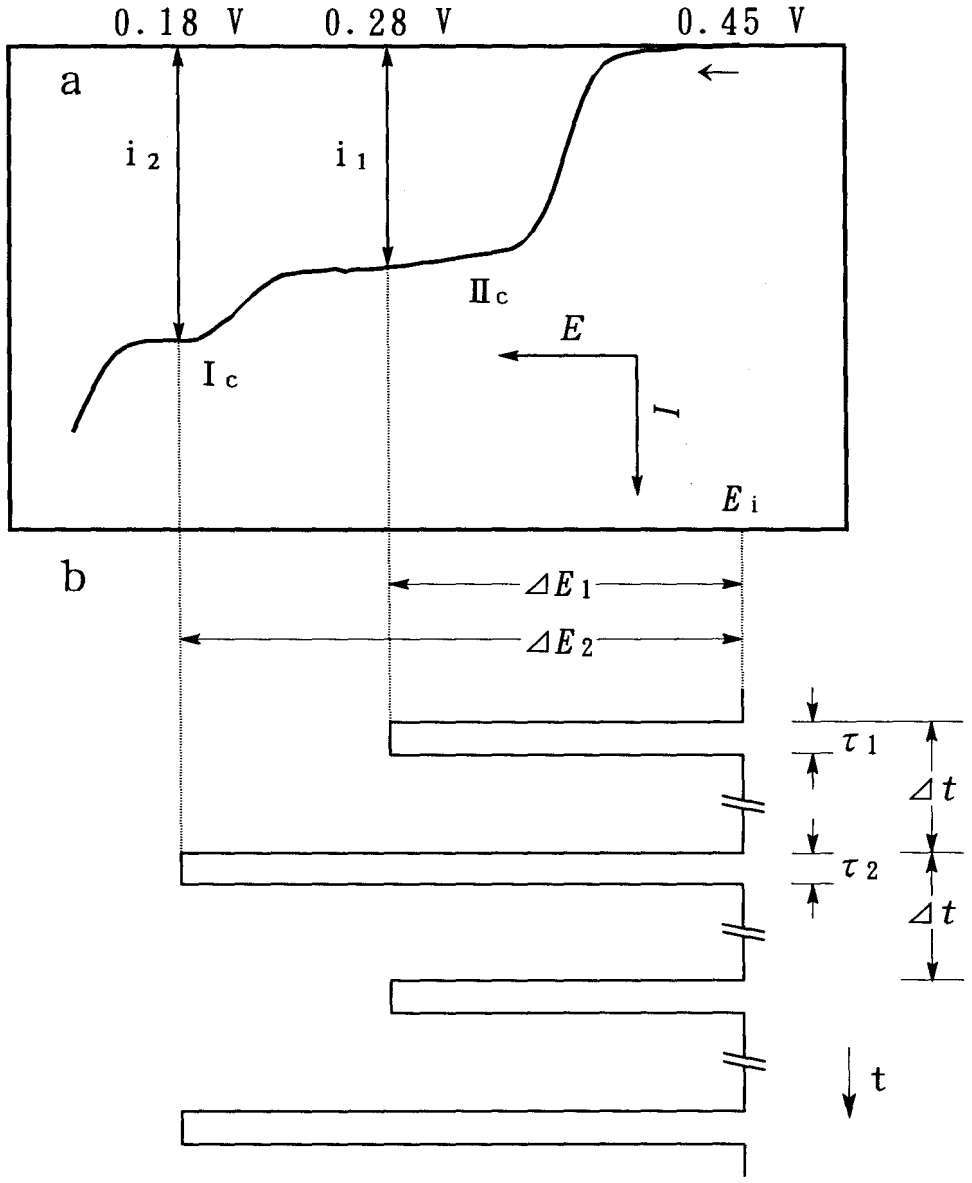

Fig. 4-2.

(a) Normal pulse voltammogram of the transfer across the NB/W interface of the heteropolyanions formed in the W phase ([Ge] = 200 μM, [Mo] = 24 mM, and pH 3.3). Sampling time, 100 ms.

(b) Dual pulse amperometry : on the initial applied potential, E_i, the potential pulse of amplitude ΔE_1 and ΔE_2 and of the width of τ (= τ_1 and τ_2) are applied alternatively at the time interval of Δt.

an approximation: $D_{II}^{W} = D_{I}^{W} = D^{W}$. Thus, we obtain

$$[I] = -\frac{\sqrt{\pi\tau}}{5FA\sqrt{D^{W}}}(i_2-i_1) \qquad (4\text{-}42)$$

and

$$[II] = -\frac{\sqrt{\pi\tau}}{4FA\sqrt{D^{W}}}i_1 \qquad (4\text{-}43)$$

Equations 4-42 and 4-43 show that if D^{W} was known, [I] are [II] were estimated by (i_2-i_1) and i_1, respectively. The values of D^{W} for X = Si and Ge can be assumed to be equal [108], because there is little difference in size between $[SiMo_{12}O_{40}]^{4-}$ [109] and $[GeMo_{12}O_{40}]^{4-}$ [110]. Here, the values of D^{W} were determined to be 2.46×10^{-6}, 2.49×10^{-6}, and 2.51×10^{-6} cm^2s^{-1} at 5, 15, and 25 ℃ from the limiting currents i_1 for the transfer of $[SiMo_{12}O_{40}]^{4-}$ at [Si] = 0.333 mM, [Mo] = 24 mM, and pH 2.5; under these conditions, almost all Si species are consumed for the formation of $[SiMo_{12}O_{40}]^{4-}$ (see section 3.3.1).

Thus the amperometric detection of the transfer currents of heteropolyanions enables us to follow directly their formation. In the following, the results obtained for X=Si and Ge at various pH's (2.5-3.5) and temperatures (5, 15, and 25 ℃) will be presented.

12-molybdosilicate Formation

Figure 4-3 shows a result of DPA for a test solution ([Mo] = 24 mM, $[Si]_o$ = 100 μM, pH 3.5) at 25 ℃. Curves (a) and (b) show [I] and [II] estimated by Eqs. 4-42 and 4-43, i.e. formation curves of species I and II. As seen in the figure, [I] increased rapidly until it reached a peak, then gradually decreased. On the other hand, [II] increased monotonously until it reached a constant. In this case, $[I]_{eq}$ is negligibly small and $[II]_{eq}$ is equal to $[Si]_o$; accordingly, the decomposition of species II may be neglected. Thus the formation mechanism is regarded as scheme 1B or 2B. In order to know which reaction scheme can be applied to elucidate such formation curves, the following analysis was performed.

First, the author examined the applicability of reaction scheme 1B , i.e. a two-step successive reaction. A data fitting of curve (a) in Fig. 4-3 to Eq. 4-12 was performed using a non-linear least square method (Gauss-Newton method). The parameters obtained by the regression analysis were: A = 54.2 μM, $\alpha = 5.62\times10^{-3}$ s^{-1}, and $\beta = 2.17\times10^{-2}$ s^{-1}. By using Eqs. 4-11, 4-14, and 4-15, the rate constants, k_1, k_2, and k_3 were calculated from A, α, and β as $k_1 = 8.7\times10^{-3}$, $k_2=1.4\times10^{-2}$, and $k_3 = 4.6\times10^{-3}$ s^{-1}. By substituting these rate constants in Eq. 4-13, the calculated concentration-time profiles for species I (□) and II (○) were obtained and plotted. As seen in the figure, the calculated values were in good agreement with the experimental data.

Next, the applicability of reaction scheme 2B, i.e. a competitive reaction, was examined. The data fitting of curve (a) using Eq. 4-36 yielded parameters A = 54.2 μM, $\alpha = 5.62\times10^{-3}$ s^{-1}, and $\beta = 2.17\times10^{-2}$ s^{-1} (note that Eq. 4-36 is identical to Eq. 4-12). From these parameters, however, the rate constants could not be determined because the simultaneous equations, 4-38 and 4-39, gave no solutions for the rate constants. Thus, this reaction scheme was excluded.

Thus, the formation kinetics of $[SiMo_{12}O_{40}]^{4-}$ can be elucidated by the two-step successive reaction scheme:

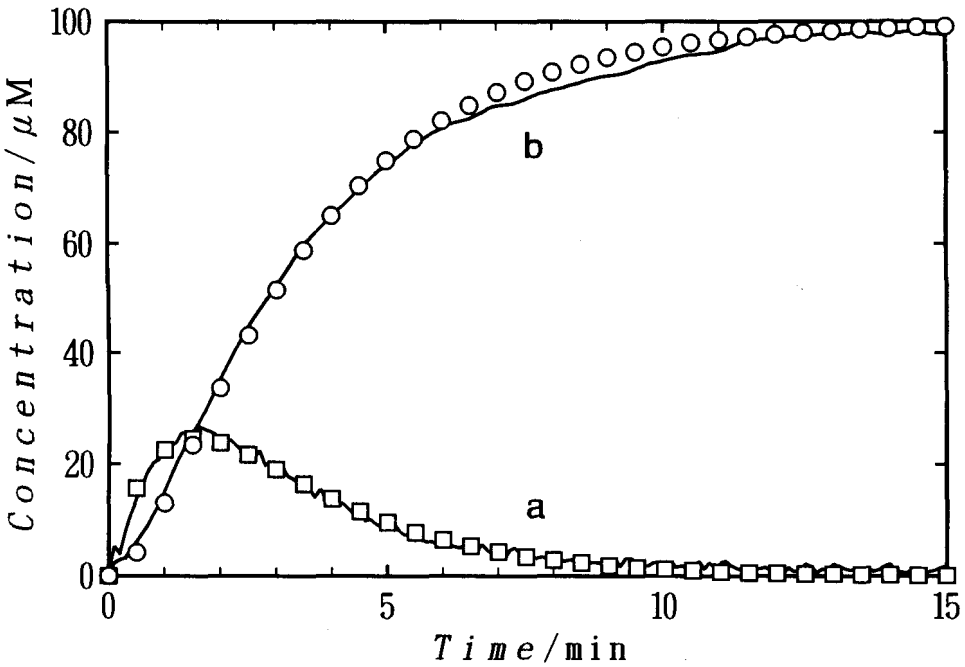

Fig. 4-3. Formation curves of species I (a) and II (b) obtained for a test solution ([Mo] = 24 mM, $[Si]_0$ = 100 μM, pH 3.5) at 25 ℃.

$$Si + Mo(excess) \rightleftharpoons H_3SiMo_{11}O_{39}^{5-} \longrightarrow [SiMo_{12}O_{40}]^{4-}$$

In order to examine the validity of the assumption that the respective reaction steps obey first-order kinetics, the rate constants, k_1, k_2, and k_3, were determined at various $[Si]_o$'s (20 - 200 μM). As expect, the rate constants determined were virtually constant: k_1 = $(8.4\pm0.3)\times10^{-3}$, k_2 = $(3.8\pm1.0)\times10^{-3}$, and k_3 = $(1.3\pm0.3)\times10^{-2}$ s^{-1}. This clearly indicates that the above assumption is valid when [Mo] is much higher than $[Si]_o$.

In a similar manner, the measurement and the analysis were performed at various pH's and temperatures. At any condition, $[II]_{eq} = [Si]_o$, i.e. no decomposition of species II was observed. The rate constants were then determined by the regression analysis for reaction scheme 1B, but not for scheme 2B.

The results are summarized in Table 4-1. In general, the formation rate constants, k_1 and k_3, became larger with a lowering of pH, whereas the decomposition rate, k_2, was not very dependent on pH.

Table 4-1. Rate constants of the formation of $[H_3SiMo_{11}O_{39}]^{5-}$ and $[SiMo_{12}O_{40}]^{4-}$ at various pH values and temperatures.

Rate constants[a] (s^{-1})	pH	Temperature(℃)		
		5	15	25
k_1	2.5	1.2×10^{-2}	1.6×10^{-2}	
	3.0	5.0×10^{-3}	8.1×10^{-3}	2.3×10^{-2}
	3.5	9.0×10^{-4}	1.8×10^{-3}	8.7×10^{-3}
k_2	2.5	2.8×10^{-2}	3.8×10^{-2}	
	3.0	1.2×10^{-2}	1.2×10^{-2}	1.3×10^{-2}
	3.5	2.2×10^{-3}	2.4×10^{-3}	4.6×10^{-3}
k_3	2.5	1.1×10^{-2}	2.4×10^{-2}	
	3.0	1.1×10^{-2}	2.5×10^{-2}	4.7×10^{-2}
	3.5	2.9×10^{-3}	5.1×10^{-2}	1.4×10^{-2}

a) rate constants defined as

$$Si \underset{k_2}{\overset{k_1}{\rightleftharpoons}} [H_3SiMo_{11}O_{39}]^{5-} \xrightarrow{k_3} [SiMo_{12}O_{40}]^{4-}$$

12-molybdogermanate Formation

Figure 4-4 shows a result of DPA for a test solution ([Mo] = 24 mM, $[Ge]_o$ = 100 μM, pH 3.5) at T = 25 ℃. Under the conditions at higher pH's (≥ 3.0), $[I]_{eq}$ showed a certain value (= 21.0 mM), whereas $[II]_{eq}$ (= 19.7 mM) was less than $[Ge]_o$. This demonstrates that an equilibrium exists between species I and II. The decomposition of species II is not negligible in contrast to the case of molybdosilicates. Hence, the mechanism of their formations should be regarded as scheme 1A or 2A. In order to know which reaction scheme is applicable, the following analysis was performed.

First, the author examined the applicability of reaction scheme 1A, i.e. a two-step successive reaction. In this case, the value of $[I]-[II]([I]_{eq}/[II]_{eq})$, calculated using curves (a) and (b) in Fig. 4-4 was plotted against time, and the regression analysis was performed using Eq. 4-10. The parameters obtained by the regression analysis were: $\alpha = 4.43\times10^{-3}$, $\beta = 6.33\times10^{-2}$, and A = 26.8. By using Eqs. 4-4, 4-5, 4-8, and 4-11, the rate constants k_1, k_2, k_3, and k_4 were calculated from $[I]_{eq}$, α , β, and A as $k_1 = 1.6\times10^{-2}$, $k_2 = 4.5\times10^{-2}$, $k_3 = 3.5\times10^{-3}$, and $k_4 = 3.7\times10^{-3}$ s^{-1}. By substituting these rate constants in Eqs. 4-6 and 4-7, the values of [I] and [II] were obtained. In Fig. 4-4, the values of [I] (□) and [II](○) calculated by the regression analysis are plotted. As shown in the figure, the calculated values were in harmony with the experimental data.

Next, the applicability of reaction scheme 2A, i.e. a competitive reaction, was examined. The data fitting for the $[I]-[II][I]_{eq}/[II]_{eq}$ vs. t plot using Eq. 4-34 yielded parameters: $\alpha = 4.43\times10^{-3}$, $\beta = 6.33\times10^{-2}$, and A = 26.8 (note that Eq. 4-34 is identical to 4-10). By using Eqs 4-25, 4-26, 4-32, and 4-35 the rate constants could be also calculated from $[I]_{eq}$, α , β, and A as $k_1 = 1.7\times10^{-2}$, $k_2 = 4.6\times10^{-2}$, $k_3 = 1.4\times10^{-3}$, and $k_4 = 3.5\times10^{-3}$ s^{-1}. The calculated values of [I] and [II] are necessarily equivalent to those for reaction scheme 1A, i.e., (□) and (○) in Fig. 4-4. Thus neither reaction scheme was excluded.

However, a favorable choice of the conditions enable us to

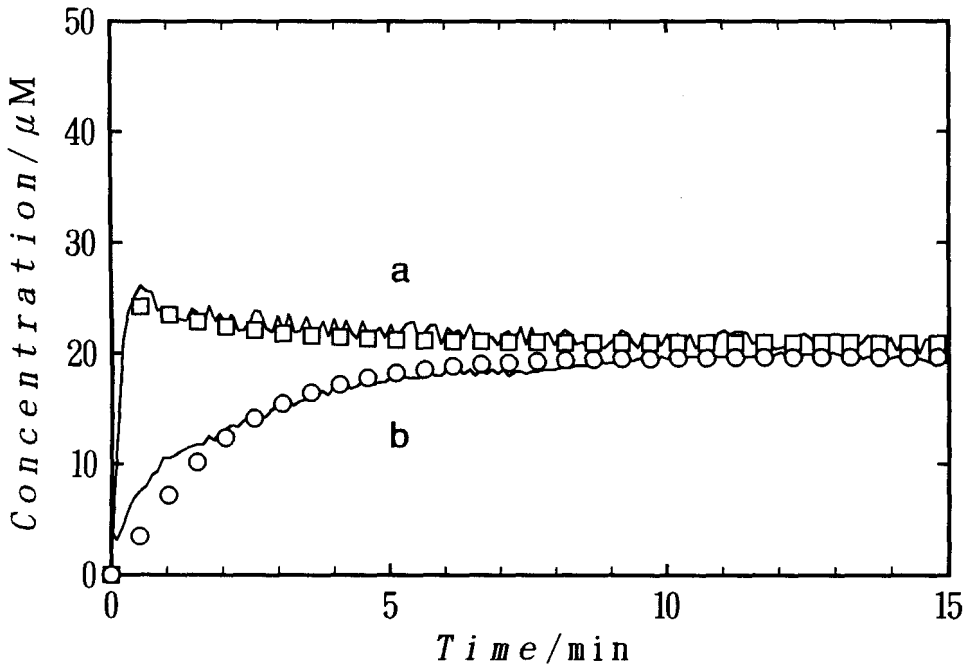

Fig. 4-4. Formation curves of species I (a) and II (b) obtained for a test solution ([Mo] = 24 mM, $[Ge]_0$ = 100 μM, pH 3.5) at 25 ℃.

determinate the reaction mechanism (see Table 4-2).

In Fig. 4-5 is shown a result which was obtained for a test solution ([Mo] = 24 mM, $[Ge]_o$ = 100 μM, pH 2.5) at a lower temperature (5 ℃). Since both $[I]_{eq}$ is negligibly small and $[II]_{eq}$ is equal to $[Ge]_o$, the decomposition of species II is reasonably negligible. Accordingly, the formation mechanism is regarded as scheme 1B or 2B, (i.e. the simplified case for reaction scheme 1A or 2A). Thus, the regression analysis could be treated in a manner similar to that for the case of molybdosilicate anions.

By using reaction scheme 1B, the rate constants could be calculated as $k_1 = 8.7\times10^{-3}$, $k_2=1.4\times10^{-2}$, and $k_3 = 4.6\times10^{-3}$ s^{-1}. As shown in Fig. 4-5, the values calculated with these rate constants were in good agreement with the experimental data. However, the use of reaction scheme 2B did not enable us to determine the rate constants. Thus, this reaction scheme was excluded. Although there was no sign of decomposition for species II in the test solution (pH 2.5) at the higher temperatures, 15 and 25 ℃, the regression analysis was unsuccessful because the formation rate of species I was quite rapid.

The analysis for a test solution (pH 3.0) also showed that reaction scheme 2B is excluded. Thus, the formation kinetics of $[GeMo_{12}O_{40}]^{4-}$ has been also found to be elucidated by the two-step successive reaction scheme:

$$Ge + Mo(excess) \rightleftharpoons H_3GeMo_{11}O_{39}^{5-} \rightleftharpoons [GeMo_{12}O_{40}]^{4-}$$

The sets of rate constants at various pH values and temperatures are shown in Table 4-2.

In general, the rate constants for the formation of species I and II, k_1 and k_3, become larger with a lowering of pH, whereas that for the decomposition of species II, k_4, becomes smaller with an increase of pH. However, the pH-dependence of k_2 is somewhat complex.

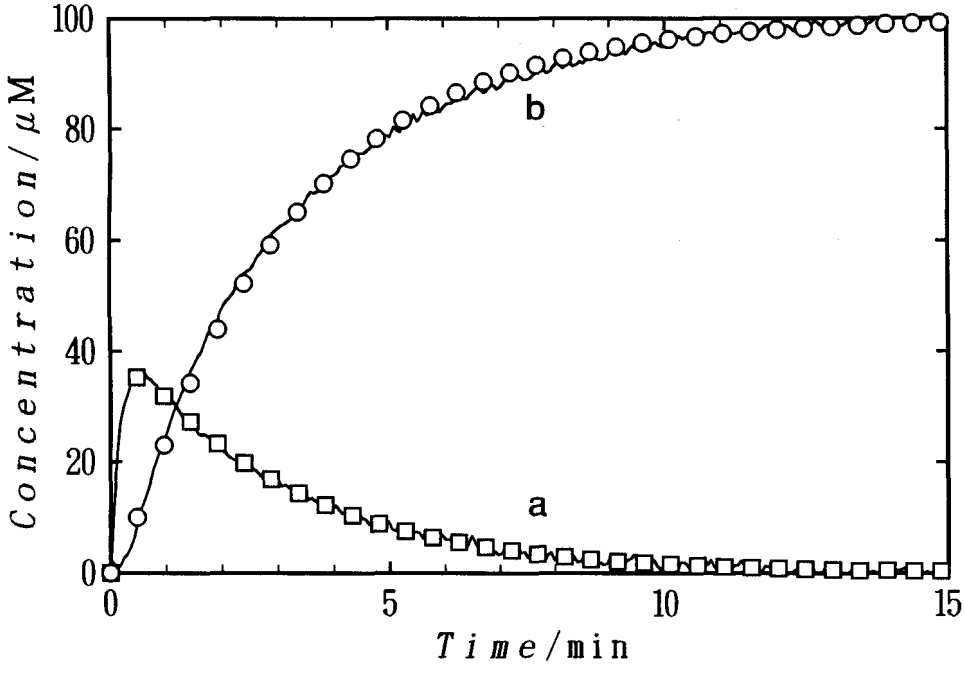

Fig. 4-5. Formation curves of species I (a) and II (b) obtained for a test solution ([Mo] = 24 mM, $[Ge]_0$ = 100 μM, pH 2.5) at 5 ℃.

Table 4-2. Rate constants of the formation of $[H_3GeMo_{11}O_{39}]^{5-}$ and $[GeMo_{12}O_{40}]^{4-}$ at various pH values and temperatures.

Rate constants[a] (s^{-1})	pH	Temperature(℃)		
		5	15	25
k_1	2.5b)	2.6×10^{-2}		
	3.0b)	1.3×10^{-2}	1.8×10^{-2}	
	3.5c)	4.1×10^{-3}	8.0×10^{-2}	1.6×10^{-2}
k_2	2.5	3.1×10^{-2}		
	3.0	1.8×10^{-2}	2.2×10^{-2}	
	3.5	2.0×10^{-2}	2.5×10^{-2}	4.5×10^{-2}
k_3	2.5	7.9×10^{-3}		
	3.0	1.3×10^{-3}	2.6×10^{-3}	
	3.5	1.1×10^{-3}	1.7×10^{-3}	3.5×10^{-3}
k_4	2.5	$\simeq 0$		
	3.0	2.8×10^{-4}	5.4×10^{-4}	
	3.5	1.0×10^{-3}	1.7×10^{-3}	3.7×10^{-3}

a) rate constants defined as

$$Ge \underset{k_2}{\overset{k_1}{\rightleftharpoons}} [H_3GeMo_{11}O_{39}]^{5-} \underset{k_4}{\overset{k_3}{\rightleftharpoons}} [GeMo_{12}O_{40}]^{4-}.$$

b) reaction mechanism could be determine to above equation.

c) reaction mechanism could not be determine.

4.5. Discussion

The results clearly demonstrate that the Keggin anions, $[SiMo_{12}O_{40}]^{4-}$, and $[GeMo_{12}O_{40}]^{4-}$ form via lacunary anions, $[H_3SiMo_{11}O_{39}]^{5-}$ and $[H_3SiMo_{11}O_{39}]^{5-}$ in aqueous solutions.

For comparison, the rate constants (s^{-1}) for the Si-Mo and Ge-Mo systems determined under a certain condition (pH 3.5, T = 25℃, [Mo] = 24 mM , and $[X]_o$ = 100 μM) are shown below:

$$\text{Si} \quad \underset{1.4\times10^{-2}}{\overset{8.7\times10^{-3}}{\rightleftharpoons}} [H_3SiMo_{11}O_{39}]^{5-} \xrightarrow{4.6\times10^{-3}} [SiMo_{12}O_{40}]^{4-}$$

$$\text{Ge} \quad \underset{4.5\times10^{-2}}{\overset{1.6\times10^{-2}}{\rightleftharpoons}} [H_3GeMo_{11}O_{39}]^{5-} \underset{3.7\times10^{-3}}{\overset{3.5\times10^{-3}}{\rightleftharpoons}} [GeMo_{12}O_{40}]^{4-}$$

The formation rate of $[H_3GeMo_{11}O_{39}]^{5-}$ is faster than that of $[H_3SiMo_{11}O_{39}]^{5-}$, whereas the formation rate of $[GeMo_{12}O_{40}]^{4-}$ is slower than that of $[SiMo_{12}O_{40}]^{4-}$. This seems to result from a structural factor: because the ionic size of germanate is larger than that of silicate, the MoO_6 octahedra of $[GeMo_{12}O_{40}]^{4-}$[110] is slightly distorted from that of a structurally stable $[SiMo_{12}O_{40}]^{4-}$[109].

Since the rate constants k_n (n = 1 - 4) in tables 4-1 and 4-2 are determined under the assumption of first-order kinetics, they are regarded as apparent rate constants as a function of $[H^+]$ and the concentration of free molybdate or isopoly species. However, since the equilibria of isopolyanions are rather complex (e.g., section 3.3.1), it seems premature to determine the species associated with the formation of species I and II. Further study should be needed for a detailed discussion of the formation mechanisms.

CHAPTER V

Analytical Application – A Voltammetric Phosphate Sensor[h,i] –

5.1. Introduction

To date, a variety of phosphate-selective electrodes based on metal-metal phosphate electrodes, enzyme electrodes, liquid-liquid or polymer-membrane electrodes, etc., have been developed [111-118](for review, see [119]). Despite these efforts, however, none of these electrodes has reached commercial production mainly because of their poor selectivity. The electrodes based on metal-metal phosphates [111,112] have a fair performance in chloride-free solutions, but their application seems to be limited. The enzyme electrode systems [116-118] are very complicated. Recently, it has been shown that polymer-membrane electrodes based on organotin compounds display a relatively high level of selectivity for dibasic phosphate over many common anions [113-115]. However, many questions remain unanswered concerning the fundamental chemistry responsible for selectivity of the membrane electrodes. Further investigation seems to be needed for practical application of these membrane electrodes.

The formation of heteropolymolybdate complexes has long been used as the basis of the spectrophotometric determination of phosphate ion [120]. The application of the heteropoly compounds to the phosphate-selective electrode is promising; however, a few attempts to develop potentiometric electrodes were unsuccessful [121].

In a previous study [32], the electrochemical formation of a heteropoly molybdophosphate complex at NB/W interface was reported: When an isopolyanion $Mo_6O_{19}^{2-}$ transfers form NB to W, the anion rapidly decomposes in W to liberate some Mo(VI) species, which subsequently forms a molybdophosphate complex $[H_3PMo_{11}O_{39}]^{5-}$ with phosphate ion. The heteropolyanion formed in W gives a voltammetric current due to its transfer back to NB. The current has been found to be proportional to the phosphate concentration in W. This result shows the possibility

of a new type of sensor based on amperometric detection of phosphate ion (note that all phosphate electrodes so far developed [111-115], except the enzyme electrodes [116-118], are based on potentiometry). In this study, a voltammetric sensor for phosphate ion has been constructed and its performance has been examined.

5.2. Experimental

Chemicals

The *n*-tetrapentylammonium hexamolybdate $(TPnA)_2[Mo_6O_{19}]$ was prepared by the addition of solid *n*-tetrapentylammonium bromide (1.5 g) to a 120 mM Mo(VI) - 0.5 M HCl - 70% (v/v) acetone system (100 ml) [122]. The resultant yellow salt was subsequently recrystallized from acetone. The preparations of a NB solution of TPnATPB and a stock solution of TPnACl for preparing the internal solution are described in section 1.2. Other chemicals used were of analytical grade. Distilled water was used for preparing all aqueous solutions.

Sensor Construction

The voltammetric phosphate sensor is schematically illustrated in Figure 5-1. A dialysis membrane (Union Carbide Corp., 20.3 μm thick) impregnated with distilled water was spread at the cut end (3.0-mm inner diameter) of glass tube "A" by means of a Teflon tube. A 0.1 M TPnATPB NB solution was poured into the glass tube. The inner surface of the a glass tube, which should be in contact with the NB solution, was siliconized in advance with dimethyldichlorosilane vapor. Next, about 40 mg of the $(TPnA)_2Mo_6O_{19}$ salt finely ground in an agate mortar was dropped into the NB solution; the salt was partly dissolved, but the majority remained the undissolved on the dialysis membrane. An internal solution containing 0.02 M TPnACl and 0.1 M $MgSO_4$ was then

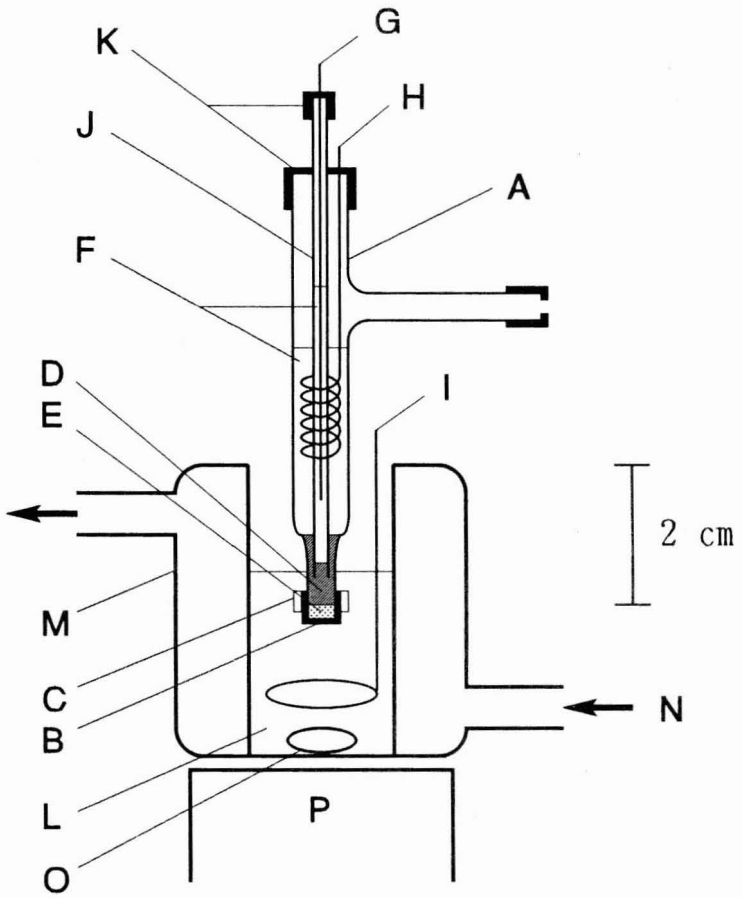

Fig. 5-1. Scheme of the phosphate sensor system : (A) glass tube, (B) dialysis membrane, (C) Teflon tube, (D) 0.1 M TPnATPB NB solution, (E) $(TPnA)_2Mo_6O_{19}$ powder, (F) internal solutions (0.02 M TPnACl + 0.1 M $MgSO_4$), (G,H,I) Ag/AgCl electrodes, (J) Luggin capillary, (K) rubber caps, (L) test aqueous solution (χ mM KH_2PO_4 + 0.5 M $MgCl_2$; typically pH 3.5), (M) water-jacketed vessel, (N) thermostated water (25±0.1℃), (O) stirring bar, and (P) magnetic stirrer.

gently applied onto the NB solution. A Luggin capillary and spiral Ag/AgCl electrode, both held by a rubber cap, were immersed into the internal solution. As shown in Fig. 5-1, the end of Luggin capillary, being siliconized in advance, was located in the NB solution. Finally, another Ag/AgCl electrode was placed in the Luggin capillary filled with the internal solution. The sensor was conditioned by dipping its end in distilled water for at least 12 hours at room temperature. When not in use, it was stored in the same manner.

Apparatus are described in Chapter I.

Procedure

The phosphate sensor system was constructed as shown in Fig. 5-1. Four ml of a test aqueous solution (x mM KH_2PO_4 + 0.5 M $MgCl_2$, typically pH 3.5) was transferred to a water-jacketed vessel thermostated at 25±0.1 ℃; the pH of the test solution was adjusted with a CH_3COOH-$(CH_3COO)_2Mg$ buffer ($[CH_3COO^-]$ = 0.1 M). A voltammetric measurement was carried out after stirring the test solution by means of a magnetic stirrer for about 1 minute (the distribution equilibrium of phosphate ion between the dialysis membrane and the test solution was reached in the time). The potential sweep was applied in the positive direction from 0.29 V to 0.35 V, followed by the negative to 0.16 V, then the positive back to the initial potential; in this cycle, the electrode potential was held at 0.35 V for 30 seconds (unless otherwise noted). The sweep rate was usually 0.02 V s^{-1}. After the voltammetric measurement was accomplished, 2 ml of 1 M $(CH_3COO)_2Mg$ solution was added to the test solution (the pH became 6.0), followed by stirring for about 1 minute; the heteropoly complex formed in the dialysis membrane was perfectly removed in this operation. After the test solution was sucked off, the sensor was rinsed twice with distilled water and then used for the next assay.

A freshly prepared sensor must be pretreated by repeating the above-mentioned voltammetric measurement several times until a steady current

response for phosphate ion was obtained. Once pretreated, the sensor gave stable response all through the experiment.

5.3. Results and Discussion

Figure 5-2 shows cyclic voltammograms in the presence and absence of phosphate ion in the test solution. The anodic current observed on the initial positive scan from 0.29 V to 0.35 V is due to the transfer of $Mo_6O_{19}^{2-}$ from NB to W (i.e., dialysis membrane, see below). This anodic current was not followed by a cathodic current due to the transfer of $Mo_6O_{19}^{2-}$ back to NB. This shows that the anion decomposed rapidly into some Mo(VI) species (see section 3.3.1) after being transferred from NB to W. In this measurement, the potential was held at 0.35 V for a definite time (e.g., 30 seconds in Fig. 5-2) in order to generate Mo(VI) enough for the subsequent formation of a heteropoly complex. In the presence of phosphate ion in the test solution, a well-defined wave with cathodic and anodic peaks appeared around 0.25 V. As reported previously (Ref. 32 and Chapter III), this wave is due to the interfacial transfer of a lacunary Keggin anion ($[H_3PMo_{11}O_{39}]^{4-}$) formed in the W phase in the vicinity of the interface; the cathodic peak corresponds to the transfer of $[H_3PMo_{11}O_{39}]^{4-}$ from W to NB, while the anodic peak corresponds to its transfer back to W. Under suitable conditions, the cathodic peak current (I_{pc}) was proportional to the phosphate concentration, as shown below.

Although the voltammogram shown in Fig. 5-2 was recorded for a quiet test solution, stirring of the test solution had no effect on the voltammetric curve. This shows that the formation of the heteropoly complex takes place in the dialysis membrane impregnated preferentially with the test aqueous solution. Accordingly, it can be assumed that the NB/W interface is formed at the inner surface of the dialysis membrane. This is in line with the previous study on the electrochemical characteristics of the membrane-covered ion-selective electrodes [116].

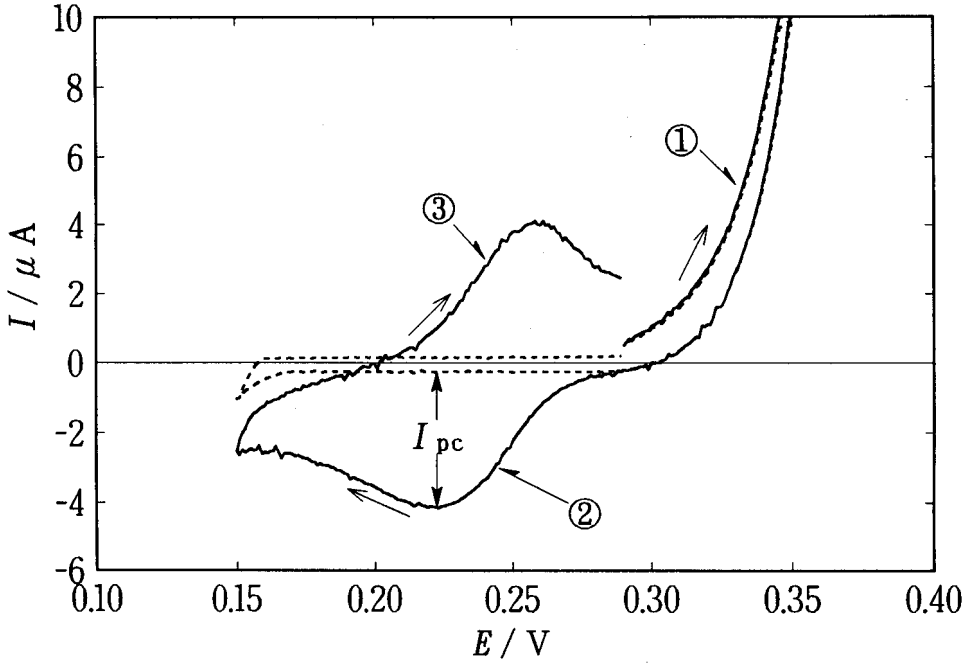

Fig. 5-2. Cyclic voltammograms in the presence (—) and absence (---) of 0.4 mM phosphate ion in the test solution (pH 3.5). The potential was held at 0.35 V for 30 s. Scan rate : 20 V s^{-1}. The voltammetric currents denoted by (1-3) are due to the corresponding processes in Fig. 5-3.

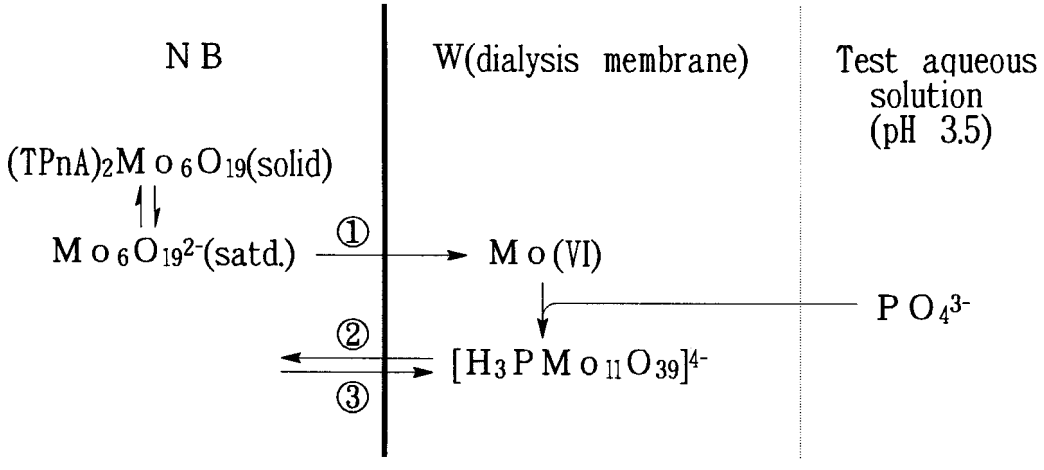

Fig. 5-3. Principle of the voltammetric phosphate sensor. See text for details.

Figure 5-3 illustrates the principle of the voltammetric phosphate sensor. Thus, the Mo(VI) species required to form the heteropoly complex is provided by the interfacial transfer of $Mo_6O_{19}^{2-}$. Although $Mo_6O_{19}^{2-}$ in NB is consumed for each measurement, it is supplied by quick dissolution of excess solid $(TPnA)_2Mo_6O_{19}$, which makes it possible to use the sensor repeatedly (at least 200 times) without any particular treatment.

The effects of pH, phosphate concentration, and potential-holding period on the voltammetric response were examined. Figure 5-4 shows the pH dependence of the voltammetric response. As pH was increased form 3.1 to 5.1, the wave for the heteropolyanion transfer shifted to negative potentials. The I_{pc} was not very dependent on pH in the range from 3.1 to 4.1 but decreased at higher pH. In the following experiments, the test solution of pH 3.5 was employed.

The dependence of I_{pc} on the phosphate concentration for various potential holding periods (τ 's) is shown in Fig. 5-5. The decrease in I_{pc} at the τ 's shorter than 30 seconds may be attributed to a deficiency of Mo(VI). When τ was 30 seconds, the I_{pc} was proportional to the phosphate concentration in the range from 0.02 to 0.5 mM. Under these conditions, the I_{pc} was controlled only by the diffusion of phosphate ion in the dialysis membrane. When τ was longer than 60 seconds, the reproducibility of I_{pc} became poor (data not shown). Possibly this is because the diffusion layer of phosphate ion was no longer confined within the dialysis membrane and reached the solution phase where the diffusion layer might be disrupted by convection. Consequently, the τ of 30 seconds was determined as optimum.

Interference studies were conducted on silicate, arsenate, and germanate ions in some detail, because they could possibly form heteropoly complexes (see Chapter III). The results showed that only silicate ion interfered with the determination of phosphate ion. As shown in Fig. 5-6, the addition of silicate ion caused the wave for the molybdophosphate anion to shift to negative potentials with a decrease in current. The current around the negative switching potential (i.e. 0.16 V) increased with an increase in the silicate concentration,

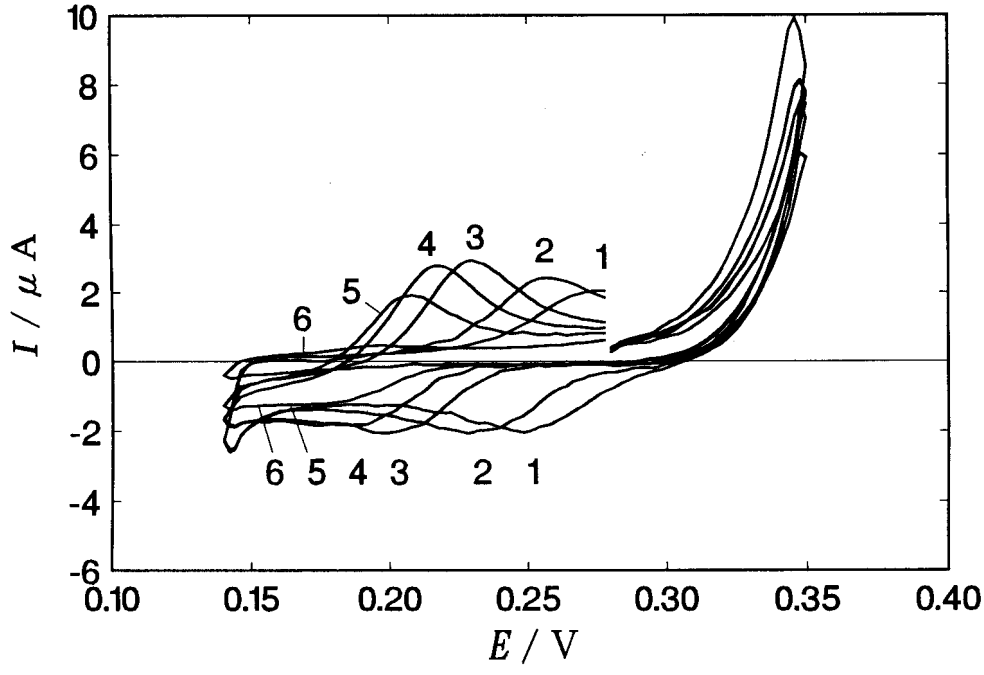

Fig. 5-4. pH dependence of the voltammetric response. pH : (1) 3.1, (2) 3.5, (3) 4.1, (4) 4.3, (5) 4.7, and (6) 5.1. Phosphate : 0.2 mM. Other conditions are as in Fig. 5-2.

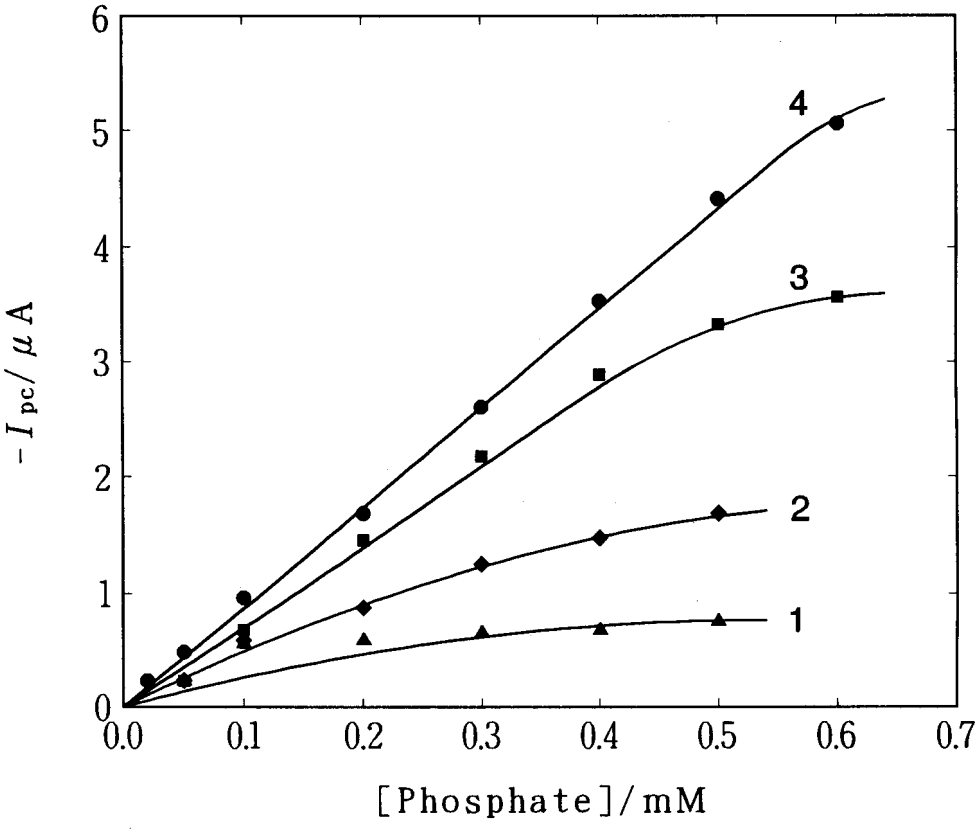

Fig. 5-5. Dependence of the cathodic peak current on the phosphate concentration. Potential holding period : (1) 0, (2) 1, (3) 5, and (4) 30 s.

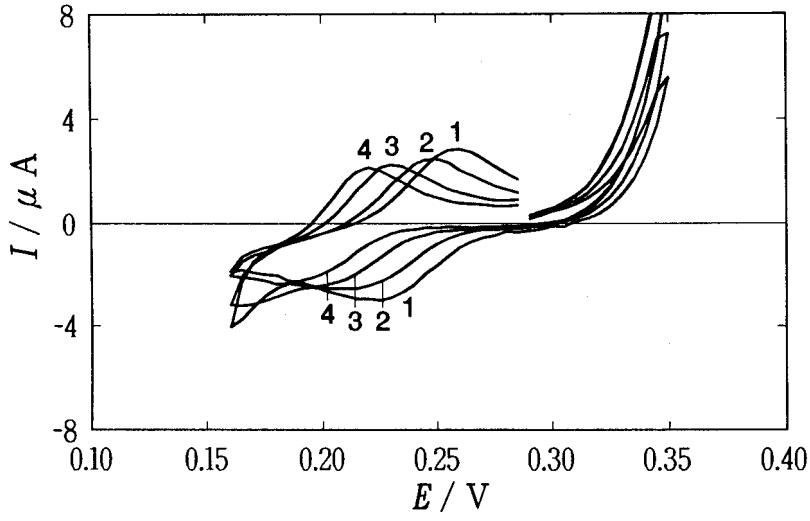

Fig. 5-6. Effect of silicate ion on the determination of phosphate ion. Phosphate : 0.2 mM. Silicate : (1) 0.0, (2) 0.2, (3) 1.0, and (4) 2.0 mM. Other conditions are as in Fig. 5-2.

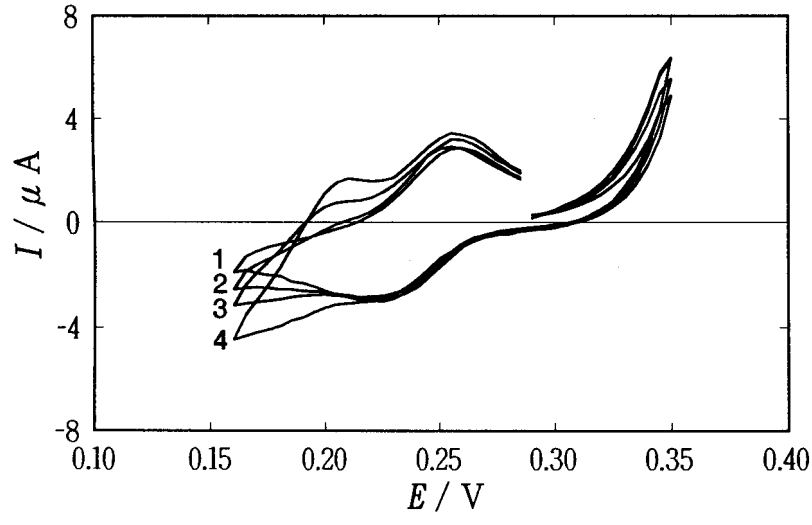

Fig. 5-7. Effect of arsenate ion on the determination of phosphate ion. Posphate : 0.2 mM. Arsenate : (1) 0.0, (2) 0.1, (3) 0.2, and (4) 0.5 mM. Other conditions are as in Fig. 5-2.

suggesting that a certain molybdosilicate complex, 11-molybdosilicate (see section 3.3.1 and section 4.4), was formed along with the molybdophosphate complex. On the other hand, as shown in Figs. 5-7 and 5-8, arsenate and germanate ions in comparable amounts caused no significant interference, though these ions, as well as silicate ion, gave voltammetric waves around 0.16 V due to the transfer of the corresponding heteropolyanions formed (see Chapter III).

Furthermore, interference studies were conducted on many other common ions, namely, NO_3^-, ClO_4^-, SO_4^{2-}, SCN^-, Br^-, Li^+, Na^+, K^+, and NH_4^+ (2.0 mM each). All the ions examined, except SCN^- and ClO_4^- had no effect on the voltammetric response for phosphate ion; SCN^- and ClO_4^- led to positive errors (+7 and +180%, respectively) in the determination of phosphate ion (0.2 mM), because the currents due to their own transfer from W to NB were superimposed upon the cathodic peak current to be measured.

With the present phosphate sensor, about 20 samples can be assayed for an hour. In addition, the voltammetric response was reproduced within ±5% (in I_{pc}) for at least a week and 200 assays.

As stated above, the present voltammetric sensor displayed a relatively high level of selectivity for phosphate ion. Accordingly, the utility of this sensor may be recognized. But the concentration range showing the linear current response is not very wide (5×10^{-4} - 2×10^{-5} M) compared with that showing the Nernstian response for a usual potentiometric electrode (e.g., in [113], the range is 10^{-2} - 10^{-5} M). This is because this sensor is based on amperometric detection of phosphate ion. In general, however, amperometric (or voltammetric) electrodes, giving the current response directly proportional to analyte concentration, are more suitable for detecting small differences in analyte concentration than potentiometric electrodes giving the potential response proportional to the logarithm of analyte activity (concentration).

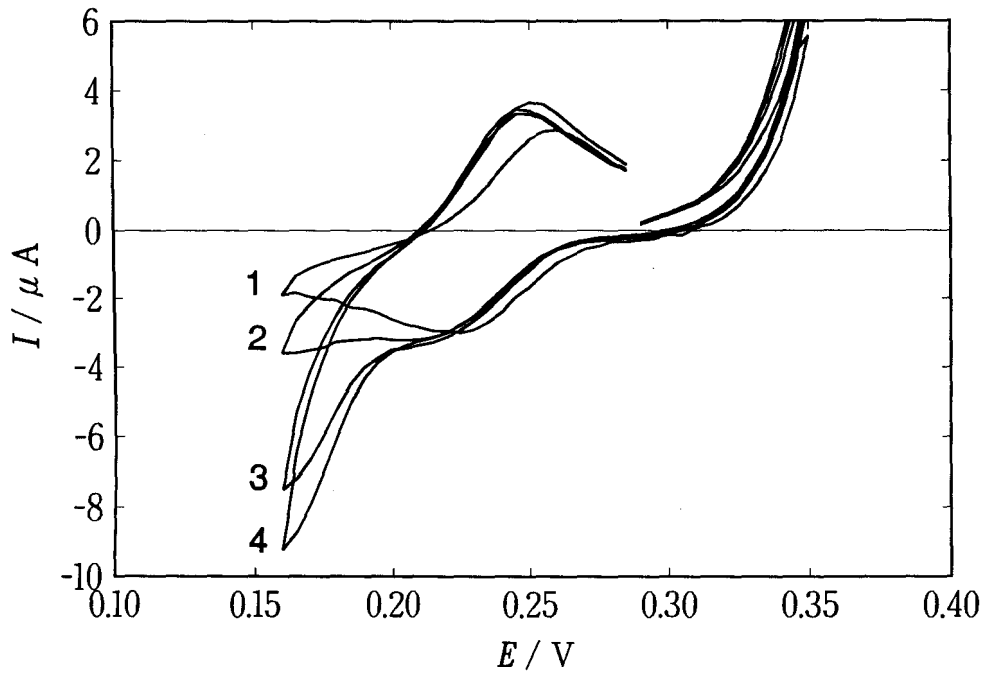

Fig. 5-8. Effect of germanate ion on the determination of phosphate ion. Phosphate : 0.2 mM. Germanate : (1) 0.0, (2) 0.2, (3) 0.5, and (4) 1.0 mM. Other conditions are as in Fig. 5-2.

CONCLUSION

In this study, the formation of heteropolyanions in solutions has been studied by means of ion-transfer voltammetry using the oil/water interface.

In Chapter I, the transfer of polyanions at the nitrobenzene/water interface has been studied. Through analyses of the voltammetric waves, the values of the standard ion-transfer potential ($\Delta_{O}^{W}\phi^{\circ}$) were determined for the polyanions of various size and ionic charge. Since all of the space of the polyanion structure is taken up by bulky oxygen atoms, the charge density can be regarded as being proportional to $|z|/n^{2/3}$ (z, ionic valence; n, number of oxygen atoms). The plot of $\Delta_{O}^{W}\phi^{\circ}$-values against this quantity showed a simple relationship, i.e.,

$$\Delta_{O}^{W}\phi^{\circ}(V) = -1.981(|z|/n^{2/3}) + 0.749$$

This linear relationship shows that the $|z|/n^{2/3}$-value can be used as a hydrophobicity scale of polyanions. According to the $|z|/n^{2/3}$-value, polyanions may be classified as being either hydrophobic or hydrophilic. As a whole, polyanions with $|z|/n^{2/3}$-values smaller than 0.3 are classified as being "hydrophobic"; they are known to be stable in mixed organic solvent. Whereas polyanions with $|z|/n^{2/3}$-values larger than 0.3 are classified as being "hydrophilic"; they are known to be stable in mixed organic solvent. Thus, the author proposes the $|z|/n^{2/3}$-value to be used for the discussion of hydrophobic behaviors of polyanions.

In Chapter II, Ion-transfer voltammetric measurements have been extended to the 1,2-dichloroethane/W interface. The plots of "apparent" ion-transfer potentials against $|z|/n^{2/3}$ at several concentrations of organic phase gave also straight lines. Since the slope of each straight line was almost the same, there were no marked differences in the effect of ion pairing between the polyanions tested. Thus, the linear relationship between $\Delta_{O}^{W}\phi^{\circ}$ and $|z|/n^{2/3}$ was also obtained for this system.

$$\Delta_{O}^{W}\phi^{\circ}(V) = -1.781(|z|/n^{2/3}) + \text{const}$$

By using the Uhlig formula, the "electrostatic" part of $\Delta_{O}^{W}\phi^{\circ}$ $\{\Delta_{O}^{W}\phi^{\circ}(el)\}$ was estimated. The $\Delta_{O}^{W}\phi^{\circ}(el)$-value also depends linearly on $|z|/n^{2/3}$. Thus, the electrostatic part of the Gibbs transfer energy $\{\Delta G_{tr}^{\circ,\circ\rightarrow W}(el)\}$ could be expressed as

$$\Delta G_{tr}^{\circ,\circ\rightarrow W}(el) = a(z^2/n^{2/3}) - bz$$

Such a dependence conflicts with Bornian (long-range) electrostatic solvation energy. This non-Bornian dependence suggest that short-range interactions (i.e., donor-acceptor effects or hydrogen bonds) of the polyanion with the solvent molecules play the most significant role.

In Chapter III, ion-transfer voltammetry using the nitrobenzene/water interface has been applied to characterize aqueous molybdate solutions containing such a heteroanion as silicate, germanate, phosphate, or arsenate. Some solute species have been identified and their formation equilibria could be discussed on the basis of the hydrophobicity scale proposed in Chapter I. The Keggin anions with pentavalent heteroatoms, $[PMo_{12}O_{40}]^{3-}$ and $[AsMo_{12}O_{40}]^{3-}$, having higher hydrophobicity ($|z|/n^{2/3}$ = 0.256), have never been observed in test aqueous solutions (pH $\leq$ 0.9), whereas those with tetravalent heteroatoms, $[SiMo_{12}O_{40}]^{4-}$ and $[GeMo_{12}O_{40}]^{4-}$, having lower hydrophobicity ($|z|/n^{2/3}$ = 0.342), were rather stable even at lower acid concentrations. The 11-heteropolymolybdate anions, $[H_3SiMo_{11}O_{39}]^{5-}$, $[H_3GeMo_{11}O_{39}]^{5-}$, and $[H_3PMo_{11}O_{39}]^{4-}$, were observed in all systems except for the arsenate-molybdate system. Only in the arsenate-molybdate system, however, so-called "reversed" Keggin anion, $[H_2As_4Mo_{12}O_{50}]^{6-}$, exists instead of 11-molybdoarsenate.

In Chapter IV, the author has also developed a new electrochemical method for the kinetic study of the formation of Keggin anions, $[SiMo_{12}O_{40}]^{4-}$ and $[GeMo_{12}O_{40}]^{4-}$. This method named dual pulse amperometry is based on the amperometric detection of polyanions by means of two potential pulses of different amplitudes. The formation

curves of the Keggin anions and the lacunary anions, $[H_3SiMo_{11}O_{39}]^{5-}$ and $[H_3GeMo_{11}O_{39}]^{5-}$, have been obtained. The analysis of the formation curves clearly demonstrated that the Keggin anions form via the lacunary anions in aqueous solutions. The formation rate of $[H_3GeMo_{11}O_{39}]^{5-}$ was faster than that of $[H_3SiMo_{11}O_{39}]^{5-}$, whereas the formation rate of $[SiMo_{12}O_{40}]^{4-}$ was slower than that of $[GeMo_{12}O_{40}]^{4-}$.

In Chapter V, a voltammetric phosphate sensor, which relies on electrochemical formation of the molybdophosphate at the NB/W interface, has been constructed and its performance has been examined. Under optimal conditions, the voltammetric current is proportional to the phosphate concentration in the range from 0.02 to 0.5 mM. Though silicate ion interferes with the determination of phosphate ion, arsenate and germanate ions cause no significant interference. About 20 samples could be assayed for an hour. The voltammetric response was reproduced within ±5% for at least a week and 200 assays. Thus, this sensor appears to be quite promising for the accurate determination of phosphate ion in a variety of media.

Acknowledgement

The author wishes to express his sincere thanks to Dr. Atsuyoshi Saito, Professor of Kobe University, for his gracious guidance and encouragement throughout the course of this study. His scientific insight has contributed much to this work. The author also expresses his deep appreciation to Dr. Sadayuki Himeno, Professor of Kobe University, for his helpful direction and opinion. His learning and experience in solution chemistry have also made a greater contribution. The author is also grateful to Dr. Toshiyuki Osakai for his continuous guidance and invaluable advice. His stimulating discussions has been of great help for the author's study. Thanks are also due to Dr. Kohji Maeda (present address: Fukui prefectural University) for his helpful suggestions. The author has exceedingly referred to his earnest and active attitudes towards research. The experiments were carried out in collaboration with Tadaharu Ueda, Miss Tomomi Kubo, and Miss Hiroko Hayamizu. The author has been indebted to them for their sincere assistance.

REFERENCES

1) M. T. Pope, "Heteropoly and Isopoly Oxometalates," Springer-Verlag, Berlin (1983).

2) M. T. Pope and A. Müller, *Angew. Chem.*, **103**, 56 (1991)

3) For reviews, see: a) I. V. Kozhevnikov and K. I. Matreev, *Appl. Catal.*, **5**, 135 (1983); b) M. Misono, "Proceedings of the Climax Fourth International Conference on the Chemistry and Uses of Molybdenum," ed by H. F. Barry and P. C. H. Mitchell, Climax Molybdenum Co., Ann Arbor, Michigan (1982), pp. 289-295; c) M. Misono, *Catal. Rev. Sci. Eng.*, **29**, 269 (1987); d) I. V. Kozhevnikov, *Russ. Chem. Rev. (Engl. Transl.)*, **56**, 811 (1987).

4) a) A. Negin, *Clin. Chem.*, **15**, 829 (1969); b) A. B. Sanyal and P. Ganguly, *Biochem. Biophys. Acta*, **133**, 535 (1967); c) J. C. Chermann, F. Sinoussi, and C. Jatmin, *Biochem. Biophys. Res. Commun.*, **65**, 1229 (1975); d) J. E. Scott, *J. Histochem. Cytochem.*, **19**, 689 (1971); e) J. E. Scott, *Acta Histochem.*, **15**, 213 (1975).

5) a) J. van R. Smit, *Nature*, **181**, 1530 (1958); b) J. Krtil and V. Kourim, *J. Inorg. Nucl. Chem.*, **12**, 367 (1960).

6) T. Hori, O. Tamada, and S. Himeno, *J. Chem. Soc., Dalton Trans.*, 1491 (1989).

7) S. Himeno, T. Hori, and A. Saito, *Bull. Chem. Soc. Jpn.*, **62**, 2184 (1989).

8) S. Himeno, T. Hori, and A. Saito, *Bull. Chem. Soc. Jpn.*, **63**, 1602 (1990).

9) S. Himeno, T. Hori, M. Hasegawa, and A. Saito, *Inorg. Chim. Acta.*, **131**, 11 (1987).

10) S. Himeno, T. Osakai, A. Saito, and T. Hori, *Bull. Chem. Soc. Jpn.*, **65**, 799 (1992).

11) T. Hori and S. Himeno, *Bunseki Kagaku*, **40**, 507 (1991).

12) P. Souchay and R. Contant, *C. R. Acad. Sci., Ser. C*, **265**, 723 (1967).

13) J. M. Fruchart and R. Contant, *C. R. Acad. Sci., Ser. C*, **266**, 1571 (1968).

14) G. A. Tsigdinos and C. J. Hallada, *J. Less-Common Met.*, **36**, 79 (1974).

15) D. N. Bernhart and A. R. Wreath, *Anal. Chem.*, **27**, 440 (1955).

16) A. Halász and E. Pungor, *Talanta*, **18**, 569 (1971).

17) T. Fujinaga, M. Koyama, and T. Hori, Talanta, **18**, 960 (1971).

18) T. Hori and T. Fujinaga, *Talanta*, **30**, 925 (1983)

19) T. Hori and T. Fujinaga, *Bull. Chem. Soc. Jpn.*, **58**, 1380 (1985).

20) J. Koryta, *Electrochim. Acta*, 24, 293 (1979); 29, 445 (1984); **33**, 189 (1988)

21) P. vanýsek, *Anal. Chem.*, 62, 872A (1990).

22) M. Senda, T. Kakiuchi, and T. Osakai, *Electrochim. Acta*, **36**, 253 (1991).

23) Le Q. Hung, *J. Electroanal. Chem. Interfacial Electrochem.*, **115**, 159 (1980).

24) T. Kakutani, Y. Nishiwaki, and M. Senda, *Bunseki Kagaku*, **33**, E175 (1984).

25) Z. Yoshida and H. Freiser, *Inorg. Chem.*, **23**, 3931 (1984).

26) J. Koryta, *J. Electroanal. Chem. Interfacial Electrochem.*, **213**, 323 (1986).

27) J. Koryta and M. Skalický, *J. Electroanal. Chem. Interfacial Electrochem.*, 229, 265 (1987).

28) J. Koryta, *Electrochim. Acta*, **32**, 419 (1987).

30) T. Osakai, S. Himeno, and A. Saito, *Anal. Sci.*, **5**, 771, (1989).

31) T. Osakai, S. Himeno, and A. Saito, *J. Electroanal. Chem. Interfacial Electrochem.*, **302**, 145, (1991).

32) T. Osakai, S. Himeno, and A. Saito, *Bull. Chem. Soc. Jpn.*, **64**, 1313 (1991).

33) T. Osakai, S. Himeno, and A. Saito, *J. Electroanal. Chem. Interfacial Electrochem.*, **332**, 169 (1992).

34) H. Katano, T. Osakai, S. Himeno, and A. Saito, *Rev. Polarogr. (Kyoto)*, **37**, 41 (1991).

35) A preliminary accound of the result was reported at the "36th Annual Meeting on Polarography and Electroanalytical Chemistry," Tokyo December 1990; Abstr., T. Osakai, S. Himeno, and A. Saito, *Rev. Polarogr. (Kyoto)*, **36**, 61 (1990).

36) S. Himeno, T. Osakai, and A. Saito, *Bull. Chem. Soc. Jpn.*, **64**, 21 (1991).

37) W.G. Klemperer and W. Shum, *J. Am. Chem. Soc.*, **98**, 8291 (1976).

38) T. Kakutani, T. Osakai, and M. Senda, *Bull. Chem. Soc. Jpn.*, **56**, 991 (1983).

39) T. Osakai, T. Nuno, Y. Yamamoto, A. Saito, and M. Senda, Bunseki Kagaku, 38, 479 (1989).

40) In this study, all the potentials refer to the reversible half-wave potential of tetramethylammonium ion [38], $E^{rev}_{1/2,TMA}$(= 0.367 V in cell A), $\Delta^{W}_{NB}\phi^{\circ}_{TMA}$ being 0.035 V (J. Koryta, P. vanýsek, and M. Brezina, *J. Electroanal. Chem. Interfacial Electrochem.*, **75**, 211 (1977)). From Eqs. 1-1 and 1-2 with γ^{o}/γ^{w} = 1 and D^{w}/D^{o} = 2.07 [42], ΔE_{ref} was evaluated to be 0.323 V for cell A.

41) By assuming that the $\Delta^{W}_{O}\phi^{\circ}$-value of a protonated anion, $[HVMo_5O_{19}]^{2-}$, equals to that of $[Mo_6O_{19}]^{2-}$ with the identical charge and structure, i.e., 0.164 V (Table 1-1), the ratio of the protonation constants in W and NB can be estimated as $K^{w}/K^{o}=5.4\times10^{-18}$ (see Eqs. A10-A13 and Eq. A16 in Ref. 31). This means that the protonation reaction in W can be neglected.

42) T. Osakai, T. Kakutani, Y. Nishiwaki, and M. Senda, *Bunseki Kagaku*, **32**, E81 (1983).

43) T. Kurucsev, A.M. Sargeson, and B.O. West, *J. Phys. Chem.*, **61**, 1567 (1957).

44) C. Wadelin and M.G. Mellon, *Anal. Chem.*, **25**, 1668 (1953).

45) M. Ishibashi and M. Tabushi, *Bunseki Kagaku*, **8**, 588 (1956).

46) S.J. Simon and D.F. Boltz, *Anal. Chem.*, **47**, 1758 (1975).

47) V.S. Markin and A.G. Volkov, *Electrochim. Acta*, **34**, 93 (1989);

48) Y. Marcus, *Pure Appl. Chem.*, **55**, 977 (1983).

49) M. Born, *Z. Phys.*, **1**, 45 (1920).

50) Y. Marcus, "Ion Solvation," Willey, Chichester (1985), pp. 44-47.

51) M.H. Abraham and A.F. Danil de Namor, *J. Chem. Soc. Faraday Trans.* I, **72**, 955 (1976).

52) M.H. Abraham and A.F. Danil de Namor, *J. Chem. Soc. Faraday Trans.* I, **74**, 2101 (1978).

53) J. Rais, *Collect. Czech. Chem. Commun.*, **36**, 3253 (1971).

54) J. Czapkiewicz and B. Czapkiewicz-Tutaj, *J. Chem. Soc. Faraday Trans.* I, **76**, 1663 (1980).

55) M. H. Abraham and J. Liszi, *J. Chem. Soc. Faraday Trans.* I, **74**, 1604 (1978).

56) M. H. Abraham and J. Liszi, *J. Chem. Soc. Faraday Trans.* I, **74**, 2858 (1978).

57) A. A. Kornyshev and A. G. Volkov, *J. Electroanal. Chem.*, **180**, 363 (1984).

58) E. Makrlik and Le Q. Hung, *J. Electroanal. Chem.*, **158**, 277 (1983).

59) Z. Samec, V. Marecēk, and M. P. Colombini, *J. Electroanal. Chem.*, **257**, 147 (1988).

60) T. Wandlowski, V. Marecēk, and Z. Samec, *Electrochim. Acta*, **35**, 1173 (1990).

61) K. Maeda, S. Kihara, M. Suzuki, and M. Matsui, *J. Electroanal. Chem.*, **295**, 183 (1990).

62) H. H. Uhlig, *J. Phys. Chem.*, **41**, 1215 (1937).

63) T. Kakiuchi, M. Nakanishi, and M. Senda, *Bull. Chem. Soc. Jpn.*, **61**, 1845 (1988).

64) P. Souchay and J. Faucherre, *Bull. Soc. Chim. Fr.*, 355 (1991).

65) L. Pettersson, *Chem. Scr.*, **7**, 145 (1975)

66) R. Contant, *Bull. Soc. Chim. Fr.*, 3277 (1973).

67) R. Contant and P. Souchay, *Bull. Soc. Chim. Fr.*, 3287 (1973).

68) L. Lyhamm and L. Pettersson, *Chem. Scr.*, **16**, 52 (1980).

69) L. Pettersson, *Acta Chem. Scand.*, **A29**, 677 (1975).

70) G. Johansson, L. Pettersson, and N Ingli, *Acta Chem. Scand.*, Ser. A, (a) **28**, 1119 (1974); (b) **32**, 407 (1978).

71) M. S. Kasprzak, S. R. Crouch, and G. E. Leroi, *Appl. Spectrosc.*, **32**, 537 (1978)

72) K. Murata and S. Ikeda, *Polyhedron*, (a) **2**, 1005 (1983); (b) **6**, 1681 (1987)

73) (a) T. Fujinaga, M. Koyama, and T. Hori, *Bull. Inst. Chem. Res. Kyoto Univ.*, **48**, 210 (1970); (b) T. Hori, *J. Inorg. Nucl. Chem.*, **39**, 2173 (1977).

74) C. C. Kircher and S. R. Crouch, *Anal. Chem.*, (a) **54**, 879 (1982); (b) **55**, 242 (1983)

75) L. Pettersson, I. Andersson and L.-O. Öhman, *Acta Chem. Scand.*, Ser. A, **39**, 53 (1985).

76) J. A. Rob van Veen, O. Sudmeijer, C. A. Emeis and H. de Wit., *J. Chem. Soc. Dalton Trans.*, 1825 (1986).

77) L. A. Combs-Walker and C. L. Hill, *Inorg. Chem.*, **30**, 4016 (1991).

78) J. D. H. Strickland, *J. Am. Chem. Soc.*, **74**, (a) 872, (b) 862, and (c) 868 (1952).

79) R. Massart *Ann. Chim.*, **4**, 285 (1969); (b) 635 (1969); (C) R. Massart and G. Herve, Rev. *Chimie Minerale*, **5**, 501 (1968).

80) R. Massart, *Ann. Chim.*, **3**, 507 (1968).

81) V. W. Truesdale and C. J. Smith, *Analyst*, 100, (a) 203 and (b) 797 (1975).

82) V. W. Truesdale, C. J. Smith, and P. J. Smith, *Analyst*, 102, 73 (1977).

83) P. Souchay and Tchakirian, *Ann. Chim.*, 1, 248 (1946).

84) C. M. Tourne, G. F. Tourne, S. A. Malik and T. J. R. Waeakley, *J. Inorg. Nucl. Chem.*, 32, 3875 (1970).

85) M. Fournier and R. Massart, *C. R. Acad. Ser. C*, **279**, 875 (1974).

86) C. Rocchiccioli-Deltcheff, M. Fournier, R. Frank, and R. Thouvenot, *Inorg. Chem.*, **22**, 207 (1983).

87) Sanchez, J. Livage, J. P. Launay, M. Fournier and Y. Jeannin, *J. Am. Chem. Soc.*, **104**, 3194 (1982).

88) K. Y. Matsumoto and Y. Sasaki, Bull. *Chem. Soc. Jpn.*, **49**, 156 (1976).

89) The structures of β-type XM_{11} are shown in Ref. 1, pp. 59.

90) R. Strandberg, *Acta Chem. Scand., Ser. A.* **28**, 217 (1974).

91) M. Filowitz, K. C. Ho, W. G. Klemperer, and W. Shum, *Inorg. Chem.*, **18**, 93 (1979).

92) K. Nishikawa and Y. Sasaki, *Chem. Lett.*, 1185 (1975).

93) a) Y. Sasaki, I. Lindqvist, and L. G. Sillén, *J. Inorg. Nucl. Chem.*, **9**, 93 (1959); b) Y. Sasaki and L. G. Sillén, *Arkiv Kemi*, 29, 253 (1967).

94) O. W. Howarth and P. Kelly, *J. Chem. Soc., Dalton Trans.*, 1236 (1988).

95) O. W. Howarth , P. Kelly, and L. Pettersson, *J. Chem. Soc., Dalton Trans.*, 81 (1990).

96) T. Ozeki and H. Kihara, *Anal. Chem.*, **60**, 2055 (1988).
97) J. Aveston, E. W. Anacker, and J. S. Johnson, *Inorg. Chem.*, **3**, 735 (1964).
98) K. H. Tytko, G. Baethe, E. R. Hirschfeld, K. Mehmke, and D. Stellhron, *Z. Anorg. Allg. Chem.*, **503**, 43 (1983); K. H. Tytko, G. Baethe, and J. J. Cruywagen, *Inorg. Chem.*, **24**, 3132 (1985).
99) M. Isobe, F. Maruno, T. Yamase, and T. Ikawa, *Acta Cryst.*, **B34**, 2728 (1978); T. Yamase, *J. Chem. Soc., Dalton Trans.*, 283 (1978).
100) L. Pettersson, I. Andersson and L.-O. Öhman, *Inorg. Chem.*, **25**, 4726 (1986).
101) W. H. Knoth and R. L. Harlow, *J. Am. Chem. Soc.*, **103**, 1865 (1981).
102) R. S. Nicholson and I. Shain, *Anal. Chem.*, **36**, 706 (1964).
103) A. Tézé and D. Hervé, *J. Inorg. Nucl. Chem.*, **39**, 999 (1977).
104) A. Tézé and D. Hervé, *Private Communications*, 1981 (1979).

105) V. W. Truesdale, P. J. Smith, and C. J. Smith, *Analyst*, **104**, 1243 (1979).
106) C. Cappellos and B. H. J. Bielski, "Kinetic Systems," Willey, New York (1972).
107) Y. Yamamoto, T. Osakai, and M. Senda, *Bunseki Kagaku*, **39**, 655 (1990).
108) This is supported by the fact that the saturating Ipc-values in the certain curves of the distribution diagrams both for the Si-Mo system (Fig. 3-13) and for the Ge-Mo system (Fig. 3-17) are almost equivalent (21.6 μA).
109) H. Ichida, A. Kobayashi, and Y. Sasaki, *Acta Cryst.*, **B36**, 1382 (1980).
110) R. Strandberg, *Acta Cryst.*, **B33**, 3090 (1977).
111) E. W. Grabner, I. Vermes, and K.-H. König, *J. Electroanal. Chem.*, **214**, 135 (1986).
112) I. Vermes and E. W. Grabner, *J. Electroanal. Chem.*, **284**, 315(1990).
113) S. A. Glazier and M. A. Arnold, *Anal. Chem.*, **60**, 2542 (1988).
114) S. A. Glazier and M. A. Arnold, *Anal. Lett.*, **22**, 1075 (1989).
115) S. A. Glazier and M. A. Arnold, *Anal. Chem.*, **63**, 754 (1991).

116) G. G. Guilbault and M. Nanjyo, *Anal. Chim.* Acta, **78**, 69 (1975).
117) G. G. Guilbault and T. Cserfalvi, *Anal. Lett.*, **9**, 277 (1976).
118) F. Schubert, R. Renneberg, F. W. Scheller, and L. Kirstein, *Anal. Chem.*, **56**, 1677 (1984).
119) D. Midgley, *Ion-Selective Electrodes Rev.*, **8**, 3 (1986).
120) W. Rieman III and J. Beukenkamp: *Phosphorus, in Treatise on Analytical Chemistry, Part II*, I. M. Kolthoff and P. J. Elving, Eds., Interscience, New York, 1961, vol. 5, pp. 317-402.
121) G. G. Guilbault and P. J. Brignac, Jr., *Anal. Chim. Acta*, **56**, 139 (1971).
122) S. Himeno, N. Ishii, M. Hasegawa, A. Saito, and T. Hori, *Inorg. Chim. Acta*, **131**, 11 (1987).
123) S. Sawada, T. Osakai, and M. Senda, *Bunseki Kagaku*, **39**, 539 (1990).

List for Publications

a) T. Osakai, H. Katano, K. Maeda, S. Himeno, and A. Saito, "A Hydrophobicity Scale of Heteropoly- and Isopolyanions Based on Voltammetric Studies", *Bull. Chem. Soc. Jpn.*, **66**, 1111 (1993).

b) T. Osakai, S. Himeno, A. Saito, K. Maeda, and H. Katano, "Linear Dependence of the Standard Ion Transfer Potentials of Heteropoly and Isopoly Anions at the 1,2-dichloroethane-Water Interface on their Surface Charge Densities", *J. Electroanal. Chem.*, in press.

c) T. Osakai, S. Himeno, A. Saito, K. Maeda, and H. Katano, "Linear Dependence of the Standard Ion Transfer Potentials of Heteropoly- and Isopolyanions at ITIES on the Surface Charge Densities", Proceedings of 183rd Meeting of the Electrochemical Society, Inc, 2540 (1993).

d) H. Katano, K. Maeda, T. Osakai, S. Himeno, and A. Saito, "Study of Heteropoly- and Isopolyanions in Aqueous Solutions by Ion-transfer Voltammetry with the Nitrobenzene/Water Interface — A Consideration using Hydrophobicity Scale of Polyanions", *Bull. Chem. Soc. Jpn.*, to be submitted.

e) K. Maeda, H. Katano, T. Osakai, S. Himeno, and A. Saito, "One-electron Redox Potential of Keggin-Type Heteropolyoxometalate Anions with Various Charge", in preparation.

f) H. Katano, T. Osakai, S. Himeno, and A. Saito, "11-Molybdogermanate Anion as the Intermediate of the Keggin Anion", *Chem. Lett.*, to be submitted.

g) H. Katano, T. Osakai, S. Himeno, and A. Saito, "Kinetics of the Formation of Keggin-type Molybdosilicate and -germanate Anions — Using Ion-transfer Voltammetry with the Nitrobenzene/Water Interface", *Anal. Chem.*, to be submitted.

h) T. Osakai, H. Katano, S. Himeno, and A. Saito, "Electrochemical Formation of Heteropolymolybdate Anions at the Oil/Water Interface and its Application to Oxoanion Sensors", Proceedings of the International Congress on Analytical Sciences 1991 (ICAS'91), Makuhari-Messe, Chiba, *Anal. Sci.*, 7-supplement, 1657 (1991).

i) T. Osakai, S. Himeno, A. Saito, and H. Katano, "A Voltammetric Phosphate Sensor Based on Heteropolyanion Formation at the Nitrobenzene/Water Interface", *Electroanalysis*, **5**, 215 (1993).